

Mouse models of systemic sclerosis-interstitial lung disease:
hypochlorous acid (HOCl)-induced or bleomycin delivered by osmotic
minipump?

Arina Morozan

MSc Candidate

Division of Experimental Medicine

McGill University, Montreal

November 2022

A thesis submitted to McGill University in partial fulfillment of the requirements of
the degree of Master of Science in Experimental Medicine

© Arina Morozan, 2022

Abstract

Background: Systemic sclerosis (SSc; scleroderma) is an autoimmune disease characterized by excessive collagen synthesis by fibroblasts, vascular abnormalities, and immune system activation, culminating in fibrosis of the skin and internal organs. Interstitial lung disease (ILD; lung fibrosis) is a frequent complication of SSc and one of its leading causes of death. Current treatments are of limited efficacy. To test new anti-fibrotics, reliable animal models that closely resemble human SSc-ILD are required. Two mouse models are favored in the literature – the repeated intradermal administration of hypochlorous acid [(HOCl)-SSc model] and the subcutaneous administration of bleomycin by osmotic minipump [(BLM-MP) model]. Both models reportedly induce skin and lung fibrosis. The HOCl-model has anti-topoisomerase 1 autoantibodies (anti-Scl-70) and elevated advanced oxidation protein product (AOPP) levels in serum. We performed an in-depth characterization focused on pulmonary involvement comparing these models.

Methods: HOCl model: 6-week-old female BALB/c mice were treated with daily intradermal HOCl injections for 6-weeks. Experiment termination: 42 days (D).

BLM-MP model: 10-week-old male C57BL/6 mice were implanted subcutaneously with osmotic minipumps containing BLM (60mg/kg) or phosphate-buffered saline (PBS) delivered continuously for 7 days. Experiment termination: 4 weeks

Readouts: 1) body weight; 2) skinfold (caliper) and dermal thickness (histology); 3) lung histology and compliance (flexiVent™); 4) mRNA expression of profibrotic markers in the lung; 5) serum levels of AOPP and anti-Scl-70; 6) lung radiodensity and percent of poorly aerated tissue (micro-computer tomography *in vivo*).

Results: HOCl-treated mice versus PBS-controls: 1) Over time there were no differences in body weight between groups. 2) In the injected area on D42, the skinfold thickness (mm) was two times

larger (HOCl vs PBS, mean \pm SEM: 1.37 ± 0.06 vs 0.66 ± 0.04) and the dermal thickness (μm) three times larger in the HOCl group (HOCl vs PBS: 639.90 ± 50.98 vs 206.40 ± 18.97). 3) HOCl treatment neither resulted in histological features of pulmonary fibrosis nor significant changes in lung compliance (HOCl vs PBS, ml/cmH₂O/g: $3.00 \times 10^{-3} \pm 4.61 \times 10^{-5}$ vs $3.50 \times 10^{-3} \pm 9.32 \times 10^{-5}$). Automated image analysis of Picrosirius red (PSR) staining of lungs of HOCl mice did not show increased collagen deposition (HOCl vs PBS, positive PSR pixels/mm²: $2,064,449 \pm 159,647$ vs $2,224,378 \pm 152,187$). 4) HOCl injections did not increase pulmonary mRNA expression of *ACTA2* (α -smooth muscle actin) (HOCl vs PBS, fold over control: 1.27 ± 0.30 vs 1.00 ± 0.38). 5) HOCl treatment did not induce the production of either AOPPs (HOCl vs PBS, $\mu\text{mol/L}$ of chloramine-T equivalents: 40.12 ± 10.87 vs 47.21 ± 11.62) or anti-Scl-70 antibodies (HOCl vs PBS, arbitrary units: $0.21 \pm 1.30 \times 10^{-2}$ vs 1.50×10^{-2}). BLM-MP animals vs PBS controls: 1) BLM-MP mice minimal weight was documented at day 15 (BLM-MP vs PBS, % change in body weight: -7.70 ± 1.37 vs 6.77 ± 0.50) and gradually recovered until D28. 2) Distal to the site of injection, dermal thickness (μm) was increased in BLM animals (BLM-MP vs PBS: 685.80 ± 32.97 vs 465.10 ± 64.00). 3) BLM-MP mice lung histology showed thickening of the alveolar septa with chronic inflammation and collagen deposition. In these mice, lung compliance was reduced (BLM-MP vs PBS, ml/cmH₂O: $3.50 \times 10^{-2} \pm 2.00 \times 10^{-3}$ vs $6.40 \times 10^{-2} \pm 2.00 \times 10^{-3}$), and micro-CT scans showed increased lung density (BLM-MP vs PBS, Hounsfield units: -331.70 ± 13.31 vs -445.40 ± 24.30).

Conclusion: In contrast to the HOCl-SSc treated mice, the BLM-MP recapitulates key features of human SSc-ILD. Prolonged systemic administration of BLM impaired lung mechanics, increased lung density on micro-CT and induced chronic interstitial inflammation with scattered

fibroblastic foci. The BLM-MP treated mice and the readouts reported are relevant for the pre-clinical assessment of novel anti-fibrotic drugs.

Résumé

Contexte : La sclérose systémique (ScS ; sclérodermie) est une maladie auto-immune caractérisée par une synthèse excessive de collagène par les fibroblastes, des anomalies vasculaires et une activation du système immunitaire, aboutissant à une fibrose de la peau et des organes internes. La pneumopathie interstitielle (PI ; fibrose pulmonaire) est une complication fréquente de la ScS et l'une de ses principales causes de décès. Les traitements actuels sont d'une efficacité limitée. Pour tester de nouveaux anti-fibrosants, il est nécessaire de disposer de modèles animaux fiables qui ressemblent étroitement à la ScS-ILD humaine. Deux modèles de souris sont privilégiés dans la littérature: l'administration intradermique répétée d'acide hypochloreux [(HOCl)-ScS] et l'administration sous-cutanée de bléomycine par minipompe osmotique [(BLM-MP)]. Ces deux modèles induiraient une fibrose de la peau et des poumons. Le modèle HOCl présente des auto-anticorps anti-topoisomérase 1 (anti-Scl-70) et des taux élevés de produits protéiques d'oxydation avancée (AOPP) dans le sérum. Nous avons effectué une caractérisation approfondie axée sur l'atteinte pulmonaire en comparant ces modèles.

Méthodes : Modèle HOCl: Des souris BALB/c femelles âgées de 6 semaines ont été traitées par des injections intradermiques quotidiennes de HOCl pendant 6 semaines. Fin de l'expérience: 42 jours (J).

Modèle BLM-MP: Des souris C57BL/6 mâles âgées de 10 semaines ont été implantées par voie sous-cutanée avec des minipompes osmotiques contenant du BLM (60mg/kg) ou une solution saline tamponnée au phosphate (PBS) délivrée en continu pendant 7 jours. Fin de l'expérience: 4 semaines

Expérimentations: 1) poids corporel; 2) pli cutané (caliper) et épaisseur dermique (histologie); 3) histologie et conformité pulmonaire (flexiVent™); 4) expression de l'ARNm des marqueurs

profibrotiques dans le poumon; 5) taux sériques d'AOPP et d'anti-Scl-70; 6) radiodensité pulmonaire et pourcentage du tissu mal aéré (tomographie par micro-ordinateur in vivo).

Résultats: Souris traitées au HOCl par rapport aux souris contrôles avec PBS : 1) Au fil du temps, il n'y avait aucune différence de poids corporel entre les groupes. 2) Dans la zone injectée au J42, l'épaisseur du pli cutané (mm) était deux fois plus important (HOCl vs PBS, moyenne \pm SEM: $1,37 \pm 0,06$ vs $0,66 \pm 0,04$) et l'épaisseur du derme (μm) trois fois plus importante dans le groupe HOCl (HOCl vs PBS : $639,90 \pm 50,98$ vs $206,40 \pm 18,97$). 3) Le traitement au HOCl n'a pas entraîné de caractéristiques histologiques de fibrose pulmonaire ni de changements significatifs de la conformité pulmonaire (HOCl vs PBS, $\text{ml}/\text{cmH}_2\text{O}/\text{g}$: $3,00 \times 10^{-3} \pm 4,61 \times 10^{-5}$ vs $3,50 \times 10^{-3} \pm 9,32 \times 10^{-5}$). L'analyse d'image automatisée de la coloration au rouge Picrosirius (PSR) des poumons des souris HOCl n'a pas montré une augmentation du dépôt de collagène (HOCl vs PBS, pixels PSR positifs/ mm^2 : $2\,064\,449 \pm 159\,647$ vs $2\,224\,378 \pm 152\,187$). 4) Les injections de HOCl n'ont pas augmenté l'expression de l'ARNm pulmonaire de ACTA2 (α -actine de muscle lisse) (HOCl vs PBS, pli par rapport au contrôle : $1,27 \pm 0,30$ vs $1,00 \pm 0,38$). 5) Le traitement par HOCl n'a pas induit la production d'AOPP (HOCl vs PBS, $\mu\text{mol}/\text{L}$ d'équivalents chloramine-T : $40,12 \pm 10,87$ vs $47,21 \pm 11,62$) ou d'anticorps anti-Scl-70 (HOCl vs PBS, unités arbitraires : $0,21 \pm 1,30 \times 10^{-2}$ vs $1,50 \times 10^{-2}$). Animaux BLM-MP par rapport aux contrôles PBS : 1) Le poids minimal des souris BLM-MP a été observé au jour 15 (BLM-MP vs PBS, % de variation du poids corporel: $-7,70 \pm 1,37$ vs $6,77 \pm 0,50$) et s'est progressivement rétabli jusqu'au J28. 2) Distalement au site d'injection, l'épaisseur du derme (μm) a augmenté chez les animaux BLM (BLM-MP vs PBS : $685,80 \pm 32,97$ vs $465,10 \pm 64,00$). 3) L'histologie pulmonaire des souris BLM-MP a montré un épaissement des septums alvéolaires avec une inflammation chronique et un dépôt de collagène. Dans ce modèle, la conformité pulmonaire était réduite (BLM-MP vs PBS, $\text{ml}/\text{cmH}_2\text{O}$: $3,50 \times 10^{-3}$

$2 \pm 2,00 \times 10^{-3}$ vs $6,40 \times 10^{-2} \pm 2,00 \times 10^{-3}$), et les scans micro-CT ont montré une augmentation de la densité pulmonaire (BLM-MP vs PBS, unités Hounsfield : $-331,70 \pm 13,31$ vs $-445,40 \pm 24,30$).

Conclusion : Contrairement au modèle HOCl-ScS, le modèle BLM-MP récapitule les principales caractéristiques de la ScS-PI humaine. L'administration systémique prolongée de BLM altère la mécanique pulmonaire, augmente la densité pulmonaire sur la micro-TDM et induit une inflammation interstitielle chronique avec des foyers fibroblastiques dispersés. Le modèle BLM-MP et les résultats rapportés sont pertinents pour l'évaluation préclinique de nouveaux médicaments anti-fibrotiques.

Acknowledgements

First, I want to thank my primary supervisor Dr. Inés Colmegna for her continued mentorship and providing me the opportunity to be a part of two laboratories. None of this work would have been possible without your guidance. Dr Colmegna has taught me about research, high standards and forced me to do my best work – and did so with considerable patience, support, and encouragement. The resilience that I have learned from my time in the Colmegna laboratory is a skill like no other.

I would also like to express my deepest gratitude to my co-supervisor Dr. James Martin for his teachings, both in life and in research. Despite his breath of knowledge across a wide range of subjects, he remains a student of life with his love of learning and native curiosity that inspires others. Dr Martin, your kind and understanding qualities are unmatched. I truly appreciate your genuine nature, willingness to help and sense of humour, all of which have kept me afloat. You have helped me develop my critical thinking skills and overall confidence. It has been a privilege working with such a dedicated researcher, inspiring teacher, and wonderful friend.

I am also grateful to my laboratory members. Utako Fujii has been extremely patient in providing mouse and flow cytometry training and answering my questions. I thank Kosuke Makita and Rui Sun for their remarkable moral support, thoughtful assistance, insights, and training me with histology and qPCR techniques. Toby McGovern has introduced me to the concepts of image analysis. Erwan Pernet and Julia Chronopoulos advised on immunophenotyping macrophage subsets. Ketsia Lola spent a substantial amount of time completing the HOCl lung image analysis. I thank Sydney Joy, Alice Pan, and Sadie Wang for their help with performing BAL cell counts,

staining skin histology slides, and performing dermal thickness measurements. Dr. Maximilien Lora has trained me in cell culture techniques. Most importantly, I am thankful to all members of the Martin and Colmegna labs for their friendships and continuous support.

I would like thank members of the Small Animal Imaging Labs (SAIL) at the RI-MUHC. Antonio Aliaga, a research assistant, performed all micro-CT scans and Guoming Xiong, PET/SPECT specialist, analyzed all the acquired scans and was patient in explaining how the analysis was conducted.

I would like to thank my academic advisor Dr. Ilan Azuelos and committee members Dr Marie Hudson, Dr. Carolyn Baglole, and Dr Elizabeth Fixman for providing their time, thoughts, and intellectual inputs on my project.

Many thanks go to Dr. Richard Fraser for providing his expertise in pulmonary pathology and Dr. Kevin Watters for his insights and assessment of skin biopsies.

I would like to acknowledge the people in the Experimental Medicine departments, from the graduate program director Dr. Anne-Marie Lauzon to the administrative staff, Marylin Lihares, Katrine Couvrette and Sandra Morrison. They have helped me every step of the way since I joined the program, their doors were always open to students and they offered all the assistance we needed to navigate through our graduate school experience.

I also extend, with great gratitude, a large thank you to the administrative coordinators of Meakins-Christie Laboratories Séverine Audusseau, Maria Makroyanni and Jacqueline Brown, and program managers Inga Murawski and Linda Karpowicz. They have helped countless times in addressing questions pertaining to training at the Meakins.

I sincerely thank my former supervisor Dr. Mark Darling and my undergraduate thesis course coordinator Dr. Zia Khan for their continued encouragement and support from day one of this journey. Dr Darling, thank you for all the chats and for reviewing histology slides at a moment's notice. Dr Khan, thank you for your honesty, your thought-provoking suggestions, and for your thorough responses to my seemingly endless questions pertaining to science and life. Thank you both for believing in me when I needed it most.

A special thank you to my parents for their unconditional love and unwavering support throughout my entire education. Thank you to my little sister for being such a bundle of joy and always managing to cheer me up. And finally, thank you to my brother for all the discussions, always having my back, his tremendous understanding, and for always making me laugh.

Contribution of Authors

All experiments presented in this thesis were performed and analyzed by Arina Morozan under the supervision of Drs. James Martin and Ines Colmegna except:

- (1) Positive Picrosirius Red Image analysis of HOC1-injected mouse lungs. Ketsia Lola, a summer research student in Dr Martin's laboratory performed the remaining analysis.
- (2) Processing, embedding, and sectioning of mouse skin biopsies was performed by the Histopathology Platform at the Research Institute of the McGill University Health Centre (RI-MUHC).
- (3) The following readouts from BLM and $Nrf2^{-/-}$ experiments: Picrosirius red (PSR) and hematoxylin and eosin (H&E) staining of skin histology slides, BAL cell counts, and dermal thickness were performed by Alice Pan, Sydney Joy, and Sadie Wang (undergraduate students in Dr Martin's laboratory).
- (4) Micro-CT imaging and analysis were performed by Antonio Aliaga (research assistant at the Small Animal Imaging Labs, SAIL) and Gouming Xiong (PET/SPECT specialist at SAIL), respectively.

Table of Contents

Abstract	2
Résumé	5
Acknowledgements	8
Contribution of Authors	11
Abbreviations	18
Chapter 1: Introduction	23
Section 1: Interstitial Lung Disease (ILD)	
1.1 Definition and etiology	23
1.2 Systemic Sclerosis (SSc)	24
1.3 Systemic sclerosis associated interstitial lung disease (SSc-ILD)	
1.3.1 Epidemiology, diagnosis, and risk factors	25
1.3.2 Diagnosis of SSc-ILD	26
1.3.3 Treatment options	27
Section 2: Animal Models of SSc	
2.1 Spontaneous Mutations	
2.1.1 Tight skin 1 mouse.....	33
2.1.2 Tight skin 2 mouse.....	34
2.1.3 Chicken (UCD-200).....	34
2.2 Transgenic mouse models	
2.2.1 Fos-related antigen 2 (Fra-2)	35
2.2.2 Friend leukemia integration factor -1 (Fli-1 ^{+/-})/Kruppel-like factor 5 (KLF5 ^{+/-}).36	
2.2.3 TGF- β 1 receptor I (TGF β -R1) gain-of-function mouse	36

2.2.4 Other emerging models.....	37
2.3 Knockout models	
2.3.1 Caveolin-1 knockout (Cav-1 ^{-/-}) mouse	38
2.3.2 Urokinase-plasminogen activator receptor knockout (uPAR ^{-/-}) mouse.....	39
2.4 Inducible models	
2.4.1 Hypochlorous acid (HOCl)- induced mouse model of SSc.....	40
2.4.1.1 Experimental protocol	40
2.4.1.2 Putative mechanisms of HOCl-induced SSc	41
2.4.1.3 HOCl-induced SSc-like phenotype in BALB/c mice	41
2.4.1.4 HOCl-induced SSc-like phenotype in Nrf2 ^{-/-} mice.....	42
2.4.2 Bleomycin (BLM) – induced mouse model	43
2.4.2.1 BLM source and clinical use.....	43
2.4.2.2 Mechanisms of BLM-induced lung fibrosis	42
2.4.2.3 Different routes BLM administration and its associated phenotypes ..	45
Chapter 2: Methods	47
2.1 Animals.....	47
2.2 Animal Models.....	48
2.2.1 Hypochlorous acid (HOCl)-Induced Systemic Sclerosis (HOCl-SSc) mouse model	
2.2.1.1 Overview of protocol	48
2.2.1.2 Preparation of HOCl solution	49
2.2.1.3 Intradermal injections	49
2.2.1.4 Skin thickness	50

2.2.2 SSc-ILD mouse model by osmotic minipump delivered bleomycin (BLM-MP)	
2.2.2.1 Overview of protocol	51
2.2.2.2 Bleomycin dose.....	52
2.3 Experimental techniques	
2.3.1 Measurement of respiratory mouse mechanics	52
2.3.2 Calculation of respiratory mechanical parameters	
2.3.2.1 Measurement of P-V curve	54
2.3.2.2 Measurement of respiratory system resistance and elastance.....	54
2.3.3 Micro-computed tomography (CT)	
2.3.3.1 Image acquisition	54
2.3.3.2 Image analysis - quantification	55
2.3.4 Bronchoalveolar lavage (BAL) fluid analysis	56
2.3.5 Lung and skin histology	
2.3.5.1 Tissue collection	56
2.3.5.2 Hematoxylin and eosin (H&E) staining	57
2.3.5.3 Masson’s Trichrome (MT) staining	57
2.3.5.4 Picrosirius Red (PSR) staining and analysis	58
2.3.6 Dermal thickness quantification	58
2.3.7 Advanced oxidation protein products (AOPPs)	58
2.3.8 Anti-topoisomerase I (Scl-70) antibodies (ELISA).....	59
2.3.9 Lung hydroxyproline assay	59
2.3.10 Lung mRNA expression of pro-fibrotic markers	
2.3.10.1 RNA isolation	60

2.3.10.2 Reverse Transcription and Real-Time quantitative <i>PCR</i>	60
2.3.11 Lung immune cell repertoires	61
2.3.12 Statistical analyses	63
Chapter 3: Results	64
3.1 HOCl-SSc model using BALB/c mice	
3.1.1 Effect of intradermal HOCl injections on body weight	64
3.1.2 Skin changes	64
3.1.3 Effect of HOCl injections on lung function and histology	66
3.1.4 Effect of HOCl injections on BAL leukocytes and macrophage phenotype	70
3.1.5 AOPPs and anti-Scl70 antibodies	73
3.2 HOCl-SSc model using <i>Nrf2</i> ^{-/-} mice	
3.2.1 Effect of intradermal HOCl injections on <i>Nrf2</i> ^{-/-} mice body weight	74
3.2.2 Skin changes in <i>Nrf2</i> ^{-/-} mice following HOCl injections.....	75
3.2.3 Effect of HOCl injections on <i>Nrf2</i> ^{-/-} mice lung function and histology.....	76
3.2.4 The effect of HOCl injections on <i>Nrf2</i> ^{-/-} mice BAL leukocytes	78
3.3 BLM-MP model	
3.3.1 Effect of different BLM doses on body weight and lung function	79
3.3.2 Skin changes following systemic administration of BLM.....	81
3.3.3 Lung function, histology, and micro-CT following BLM administration	83
Chapter 4: Discussion	89
References	98
Figures	
Figure 1. HOCl-SSc mouse model.....	48

Figure 2. Experimental readouts assessed in the HOCl-SSc model.	49
Figure 3. Validation of intradermal injections using blue food colorant.	50
Figure 4. A graphic representation showing the 3 areas on the mouse where skin thickness measurements were obtained.	50
Figure 5. Experimental readouts in the BLM-MP model.	51
Figure 6. Experimental timeline for the generation of the BLM-MP mouse model. ...	52
Figure 7. Intradermal HOCl injections did not affect BALB/c mice body weight.	64
Figure 8. HOCl injections induce local skin fibrosis with spatial heterogeneity.....	65
Figure 9. Intradermal HOCl injections (6 weeks) did not impair lung function or induce lung fibrosis.....	67
Figure 10. Intradermal HOCl injections (8 weeks) do not impair lung function or induce lung fibrosis.....	69
Figure 11. Representative flow cytometry gating strategy adapted from Pernet et al. 2019.....	71
Figure 12. HOCl injections did not induce lung inflammation.....	72
Figure 13. Intradermal HOCl injections neither induced the production of AOPPs nor anti-Scl 70 antibodies.....	73
Figure 14. 6 weeks of intradermal injections do not affect the body weight of C57BL/6 nor Nrf2 ^{-/-} mice.	74
Figure 15. HOCl injections induce comparable skin fibrosis in Nrf2 ^{-/-} and WT control animals.	75
Figure 16. HOCl injections neither impaired lung function nor induced lung fibrosis in Nrf2 ^{-/-} mice.	76, 77

Figure 17. HOCl treatment did not induce lung inflammation in Nrf2^{-/-} mice.79

Figure 18. Time course of percent body weight change following exposure to different bleomycin doses or saline treatment.80

Figure 19. Dose dependent decline in lung function associated with increasing BLM doses.....80

Figure 20. Systemic administration of bleomycin via minipump leads to skin fibrosis.....82

Figure 21. 28 days post pump implantation BLM impairs lung mechanics as it generates interstitial inflammation with few fibroblastic foci.84

Figure 22. Osmotic minipump delivery of BLM increases lung density and the percent of poorly aerated tissue.85

Figure 23. 14 days post pump implantation BLM impairs lung mechanics in the absence of evident fibrosis.86

Figure 24. 38 days post pump implantation lung function in BLM-MP mice improved while histological changes were similar to day 28.....87

Tables

Table 1. Classification of interstitial lung diseases based on underlying etiology.24

Table 2. Summary describing the protocols used to generate the HOCl mouse model of SSc among different papers.40

Table 3. Description of maneuvers / outcomes composing the mouse mechanics scan sequence. Adapted from references.53

Table 4. Primer sequences used for RT-qPCR.....61

Table 5. Flow cytometry antibodies.62

Abbreviations

Activator protein -1	AP-1
Advanced oxidation protein products	AOPPs
Alpha-smooth muscle actin	α -SMA
Anti-topoisomerase 1 autoantibodies	anti-Sc170
Antioxidant response element	ARE
Autologous hematopoietic stem cell transplantation	AHSCT
Bleomycin	BLM
Bronchoalveolar lavage fluid	BALF
Caveolin-1	Cav-1
Chemokine receptor 2	CCR2
Collagen type I, alpha I	Col1a1
Collagen type I, alpha II	Col1a2
Collagen type III, alpha I	Col3a1
Connective tissue growth factor	CTGF
Cyclic adenosine monophosphate	cAMP
Diffusion capacity of the lungs for carbon monoxide	D _L CO
Enzyme-linked immunosorbent assay	ELISA
European Scleroderma Trials and Research	EUSTAR

Fibrillin-1	FBN1
Fibroblast growth factor	FGF
Fibronectin	FN
Forced vital capacity	FVC
Fos-related antigen 2	Fra-2
Friend leukemia integration factor -1	Fli-1
Graft versus host disease	GVHD
Ground glass opacity	GGO
Hematopoietic stem cell transplantation	HSCT
Hematoxylin and eosin	H&E
High resolution computed tomography	HRCT
Hounsfield units	HU
Hypochlorous acid	HOCl
Hypochlorous acid -induced Systemic Sclerosis mouse model	HOCl-SSc
Idiopathic pulmonary fibrosis	IPF
Interleukin 1 Beta	IL-1 β
Interleukin 6	IL-6
Interstitial Lung Disease	ILD
Interstitial macrophages	IM

Kelch-like ECH-associated protein 1	Keap1
Keratinocyte growth factor	KGF
Kruppel-like factor 5	KLF5
Latent Transforming growth factor- β -binding proteins	LTBPs
Masson's Trichrome	MT
Mesenchymal stromal cells	MSCs
Monocyte derived alveolar macrophages	Mo-AMs
Musculoaponeurotic fibrosarcoma	MAF
Non-specific interstitial pneumonia	NSIP
Nuclear factor erythroid 2- related factor 2	Nrf2
Peptidylpropyl isomerase A	PPIA
Peripheral blood mononuclear cells	PBMCs
Phosphate-buffered saline	PBS
Phosphodiesterase	PDE
Picrosirius Red	PSR
Platelet derived growth factor	PDGF
Positive end expiratory pressure	PEEP
Potassium dihydrogen phosphate	KH ₂ PO ₄
Pressure – Volume	P-V

Pulmonary arterial hypertension	PAH
Pulmonary function tests	PFTs
Reactive oxygen species	ROS
Red blood cells	RBCs
Reverse transcription quantitative real time polymerase chain reaction	RT-qPCR
Safety and Efficacy of Nintedanib in Systemic Sclerosis	SENSCIS
Scleroderma Lung Study I	SLS I
Scleroderma Lung study II	SLS II
Single frequency oscillation technique	SFOT
Small Animal Imaging Labs	SAIL
Static compliance	C _{st}
Systemic sclerosis associated interstitial lung disease	SSc-ILD
SSc-ILD mouse model induced by osmotic minipump delivered BLM	BLM-MP
Systemic Sclerosis; Scleroderma	SSc
Tight skin 1	Tsk1
Tight skin 2	Tsk2
Tissue resident alveolar macrophages	TR-AM
Total respiratory system elastance	E _{rs}
Total respiratory system resistance	R _{rs}
Transforming growth factor – Beta	TGF-β

Transforming growth factor – beta receptor type I	TGFβ-RI
Transforming growth factor – beta receptor type II	TGFβ-RII
Tumour Necrosis Factor alpha	TNF-α
University of California at Davis line 200	UCD-200
Urokinase-plasminogen activator receptor	uPAR
Urokinase-type plasminogen activator	uPA
Usual interstitial pneumonia	UIP
Vascular endothelial growth factor	VEGF
Von Willebrand Factor	vWF
Wild-type	WT

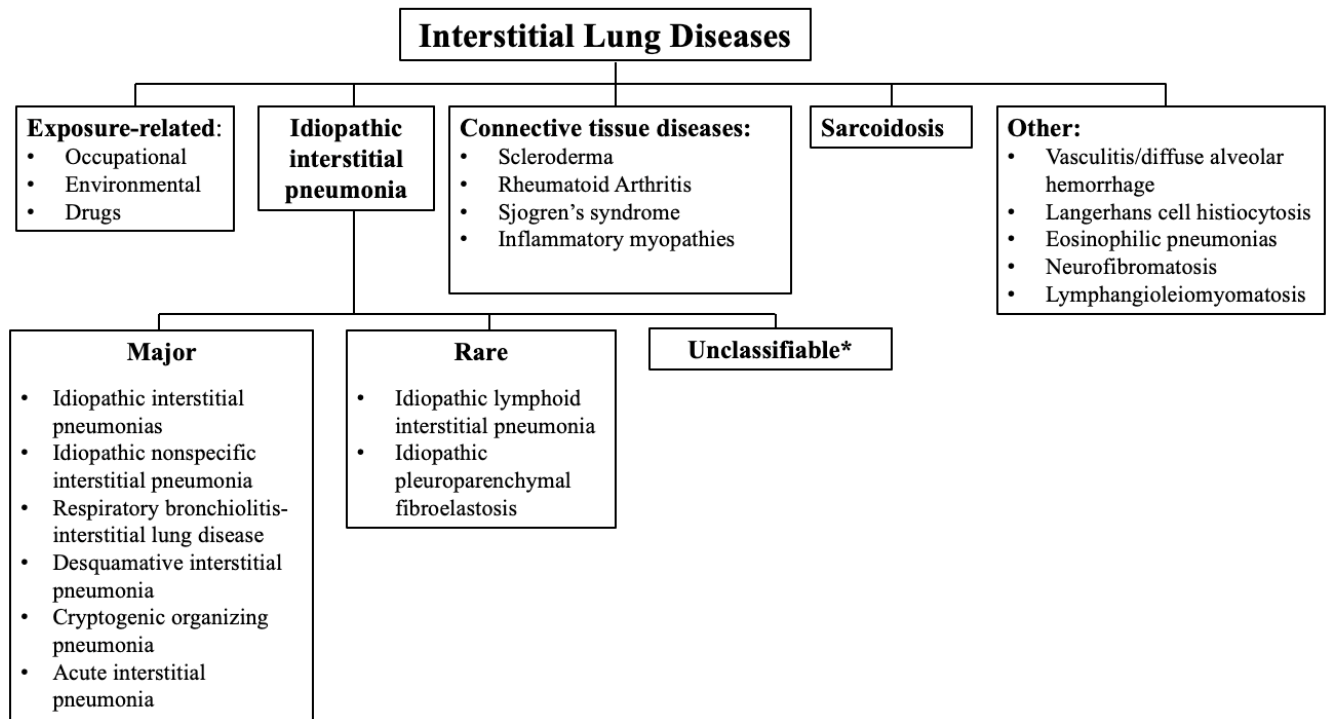
Chapter 1: Introduction

Section 1: Interstitial Lung Disease

1.1 Definition and etiology

Interstitial lung disease (ILD), describes over 200 different lung disorders characterized by varying degrees of inflammation and fibrosis affecting the lung parenchyma¹. In normal lung tissue, very few cells reside in the interstitium, the space between the alveolar epithelial cells and the vascular endothelial cells. The presence of inflammatory cells and fibrotic mediators in the interstitial space reduces alveolar function by altering their distensibility, creating ventilation to perfusion inequalities and overall lung stiffness. Lung fibrosis increases the respiratory effort and clinically manifests as progressive dyspnea, cough, and reduced exercise tolerance with impaired quality of life. ILDs can be caused by certain drugs, autoimmune diseases, and exposure to hazardous agents (Table 1)². However, in approximately 50% of cases of ILD the condition is idiopathic². Idiopathic pulmonary fibrosis (IPF) is characterized by progressive fibrosis with decline in lung function, worsening dyspnea, and early mortality³. In addition to IPF, 13-40% of ILD patients suffering from associated conditions develop a progressive fibrosis phenotype⁴. Of all ILDs, Systemic Sclerosis (SSc)- ILD is one of the types most likely to evolve into a progressive fibrosing phenotype¹.

Table 1. Classification of interstitial lung diseases based on underlying etiology^{5,6}.



Footnotes: *causes of unclassifiable idiopathic interstitial pneumonia include (1) inadequate clinical, radiologic, or pathologic data and (2) discordance between clinical, radiologic, and pathologic findings⁷.

1.2 Systemic Sclerosis

Systemic Sclerosis (SSc), or scleroderma, is a rare autoimmune rheumatic disease characterized by excessive collagen deposition in the skin and in internal organs with associated vasculopathy and autoantibody production. In the most recent study, the reported prevalence (number of affected individuals) and incidence (number of newly diagnosed cases) of SSc was 17.6% and 1.4% per 100,000 persons, respectively⁸. Endothelial cell activation and vascular injury are the earliest manifestations in SSc and were proposed to be the initiating events in the pathogenesis of the

disease⁹. The precise cause triggering vascular damage and associated immune response is not known^{9,10}. Several potential causes have been proposed including viruses, drugs, environmental and occupational exposure to organic solvent, vinyl chloride, and silica^{9,10}. SSc can occur at any age but the onset in most patients is between the ages of 30 and 50 years. Among all connective tissue diseases SSc is the one with strongest female predominance (7:1 female/male ratio)¹¹. Moreover, compared to other rheumatic diseases SSc is associated with poorer patient outcomes and lower quality of life¹². In a Norwegian cohort, factors associated with a worse SSc outcome included male sex, pulmonary hypertension, ILD, and diffuse cutaneous involvement (skin involvement proximal to the elbows and knees)¹³. ILD remains a leading cause of mortality in SSc¹⁴ accounting for 18% of all deaths¹⁵. As such, this dissertation will focus specifically on SSc-ILD.

1.3 Systemic Sclerosis associated Interstitial Lung Disease (SSc-ILD)

1.3.1 Epidemiology, diagnosis and risk factors

ILD is exceptionally common among patients with SSc and is associated with significant morbidity and mortality¹⁶. Reported prevalence rates vary widely depending on geographic location and method of detection¹⁷. In the Canadian Scleroderma Research Group registry, 65% of patients had evidence of ILD on high resolution computed tomography (HRCT), while 26% had ILD based on the presence of basilar velcro-like crackles on auscultation and 22% had ILD based on chest x-ray¹⁷. Lung involvement can range from subclinical disease to respiratory failure and death¹⁶. Diagnosis of ILD in the initial stages is a challenge as patients may be asymptomatic and often present with exertional dyspnea and dry cough, both of which are nonspecific symptoms¹⁴. As such, it is recommended that all patients suspected or known to have SSc undergo screening for ILD¹⁸. HRCT is regarded as the most sensitive and specific diagnostic modality and is suggested

to be performed in all patients at the time of diagnosis¹⁶. Pulmonary function tests (PFTs) are also routinely used in initial evaluations to assess the severity of lung involvement. Earlier reports have found 40-70% of SSc patients have PFT abnormalities^{19,20}. Recognition of risk factors associated with progressive ILD such as male sex, Afro-Caribbean ethnicity, diffuse cutaneous SSc, higher skin scores and the presence of anti-topoisomerase antibodies permits risk stratification and improved patient care²¹. Ultimately successful assessment and management of lung involvement in patients with SSc requires a high index of suspicion given the non-specific symptoms associated with respiratory manifestations and the use of a variety of diagnostic tools including HRCT, PFTs, and lung biopsy when necessary.

1.3.2 Diagnosis of SSc-ILD

SSc-ILD can be diagnosed based on lung function abnormalities, radiologic features on HRCT, and histologic patterns on lung biopsy. Non-specific interstitial pneumonia (NSIP) and usual interstitial pneumonia (UIP) are terms used to describe the histologic and radiologic patterns of ILD. In SSc patients, NSIP is the most frequently observed pattern on CT, although a UIP pattern can be seen in 36% of patients²². The NSIP pattern on CT manifests as ground glass opacities (GGO, refers to regions of increased opacity of the lung with preservation of bronchial and vascular margins²³), traction bronchiectasis, and reticulations (linear densities due to interlobular and/or intralobular septal thickening²³)²². This pattern tends to have a peripheral distribution with lower lung predominance²². In UIP, CT findings include reticular opacities and honeycomb cysts (cystic airspaces with thick fibrous walls²³) with or without traction bronchiectasis². Histologically, NSIP can be characterized by a pattern of temporally uniform lung damage with varying degrees of chronic inflammation or fibrosis²³ and can be categorized into two subtypes – cellular and fibrotic²². The majority of SSc cases can be classified within the fibrotic subtype of

NSIP, which shows fibrosis with minimal inflammation^{22,24}. In agreement with the assessment of forms of lung involvement by HRCT, the NSIP histologic pattern is more prevalent than UIP^{22,24}. Histologic sections of UIP demonstrate areas of interstitial inflammation, established fibrosis and honeycombing with intervening normal lung tissue^{23,25}. Although a lung biopsy is rarely indicated to diagnose ILD in SSc patients, it can be useful if there are inconsistencies between clinical and radiologic findings²⁶. In addition to HRCT, PFTs are also useful to diagnose, stage disease severity and monitor progression. PFTs in SSc-ILD show restrictive lung function with decreased forced vital capacity (FVC) and diffusing capacity of the lungs for carbon monoxide (D_LCO) (Table 1)¹⁴. However, it is important to note that patients with early ILD can have preserved lung volumes despite an abnormal HRCT and reduced D_LCO ¹⁴. Therefore, early detection can provide the opportunity for early therapeutic intervention.

1.3.3 Treatment Options

There is no curative treatment for SSc-ILD. However, a number of immunosuppressive and anti-fibrotic agents have been proposed for improving or slowing the rate of ILD progression.

Immunosuppressive therapies

There are several immunosuppressive drugs available for SSc-ILD but few robust clinical trial data to inform the selection of a specific agent or the best timing for treatment. One of the drugs with more supporting evidence is cyclophosphamide, an alkylating agent which inhibits DNA synthesis and prevents cell division by cross linking strands of DNA^{26,27}. The Scleroderma Lung Study I (SLS I), a large multicenter randomized controlled trial of oral cyclophosphamide versus placebo, first showed the effectiveness of cyclophosphamide in SSc-ILD²⁸. After 12 months of treatment, compared to placebo, patients on cyclophosphamide had a smaller decline of FVC (1% vs 2.53% predicted, $p < 0.03$); however, there was no difference in FVC 24 months after treatment²⁸.

This suggested that maintenance therapy might be necessary to maintain the benefit of cyclophosphamide therapy, but its long-term use may be limited by its oncogenic risk²⁸. In the second scleroderma lung study (SLS II) patients were randomized to receive cyclophosphamide for 1 year or mycophenolate mofetil for two years²⁹. After two years, both groups showed improvement in FVC % predicted (2.9% with cyclophosphamide and 2.2% with mycophenolate mofetil) but cyclophosphamide was associated with more toxicity and a higher incidence of adverse events than mycophenolate mofetil²⁹. Azathioprine, a purine synthesis inhibitor and immunosuppressant was also used for the treatment of SSc-ILD. Few studies showed promise of azathioprine in patients with progressive respiratory decline as first-line therapy³⁰ or while taking cyclophosphamide³¹. Based on evidence that mycophenolate mofetil is better tolerated than cyclophosphamide, the use of mycophenolate mofetil was recommended as first line treatment for SSc-ILD³². For severe or progressive disease, cyclophosphamide followed by mycophenolate mofetil or azathioprine is recommended³². For refractory cases, the use of cyclophosphamide, biological therapies and hematopoietic stem cell transplantation (HSCT) has been suggested.

Biological therapies

Owing to the possible role of B cells in scleroderma, rituximab, a monoclonal antibody against the CD20 surface protein has been tested. In three small open-label trials, patients treated with rituximab had stable lung function (no significant difference in FVC and DLCO at 6 months compared to baseline) and no evidence of progressive disease on HRCT³³⁻³⁵. These studies had short follow-up, small sample sizes and lacked controls which do not allow for definitive conclusions to be drawn. In attempt to address these limitations, the European Scleroderma Trials and Research (EUSTAR) study was conducted³⁶. It compared 146 SSc-ILD patients on rituximab combined with standard immunosuppressants to patients only on immunosuppressants over 2

years³⁶. Similar to the previous studies, DLCO and FVC remained stable in both groups³⁶. Rituximab was superior to cyclophosphamide in improving lung function^{37,38}. In the studies discussed above, the efficacy of rituximab treatment may have been influenced by patient differences in the extent of lung involvement and the course of ILD^{33,35-38}.

Since interleukin 6 (IL-6) seems to be a major driver of fibrosis and inflammation in SSc, its inhibition with tocilizumab was tested as a potential treatment strategy for SSc-ILD³⁹. Neves et al treated 3 patients with refractory SSc and ILD with tocilizumab and reported no progression of disease based on chest HRCT and DLCO% in two of three patients⁴⁰. More recently, two randomized controlled trials evaluating the effect of tocilizumab in early diffuse cutaneous SSc showed a smaller decline in FVC in the treatment group compared to placebo^{39,41}. In addition to these biologic therapies, antifibrotics have also been shown to slow the rate of decline in lung function.

Antifibrotics

Tissue fibrosis is one of the hallmarks of SSc and the relative lack of success of therapies focused on inflammation prompted a more direct approach with the development of antifibrotic agents. In 2014, three large randomized-controlled trials found that nintedanib and pirfenidone, two oral antifibrotics, slow the rate of FVC decline in IPF patients compared to placebo.⁴²⁻⁴⁴ This ultimately led to their approval by regulatory agencies for the treatment of IPF. Given the presumed overlap in molecular mechanisms leading to fibrosis, predisposing factors and clinical course between IPF and non IPF ILDs, pirfenidone and nintedanib were studied in SSc-ILD.⁴⁵

Nintedanib is an intracellular tyrosine kinase inhibitor, which inhibits the kinase activity of different growth factor receptors including platelet derived growth factor (PDGF), vascular endothelial growth factor (VEGF) and fibroblast growth factor (FGF)⁴⁶. Since tyrosine kinases are downstream mediators of profibrotic cytokines (e.g. TGF- β), it was suggested that blockade of these receptors, and thus downstream signalling, may slow progression of lung function decline⁴⁶. In vitro, nintedanib inhibit PDGF and TGF- β -induced proliferation of fibroblasts, myofibroblast differentiation and decreased collagen synthesis.⁴⁷ Moreover, data from animal models show that nintedanib has both anti-inflammatory and anti-fibrotic effects and this appeared to be irrespective of the method used to induce lung fibrosis⁴⁸. In the 2019 Safety and Efficacy of Nintedanib in Systemic Sclerosis (SENSCIS) trial, 576 patients with ILD affecting at least 10% of the lung on HRCT were randomly assigned to receive nintedanib twice per day or placebo for 52 weeks⁴⁹. SSc-ILD patients receiving nintedanib had a lower rate of annual FVC decline compared to placebo⁴⁹. The safety profile was similar to that observed in IPF patients with the most common side effect being diarrhea⁴⁹. Based on these data, nintedanib was approved in the US and Japan for treatment of IPF.

Pirfenidone is another antifibrotic drug approved for IPF but has yet to be approved for SSc-ILD. Although the mechanism of action of pirfenidone remains unclear, pirfenidone decreases fibroblast proliferation and expression of fibrosis-associated proteins (α -SMA, Col1)⁵⁰. A case study of 5 SSc patients with progressive ILD showed pirfenidone increased vital capacity and was well-tolerated⁵¹. In a randomized phase 2 study, pirfenidone was found to be safe and simultaneous administration of mycophenolate did not lead to increased side effects.⁵² However, compared to baseline, FVC and D_LCO at week 16 remained unchanged in subjects receiving only pirfenidone

and subjects receiving both pirfenidone and mycophenolate⁵². Another clinical trial (NCT03221257) is currently ongoing to evaluate the effect of combining pirfenidone with mycophenolate. SSc-ILD subjects are randomized to mycophenolate and placebo vs mycophenolate and pirfenidone with a follow up over 18 months and evaluating for changes in FVC and DLCO.

Recently BI 1015550, an oral selective inhibitor of phosphodiesterase (PDE) 4B, has emerged as a candidate drug for the treatment of IPF.⁵³ PDE 4B inhibitors exert their antifibrotic and anti-inflammatory effects by increasing cAMP levels which can antagonize profibrotic cascades.⁵³ They have been shown to inhibit fibroblast proliferation, differentiation and extracellular matrix deposition.⁵³ In a phase II clinical trial, B1015550 reduced the rate of FVC decline in IPF subjects over 12 weeks compared to placebo.⁵⁴ Although only 12 weeks long, these encouraging results justify a long-term phase 3 trial and testing in non-IPF ILDs, including SSc-ILD subjects, may become of interest.

Cellular therapies

Autologous hematopoietic stem cell transplantation (AHSCT) is proposed as a treatment option but only in some patients given its associated mortality. The goal of this therapy is to eliminate autoreactive cells and to re-establish an immune system which is self-tolerant. Three randomized controlled trials (ASSIST, ASTIS and SCOT) have compared AHSCT to intravenous cyclophosphamide in SSc patients with severe or progressive disease and demonstrated superiority of AHSCT.⁵⁵ These studies showed lower rate of disease progression and better overall survival in transplanted subjects.⁵⁵ Treatment related mortality was 0% at 12 months in the ASSIST trial, 10.1% in the ASTIS trial and 3% at 54 months in the SCOT trial, while in all 3 trials it was 0% for the cyclophosphamide group.⁵⁵ With respect to lung function, AHSCT increased FVC in both

ASSIST trial and ASTIS trial but no significant improvement was observed in the SCOT trial. It is important to note that these studies differed in the conditioning regimens, primary outcome, follow up duration and statistical methods used for analysis which limits their direct comparison. AHST associated toxicities limits its use. Consequently, SSc-ILD remains incurable and new therapeutic options are needed.

Mesenchymal stromal cells (MSCs) were explored in several autoimmune diseases, including SSc. MSCs are somatic progenitor cells that in vitro can differentiate into multiple lineages including adipocytes, chondrocytes and osteoblasts. They are cells with a high degree of heterogeneity and multiple factors affect their functional properties, including the tissue source. MSCs can be isolated from a variety of sources but those from bone marrow, adipose tissue and umbilical cord are most frequently used. The rationale for the therapeutic potential of MSCs derives from their anti-fibrotic and immunosuppressive capacities. Currently, MSCs are approved for the treatment of perianal fistulas in Crohn's disease and graft versus host disease (GVHD).⁵⁶

Animal models of lung fibrosis are important tools for investigating mechanisms involved in the pathogenesis of human diseases and assessing potential therapeutics. Although animal models that exhibit all aspects of SSc are not available, several induced as well as naturally occurring models, have been used.

Section 2: Animal models of SSc

Many animal models have been developed to study SSc. In this section, we will discuss several animal models that are more commonly used and recognized by researchers. These have been categorized into spontaneous mutations, transgenic and knockout models.

2.1 Spontaneous Mutations

Genetic mutations that spontaneously arose in the genome of mice and chickens resulted in increased extracellular matrix deposition.⁵⁷ This phenomenon provided three SSc animal models: tight skin 1 (TSK 1) mouse, tight skin 2 (Tsk 2) mouse, and University of California at Davis line 200 (UCD-200) chickens.⁵⁷ These animal models are useful to study skin fibrosis and vasculopathy but are of limited relevance as SSc is not hereditary.⁵⁷

2.1.1 Tight skin 1 mouse

Tight skin-1 disease was first discovered in 1967 in the B10.D2(58N)/Sn mouse strain.⁵⁷ This disease was primarily recognized by the presence of thickened skin and occurred spontaneously as a result of a partial in-frame duplication of the *fibrillin-1 (FBNI)* gene.^{57,58} Fibrillin is an extracellular matrix protein which assembles into microfibrils. It is in the microfibril form that fibrillin maintains both structural and regulatory roles.⁵⁹ Fibrillin microfibrils interact with other components of the ECM including latent TGF- β -binding proteins (LTBPs) and sequesters TGF- β from activation.^{59,60} The precise mechanism by which Tsk mutant microfibrils contribute to the Tsk phenotype is not known. However, it has been proposed that the instability of the larger fibrillin protein may result in uncontrolled release of TGF- β .⁶¹ Active TGF- β promotes tissue fibrosis by driving the differentiation of fibroblasts into myofibroblasts resulting in excessive collagen production.

Homozygous Tsk embryos (*Fbn1^{Tsk}*) die *in utero* within 8 days of gestation, whereas heterozygous mice (*Fbn1^{Tsk}/Fbn1⁺*) have a normal lifespan.⁵⁸ The phenotype of heterozygous mice includes fibrotic skin, visceral changes in the heart and lungs and the production of anti-FBN-1 autoantibodies.⁵⁷ Skin pathology is characterized by increased dermal and hypodermal thickening.⁵⁷ Other features include myocardial hypertrophy and increased growth of cartilage and bone.⁵⁷

Tight skin mice also develop lung pathology; however, histological changes are more reminiscent of emphysema than lung fibrosis.⁵⁷ Several other dissimilarities exist between Tsk-1 mice and SSc including the lack of vascular injury and mononuclear cell infiltration in the skin.⁵⁸

2.1.2 Tight skin 2 mouse

The tight skin 2 (Tsk-2) disease was first described in 1986 in the offspring of a 101/H mouse exposed to ethylnitrosourea, a mutagenic agent.⁵⁷ Mice carrying the Tsk2 mutation harbour a missense point mutation in the collagen type III, alpha I gene (*Col3a1*) gene on chromosomes 1.⁶² Similar to Tsk 1, the homozygous Tsk2 mice die *in utero* while heterozygous mice survive and develop cutaneous fibrosis.⁵⁷ Compared to wild type littermates, heterozygous Tsk-2 mice skin showed increased dermal thickness and loss of adipose both of which have been observed in the skin of SSc patients.⁶³ Infiltration of mononuclear cells in the dermis was also reported in these mice; however, this finding is not consistent in the literature.⁶³ Lungs of mice were normal. In addition to fibrosis, these mice develop a variety of autoantibodies to Scl70, centromere, and DNA suggesting aspects of autoimmunity in this model.⁵⁷

2.1.3 University of California at Davis line 200 (UCD-200) chickens

The UCD line 200 strain of chickens spontaneously develop a SSc-like condition.⁵⁷ The UCD-200 chicken was reported to display different clinical, histopathological, and serological phenotypes seen in SSc. However, in contrast to human SSc the phenotype in UCD 200 chickens appears to be more fulminant. An initial inflammatory stage occurs 1-2 weeks after hatching with the most prominent lesions observed in the comb (structure on top of the chicken's head).⁶⁴ Initially, edema and Raynaud's syndrome-like changes are observed and as a result combs become necrotic and are lost within 4 weeks.⁶⁴ At this time, the chickens develop characteristic histological

features of SSc including vascular occlusion and perivascular mononuclear cell infiltration.^{64,65} Fibrosis of the skin, esophagus and lungs were reported; however, vasculopathy was studied more extensively and seems to be more relevant in this model.^{66,67} Additionally, UCD-200 chickens produced a variety of antibodies including anti-endothelial cell antibodies and anti-nuclear antibodies that have been identified in SSc patients.^{64,68}

2.2 Transgenic mouse models

2.2.1 Fos-related antigen-2 (Fra-2) mouse

Fos-related antigen-2 (Fra-2) is a member of the activator protein (AP-1) family of transcription factors.⁶⁹ Fra-2 is overexpressed in the lungs and skin of SSc patients. It participates in a variety of cellular processes including cell migration, proliferation, differentiation, and apoptosis.⁶⁹ In contrast to the spontaneous mutation models, the Fra-2 overexpressing mice develop skin fibrosis in combination with vasculopathy and lung fibrosis.⁷⁰ Similar to human SSc, Fra-2 mice displayed dermal thickening, a reduction in the number of dermal capillaries, and increase in the perivascular inflammatory infiltrates.⁷¹ These abnormalities were preceded by endothelial cell apoptosis. Histological analyses of lungs from Fra-2 mice showed increased pulmonary arterial occlusion and increased wall thickness resembling pulmonary arterial hypertension.⁷⁰ This was accompanied by a pattern of lung injury analogous to NSIP, the most common form of SSc-ILD.⁷⁰ Assessment of the lung parenchyma showed thickening of alveolar septa by inflammation and fibrosis.⁷⁰ These structural changes manifest with functional impairment, characterized by reduced lung compliance.⁷² The Fra-2 mouse is a model of SSc-ILD and hypertension and can be used to delineate pathogenic mechanisms and test potential therapies.

2.2.2 Friend leukemia integration factor -1 (Fli-1^{+/-})/Kruppel-like factor 5 (KLF5^{+/-}) mouse

Kruppel-like factor 5 (Klf5) and Friend leukemia integration 1 (Fli1) are transcription factors that negatively regulate connective tissue growth factor (CTGF) and type I collagen transcription, respectively.⁷³ Human dermal fibroblasts transfected with Fli-1 had decreased mRNA expression of type 1 collagen whereas inhibition of Fli-1 using si-RNA resulted in the upregulation of type I collagen.⁷⁴ Fli1 and Klf5 were both found to be downregulated in dermal fibroblasts of SSc patients.⁷³ Since these two transcription factors suppress CTGF and type I collagen, it was hypothesized that mRNA expression of these genes will be increased in double heterozygous mice for Fli1 and Klf5 (*Klf5^{+/-}; Fli1^{+/-}*).⁷³ Compared to wild type littermate controls, the expression of *Colla1*, *Colla2*, *Col3a1*, *FN* and *Ctgf* genes was increased.⁷³ Histologically, there was thickening of the dermis with evidence of dense and irregular collagen fibers accompanied by loss of dermal appendages.⁷³ These are all features resembling SSc skin changes. In the lungs of 8-month-old mice, there was thickening of the alveolar septa caused by fibrosis and lymphocytic infiltrates, reminiscent of human NSIP.⁷³ *Klf5^{+/-}; Fli1^{+/-}* mice also produce antinuclear antibodies and develop vascular changes with stenosis of arterioles and thickened vascular walls in the skin and lung.⁷³

2.2.3 TGF- β Receptor 1 gain of function mice

Transforming growth factor-beta (TGF- β) is a pleiotropic growth factor which plays important roles in the regulation of immune responses, vascular morphogenesis, embryological development, and wound healing.⁷⁵ TGF- β 1 is the most abundant isoform and most frequently implicated in the pathogenesis of tissue fibrosis. TGF- β 1 is produced by many cell types including macrophages and fibroblasts and many cells have receptors for this isoform on their surface. The binding of active TGF- β 1 to type II serine/threonine kinase receptors (TGF β RII) results in the recruitment of type I serine/threonine kinase receptors (TGF β RI). TGF β RII transphosphorylates T β RI resulting

in its activation and initiation of downstream events that ultimately regulate the transcription of fibrotic genes. In the absence of TGF β RI, TGF β RII can bind TGF- β but the receptor does not transduce the signal.

A model was developed to selectively express constitutively active TGF β RI in skin fibroblasts of mice.⁷⁶ With progressing age, mice developed severe skin fibrosis characterized by increased dermal thickness, loss of adipose tissue, and epidermal thinning.⁷⁶ Blood vessels in the lung show smooth muscle hypertrophy which is a histological finding of PAH in SSc patients.⁷⁶ Immunohistochemical staining for von Willebrand Factor (vWF) show increased expression, suggesting that endothelial cell damage can be induced by aberrant TGF- β signalling.⁷⁶ Similarly, elevation of vWF was reported in the serum of SSc patients.⁷⁶ While this model reflects skin and vascular changes of SSc, there is no evidence of lung fibrosis or an autoimmune component.⁷⁶

2.2.4 Other emerging models

Recently, several additional models have emerged for the study of SSc. Mice that are haploinsufficient for A20 (A20^{+/-}), an ubiquitin-editing enzyme, were generated and were shown to develop greater fibrotic responses when treated with BLM compared to controls⁷⁷. A20^{+/-} mice showed increased dermal thickness, *Colla1* and *Colla2* mRNA expression, and number of α SMA+ myofibroblasts in the dermis⁷⁷. BLM induced exaggerated lung pathology in A20^{+/-} mice with an increased fibrotic score and collagen accumulation and more pronounced architectural distortion⁷⁷. Another animal model of SSc has been developed by injecting immunodeficient mice with peripheral blood mononuclear cells (PBMCs) derived from patients with SSc⁷⁸. Compared to immunodeficient mice that were injected with PBMCs from healthy controls, mice injected with SSc PBMCs showed increased dermal thickness, inflammation, and vasculopathy in the skin⁷⁸. In

the lungs, fibrosis, inflammatory, and vasculopathy scores were also increased in mice injected with SSc PBMCs⁷⁸. A similar model has been explored that consisted of immunodeficient mice injected with PBMCs from SSc patients that were depleted of B and T cells⁷⁹. However, this latter model study was employed to emphasize the importance of B and T cells in the development of an inflammatory response in the lungs and production of autoantibodies⁷⁹.

2.3 Knockout Models

2.3.1 Caveolin-1 knockout (Cav1^{-/-})

Another strategy to sustain TGF- β signalling is through homozygous deletion of caveolin-1 (Cav1^{-/-}). Caveolin-1 protein, encoded by the Cav1 gene, mediates lipid raft internalization which regulates the degradation of TGF- β receptors among other signalling pathways. Two endocytic pathways have been reported to independently mediate the internalization of TGF- β receptors: clathrin-mediated endocytosis and caveolin-mediated endocytosis.⁸⁰ Caveolin-mediated endocytosis is required for receptor degradation whereas clathrin-dependent internalization promotes TGF- β signalling.⁸⁰ Cav1^{-/-} mice develop vascular and fibrotic features including skin fibrosis⁸¹, lung fibrosis^{81,82}, cardiomyopathy⁸³, and pulmonary hypertension⁸³. Mice showed increased dermal thickness caused by accumulation of collagen.⁸¹ Lung histology show thickened alveolar septa consisting of inflammatory infiltrates and extracellular fibrillar deposits.⁸² Marked hypertrophy of type II alveolar cells is also observed.⁸² Compared to wild type littermates, pulmonary artery pressure is 90% higher in Cav1^{-/-} mice indicating hypertension.⁸³ This, in turn, causes right ventricular hypertrophy.⁸³ Elevated systemic levels of nitric oxide are thought to contribute to the observed cardiac phenotype.⁸³ This model also supports the idea that constitutive activation of TGF- β signalling is a key step in the development of tissue fibrosis; however, is not sufficient to explain the vascular and autoimmune components of SSc.

2.3.2 Urokinase-plasminogen activator receptor knockout (uPAR^{-/-}) mouse

The urokinase-type plasminogen activator receptor (uPAR)- deficient mouse recapitulates the vascular and fibrotic features of SSc. uPAR is an important component of the fibrinolytic system and plays a key role in angiogenesis and extracellular matrix remodelling.⁸⁴ The receptor is primarily expressed by monocytes/macrophages, fibroblasts, endothelial and smooth muscle cells.⁸⁴ Urokinase-type plasminogen activator (uPA) binds to its receptor uPAR and cleaves plasminogen to yield active plasmin which promotes extracellular matrix degradation. Patients with SSc have decreased expression of uPAR in dermal fibroblasts.⁸⁵ The function of uPAR is impaired in endothelial cells isolated from the dermis of SSc patients.⁸⁶ SSc endothelial cells have a weak response to exogenous uPA and reduced ability to form capillary like structures.⁸⁶ This demonstrates that an impaired uPA/uPAR system can diminish the angiogenic capacity of endothelial cells.⁸⁶ At 12-weeks of age, skin biopsies of uPAR deficient mice (uPAR^{-/-}) show increased dermal thickness, replacement of adipose tissue by extracellular matrix, perivascular fibrosis accompanied by inflammatory cells in the deeper dermal layers, and increased myofibroblast counts.⁸⁵ Vascular features such as endothelial cell apoptosis with subsequent decrease in microvascular density is also observed.⁸⁵ Lung histology of uPAR^{-/-} display thickened alveolar septa caused by interstitial inflammation and collagen deposition, features reminiscent of NSIP.⁸⁵

2.4 Inducible mouse models

2.4.1 Hypochlorous acid (HOCl) – induced mouse model of SSc

2.4.1.1 Experimental protocol

A recently described model of SSc is generated by daily intradermal injections of hypochlorous acid (HOCl). This model is reported to induce anti-Scl70 antibody production, oxidized serum

proteins, and fibrosis of the skin and internal organs⁸⁷⁻⁸⁹. The most recent and optimized protocol described uses female, 6-week-old mice injected with HOCl solution (consisting of NaClO and KH₂PO₄) 5 days a week for a period of 6 weeks. A total of 300µL of HOCl solution is injected in two sites (150µL each site) in the lower back of the animal⁸⁷. The majority of studies used the BALB/c strain⁸⁷⁻⁸⁹ with the exception of one group using C57BL/6 mice⁹⁰. Variations in protocols among the different published papers are described in Table 2.

Table 2. Summary describing the protocols used to generate the HOCl mouse model of SSc among different papers.

Paper	Mouse Characteristics			Injections				
	Strain	Age	Sex	Volume	[HOCl]	pH of KH ₂ PO ₄	Frequency of Injections	Route of Injections
ATJ Maria et al, Front Immunol. Nov 2018	Balb/c	6-8 weeks	F	300µL	0.096%	6.2	5 days/wk for 6 wks	ID
ATJ Maria et al, Front Immunol. Dec 2018								
F Morin et al, Free Radic Biol Med. Jul 2017								
N Kavian et al Arthritis Rheumatol. May 2012				400uL				
F Morin et al. J Immunol. Oct 2016								
X Jin et al. Int J Stem Cells. Aug 2021								
ATJ Maria et al. Arthritis Rheumatol. Oct 2015				100µL	0.0388%	7.2		SC
ATJ Maria et al. Journal of Autoimmunity. Jun 2016								
G Bagnato et al. Arthritis Res Ther. Sep 2013								
A Servettaz et al. The American Journal of Pathology. Jul 2010				200µL	6.2	ID		
A Servettaz et al. Journal of Immunology. May 2009								
N Kavian et al. Front Immunol. Aug 2018								
K Kavian et al. Arthritis & Rheumatology. Jun 2018				300µL	2.74% (?)			
X Xia et al. Oncol let. Jun 2018								
M Jeljeli et al. Nature communications. Dec 2019				200µL	6.2			
M Meng et al. Front Immunol. Aug 2019.								
Bei et al. Exp Lung Res. Feb 2016	C57BL/6			500µL	0.14%			

2.4.1.2 Putative mechanism of HOCl-induced SSc

The mechanisms by which HOCl induces fibrosis are not entirely clear⁵⁷. Initial publications proposed that HOCl-induced oxidative stress contributes to the generation of lung fibrosis⁸⁹. The theory was that injections of HOCl increase levels of reactive oxygen species (ROS) which in turn cause the production of oxidized proteins⁸⁹. These HOCl oxidized proteins generate advanced

oxidation protein products (AOPPs) which act as inflammatory mediators and are biomarkers of oxidative damage⁸⁹. *In vitro* several proteins including albumin, IgG and Scl-70 were oxidized with HOCl and AOPPs were measured⁸⁹. AOPPs generated from oxidized Scl-70 induced the greatest H₂O₂ production from endothelial cells and highest rate of fibroblast proliferation⁸⁹. These effects were not observed in AOPP depleted serum but were consistent with serum from HOCl mice and SSc patients⁸⁹. Based on these data it was proposed that AOPPs (primarily from oxidized Scl-70) contribute to the generation of lung fibrosis by propagating oxidative stress from the skin to the lungs via the bloodstream⁸⁹. However, these experiments were not sufficient to make definitive conclusions and the authors acknowledged the need for future studies.

2.4.1.3 HOCl induced SSc-like phenotype in BALB/c mice

Among the reported features of the HOCl model, the skin fibrotic phenotype is best characterized. From day 14 to day 21 of injections, there was evidence of polymorphous cellular infiltrates and increased myofibroblast activation and proliferation in the skin⁸⁷. During the second last week of injections cellular infiltrates were replaced by extracellular matrix⁸⁷. mRNA expression of pro-inflammatory cytokines IL1 β and TNF- α was greater following 21 days of injections compared to 42 days⁸⁷. Immunostaining of cellular infiltrates at 21 days showed increase number of CD3+ T cells, B cells, and F4/80 macrophages⁸⁷. At day 42, during the established fibrosis phase, mRNA expression of pro-fibrotic genes *Coll1a1*, *Col3a1*, *TGF β 1*, and *α -SMA* and collagen content was significantly increased in the skin of mice exposed to HOCl⁸⁸. This was consistent with histological findings which showed a thickened dermis caused by increased collagen deposition^{87,88}. Other features of SSc-like skin changes were observed such as loss of dermal appendages and epidermal thickening^{87,88}. HOCl injections were reported to induce kidney fibrosis with intima-media thickening of renal arteries which mimics the pathological changes of SSc⁸⁹. Several papers have

reported the development of lung fibrosis with thickening of alveolar septa and presence of inflammatory infiltrates based on qualitative assessments of histological images⁸⁷⁻⁸⁹. Immunohistochemical staining showed that inflammatory infiltrates consisted predominantly of T lymphocytes⁸⁹. Increased mRNA expression of fibrotic genes (*Colla1*, *Col3a1*, *TGFβ1*, *α-SMA*)⁸⁸ and collagen content in the lungs was also observed⁸⁸. Repetitive HOCl injections also induced the production of AOPPs and anti-Scl-70 antibodies⁸⁸.

2.4.1.4 HOCl induced a SSc-like phenotype in nuclear factor erythroid 2-related factor 2 (Nrf2^{-/-}) mice

Given that HOCl was proposed to induce fibrosis through mechanisms of oxidative stress, it was hypothesized that impairing physiological antioxidant defense mechanisms would exacerbate the effects of HOCl⁹¹. Nrf2 is a redox-sensitive transcription factor that regulates cellular responses against oxidative stress⁹². Under basal conditions Nrf2 is sequestered in the cytoplasm by Kelch-like ECH-associated protein 1 (Keap1) resulting in E3 ligase mediated polyubiquitination and its subsequent proteasomal degradation^{92,93}. Under conditions of oxidative stress, cysteine residues associated with the Keap1 redox-sensing domain are oxidized causing a conformational change such that Keap1 can no longer bind Nrf2^{92,93}. Consequently, Nrf2 translocates into the nucleus where it binds the transcriptional co-activator musculoaponeurotic fibrosarcoma oncogene homolog (MAF) and initiates transcription of antioxidant response element-associated genes⁹³. HOCl injections performed in Nrf2 knockout mice (Nrf2^{-/-}) resulted in a more pronounced skin and lung phenotype⁹¹. Nrf2^{-/-} mice that received HOCl injections had increased skin thickness, collagen content, and more severe skin pathology compared to wild type animals injected with HOCl⁹¹. Similarly, increased lung collagen content and exacerbated lung pathology was noted in Nrf2^{-/-}

HOCl-injected mice⁹¹. Additionally, levels of anti-Scl-70 antibodies were increased in the sera of HOCl-SSc mice⁹¹.

2.4.2 Bleomycin mouse model

2.4.2.1 Bleomycin source and clinical use

The Bleomycin (BLM) family of antibiotics was originally isolated from the bacteria *Streptomyces verticillus* in 1966⁹⁴⁻⁹⁶. Currently, BLM labelled indications are head and neck cancers, lymphomas, malignant pleural effusions, and testicular cancers⁹⁷. However, the use of bleomycin is limited by its dose-dependent lung toxicity⁹⁷. Up to 10% of patients can develop BLM-induced pneumonitis which can progress to lung fibrosis, of whom approximately 1% die⁹⁷. This notable side effect of BLM led to its use as an agent to induce pulmonary fibrosis in animal models.

2.4.2.2 Mechanisms of BLM-induced lung fibrosis

The induction of lung fibrosis by BLM is associated with oxidative stress. In the presence of iron and oxygen, BLM forms an activated complex that catalyzes the formation of superoxide and hydroxyl radicals. These free radicals cause DNA strand scission and lipid peroxidation^{98,99}. Consistent with this, depletion of iron with chelators attenuates bleomycin induced lung fibrosis, likely secondary to reduction in free radicals¹⁰⁰. The direct administration of antioxidants or the stimulation of Nrf2, the master transcription factor for multiple antioxidant genes are also reported to modulate fibrosis in the BLM model^{101,102}. Interestingly, the timing of the administration of BLM importantly determines the degree of lung injury as it correlates with the nadir of circadian Nrf2 activity that may be corrected with sulforaphane, the Nrf2 activator¹⁰². This observation further supports the key role of oxidative stress in the BLM lung injury.

In addition to oxidative stress, BLM induced lung fibrosis requires the lack of the inactivating enzyme bleomycin hydrolase and is influenced by genetic factors¹⁰³. The enzyme metabolizes BLM to a nontoxic molecule¹⁰⁴. Notably, the lowest concentrations of BLM hydrolase are found in the skin and lung increasing the susceptibility of these organs to BLM toxicity. The response to BLM is also strain-dependent in mice, with BALB/c being more resistant to the effects of bleomycin than C57BL/6¹⁰⁵. The strain variation is attributed to lower levels of bleomycin hydrolase in C57BL/6 mice compared to BALB/c¹⁰³.

Bleomycin alters the composition of the extracellular matrix consequently affecting the mechanical properties of the alveolar compartment. Collagen, elastin, and proteoglycans (components of the matrix) form the scaffold of the alveolar structure and are important in determining the mechanical properties of the lung parenchyma. It is suggested that changes in fiber subtypes and cross-linking of collagen fibrils are more important determinants of viscoelastic behaviour than absolute amount of collagen and elastin¹⁰⁶. Fibrotic lesions, by their nature, are characterized by significantly enhanced mechanical forces relative to healthy tissue. Increased mechanical forces within tissues activate latent transforming growth factor- β (TGF- β) through integrin dependent mechanisms driving key fibrogenic processes, including myofibroblast trans-differentiation which increases tissue stiffness and further activates TGF- β ¹⁰⁷. Bleomycin injury also leads to surfactant dysfunction making mouse lungs vulnerable to repetitive collapse which increases the degree of alveolar recruitment and decruitment during the breathing cycle¹⁰⁸. This results in alveolar wall stress and can cause inflammatory exacerbations. Alveolar stress is a well-described cause of lung injury and inflammation¹⁰⁹.

2.4.2.3 Different route of BLM administration and its associated phenotypes

BLM murine models are among the most commonly used to study pulmonary fibrosis¹¹⁰. Bleomycin can be administered through different routes. Intratracheal instillation of BLM generates an earlier lung injury with subsequent fibroblastic foci development resulting in bronchocentric distribution of fibrosis^{110,111}. This contrasts intravenous and intraperitoneal administration which induces subpleural scarring¹¹¹. Of relevance, a primary epithelial injury (intratracheal BLM) produces a similar pathological picture to a primary endothelial injury (intravenous BLM). In both instances, alveolar type I cell damage occurs and triggers a repair process mediated by hyperplasia of alveolar type II cells, epithelial to mesenchymal transition and collagen synthesis. Early studies have shown that bleomycin delivered intratracheally induces the development of fibrosis that progresses or persists for 30-90 days after a single instillation^{112,113}. However, more recent reports demonstrate a self-limiting response that begins to resolve 3-4 weeks post instillation^{114,115}. Spontaneous resolution of lung fibrosis was also observed with the BLM delivered systemically via osmotic minipump¹¹⁶.

A study has directly compared the effect of BLM delivered by the intraoral route and systemically using a subcutaneously implanted osmotic minipump¹¹⁶. In the pump model, thickening of alveolar septa was predominantly observed in the subpleural region while little change was observed in central lung area^{116,117}. This subpleural distribution of pulmonary fibrosis, a characteristic feature of NSIP, is a reproducible finding of the minipump model as reported by several other groups¹¹⁷⁻¹²⁰. This is in contrast to the intraoral route where central and subpleural regions were affected to a similar extent¹¹⁶. In addition, the pump model showed moderate inflammation in the subpleural region and no inflammation in the central region whereas extreme inflammation occurred in both lung regions with intraoral administration¹¹⁶. The investigators have also analyzed SSc-ILD lung

samples. They report the level of inflammation in lung tissues to be more similar to inflammation observed in the minipump model than the intraoral mouse model¹¹⁶.

In summary, SSc is an autoimmune disease that culminates in fibrosis of the skin and visceral organs. Although ILD is a leading cause of death among SSc patients, there is no single intervention that can reverse lung fibrosis. Research into potential treatments of SSc-ILD has been hampered by animal models which do not recapitulate key features of the human disease and whose ability to predict future clinical outcomes has been questioned. Therefore, to evaluate novel therapeutic agents of SSc-ILD a robust animal model is required.

We hypothesize that administration of repetitive intradermal HOCl injection in BALB/c mice results in an immune, skin, and lung phenotype which mimics the pathological changes seen in SSc patients. We also hypothesize that systemic delivery of BLM via osmotic minipump results in lung fibrosis resembling SSc-ILD.

The specific aims of our work are to:

1. Characterize the skin, lung, and autoimmune phenotype in the HOCl mouse model.
2. Characterize the lung phenotype in the BLM delivered by osmotic mini-pump mouse model.

Chapter 2: Methods

2.1 Animals

We followed the ‘Animal Research: Reporting of In Vivo Experiments (ARRIVE) guidelines to report animal research.¹²¹ For the HOCl-SSc mouse model, BALB/c mice were purchased from Charles River Laboratories, while NRF2^{-/-} mice on a C57BL/6 background and corresponding wild type mice were purchased from Jackson Laboratories. All mice were female between 6-8 weeks. Sex and strain were chosen based on previous literature on the model^{88,89} and the knowledge that SSc is more common in women.¹²² For the generation of the BLM mouse model, male C57BL/6, 9-10-week-old mice were purchased from Jackson Laboratories. Animals were housed in a conventional animal facility at the Research Institute of the McGill University Health Centre (RI-MUHC). Male mice develop a more severe form of BLM induced lung fibrosis compared to females¹²³. This justifies our choice of using male mice in these experiments. Animals were housed in Tecniplast GM500 cages with overall dimensions (W × D × H) of 391 × 199 × 160 mm which were replaced every 2 weeks with clean/sterile cages. Animals received chlorinated water [diluted with a bleach concentration following Canadian Council on Animal Care (CACC) guidelines] which is monitored and tested daily by the animal facility staff. The water was dispensed via an automated sipper system directly to the individual cages. The temperature in the cages was set to follow CCAC guidelines and monitored 24/7. A nesting sheet, Enviro Dri (shredded paper) was used for environmental enrichment which allowed the animals to find a secluded spot atop the inside of the cage. Animals were fed with Teklad Irradiated Diet 2918, supplied by Envigo. Animals were treated in accordance with the guidelines of the CCAC and protocols were approved by the Animal Care Committee of McGill University.

2.2 Animal Models

2.2.1 HOCl-SSc mouse model

2.2.1.1 *Overview of the protocol*

To induce lung fibrosis, we followed the methods established by Dr Alexandre Maria.^{87-89,91,124,125} Specifically, mice were anesthetized with isoflurane (4% induction, 1.5-2.5% maintenance) and received intradermal injections of HOCl in two sites of the lower back (150 μ L in each site, a total of 300 μ L) five days a week for 6 weeks. After 6 weeks, injections were discontinued, and experimental readouts were assessed. (Figure 1 & Figure 2).^{87,89} Dedicated experiments were conducted to test the effects of increasing the total volume of the injected solution to 400 μ L (200 μ L per site) and prolonging the duration of injections for 2 additional weeks (8 weeks total). Different brands of commercially available bleach were also tested.

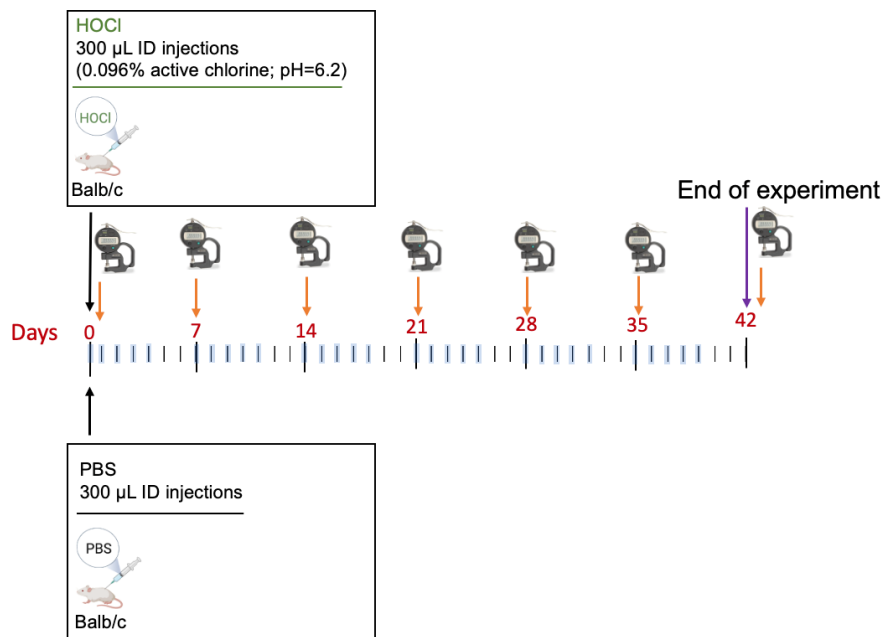


Figure 1. HOCl-SSc mouse model. 6-week-old, female, BALB/c mice received daily intradermal injections of PBS or HOCl in the lower back for 6 weeks. The graph shows days 0-42. Skin thickness was assessed weekly by caliper. Mice were sacrificed on day 42.

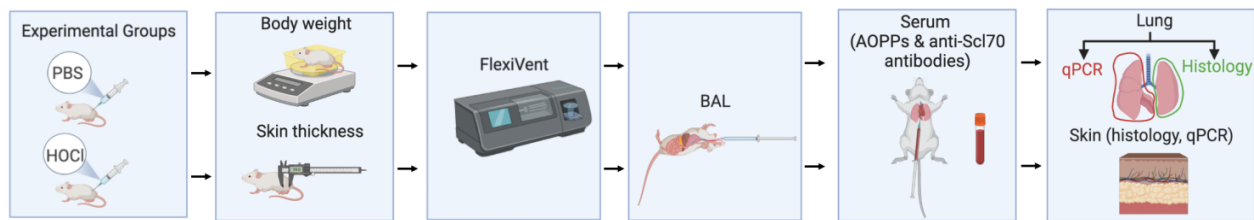


Figure 2. Experimental readouts assessed in the HOCl-SSc model. Mice were weighed daily, and skin thickness was measured weekly. After 42 days, flexiVent assessment was first performed followed by BAL and blood sample collection for evaluating levels of AOPPs and anti-Sci70 antibodies. Lastly, lungs and skin were harvested for histological assessment and quantification of mRNA expression of profibrotic genes.

2.2.1.2 Preparation of hypochlorous acid solution

Potassium dihydrogen phosphate (KH_2PO_4) buffer solution was preprepared as previously established⁸⁷ a concentration of 100mM with a pH of 6.2. The KH_2PO_4 solution was stored at 4°C for a maximum of 3 months. Commercial bleach at a concentration of 4% was used. The bleach bottle was replaced every 3 weeks, once opened. The HOCl solution was prepared at a final concentration of 0.096%. A spectrophotometer was used to ensure that the optical density measured at a wavelength of 292 nm was between 0.7 and 0.9 (arbitrary units). The HOCl solution was prepared fresh each day and its optical density was measured every day. The control group received injections of PBS.^{87,89}

2.2.1.3 Intradermal injections

The student who performed all experiments (AM) was trained in performing intradermal injections by a Clinical Veterinarian at the RI-MUHC. A blue food colorant was used to improve visualization of the injections. A circular bleb was seen upon injection of the dye indicating a

successful intradermal injection (Figure 3, a). The dorsal skin of the mouse was excised, and the dye was contained within the bleb (Figure 3, b). This confirmed that the injections were performed adequately.

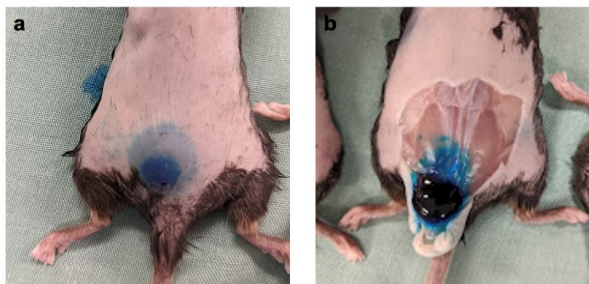


Figure 3. Validation of intradermal injections using blue food colorant. a. A successful intradermal injection shows a bleb under the skin. b. Excision of the skin shows the bleb is contained within a pocket.

2.2.1.4 Skin thickness

Skin thickness was measured using a digital caliper (Mitutoyo 547-500S) at three different locations on the lower back of the mouse where injections were performed (Figure 4). The average of the 3 measurements was recorded and compared overtime.

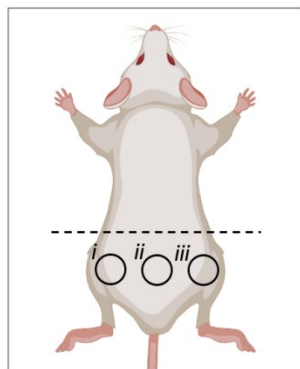


Figure 4. A graphic representation showing the 3 areas on the mouse where skin thickness measurements were obtained. This is indicated as *i,ii,iii*.

2.2.2 BLM-minipump mouse model

2.2.2.1 Overview of the protocol

We followed the methods described by Lee et al. (2014).¹¹⁶ Osmotic minipumps (ALZET 1007D; DURECT, CA) containing either 100 μ L of BLM (Adooq. Bioscience, A10152-10) or phosphate

buffer saline (PBS) were implanted subcutaneously in ten-week-old C57BL/6 mice. Minipump contents were delivered as a continuous infusion at a rate of 0.5 μ L per hour for 7 days.¹¹⁶ Prior to the implantation of the minipumps, the mice were anesthetized in an induction chamber for 5-10 minutes with isoflurane (vaporizer was set to 4%). For anesthesia maintenance, a tight-fitting mask was used and the isoflurane vaporizer was set to 1.5-2.5%. Oxygen flowmeter was adjusted to 0.8 to 1.5L/min. (McGill SOP 110.05 – Mouse Anesthesia). The upper back of the animal was shaved and skin was cleaned with chlorhexidine and ethanol. A mid scapular incision was made and a haemostat was inserted into the incision to create a pocket for the pump. The pump was inserted with the exit port towards the caudal end of the animal. The wound was closed with sutures or wound clips. Post-implantation, animals were placed inside a heated cabinet, 1mL of saline was administered subcutaneously and mice were given wet food (2918 Teklad chow mixed with drinking water) and saline (Baxter JB1302) for 3 days. Pumps were removed on day 10 as per manufacturer recommendations. Mice were sacrificed on day 28 and readouts were performed (Figure 5). The experimental timeline is shown in Figure 6.

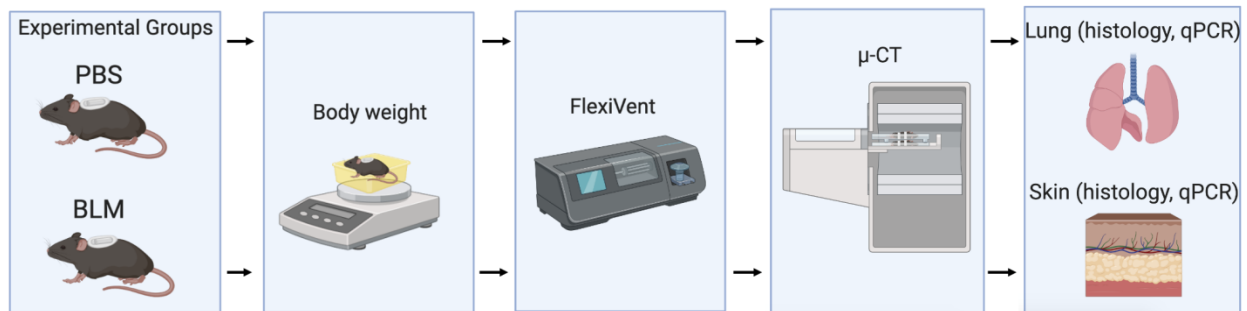


Figure 5. Experimental readouts in the BLM-MP model. Following minipump implantation mice were weighed daily. At the time of study termination, the flexiVent was performed followed by micro-CT and harvesting of organs.

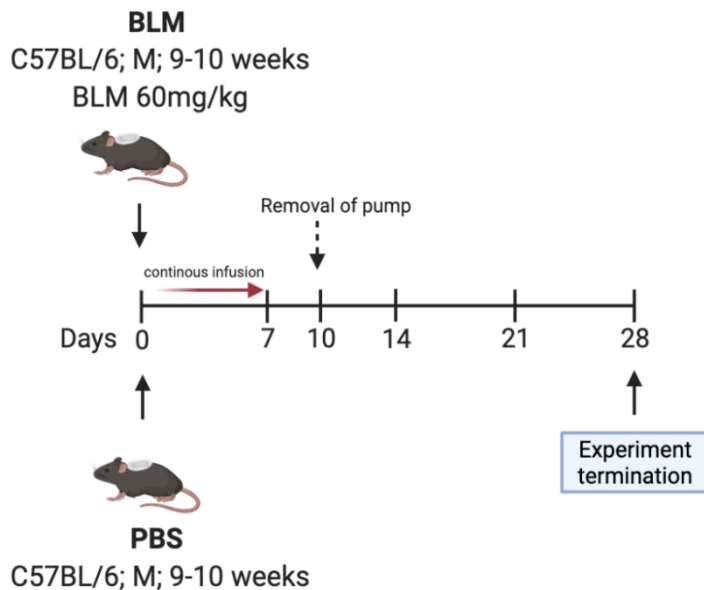


Figure 6. Experimental timeline for the generation of the BLM-MP mouse model. BLM or PBS was delivered systemically via osmotic minipump implanted in C57BL/6 mice. Outcomes were evaluated on day 28.

2.2.2.2 Bleomycin dose

Initial experiments were performed to determine the optimal BLM dose that induced lung injury and was well tolerated by the animals. Based on the results of these experiments we proceeded to further characterize lung involvement in animals treated with a BLM dose of 60mg/kg.

2.3 Experimental Techniques

2.3.1 Measurement of respiratory mouse mechanics

Methods to assess respiratory mouse mechanics were adapted from McGovern et al 2013.^{126,127} Mice were sedated with xylazine (8 mg/kg; intraperitoneally) and anesthetized with pentobarbital sodium (30 mg/kg; intraperitoneally). They were tracheostomized using an 18-gauge metal cannula; connected to a computer controlled small animal ventilator (flexiVent™, SCIREQ, Montreal, PQ, Canada) and normal tidal ventilation was initiated. Mice were mechanically ventilated at 150 breaths/minute with a positive end expiratory pressure (PEEP) of 3cmH₂O. One deep inflation maneuver was performed at 27cmH₂O to open closed airways and to normalize lung

volumes. Subsequently, a muscle relaxant was administered (rocuronium bromide; 0.2mg/kg) intraperitoneally. This was followed by 3 minutes of mechanical ventilation to allow the mice to adjust to the ventilator and for the rocuronium to have an effect. In the absence of spontaneous breathing, lung mechanical properties were assessed. This was done using a sequence of measurements integrated by default in the flexiVent operating software and referred to as the *mouse mechanics scan*.¹²⁸ The maneuvers/measurements that compose this sequence are outlined in Table 3.^{126,128}

Table 3. Description of maneuvers / outcomes composing the mouse mechanics scan sequence.

Adapted from references.^{126,128}

Maneuver	Description	Outcome
Deep inflation	Mice lungs are gradually inflated to 30cmH ₂ O over a period of 3 seconds and this pressure was held for 3s to allow alveolar pressure to equilibrate.	IC: Inspiratory capacity
SnapShot-150	1.2 second, 2.5 Hz single-frequency oscillation manoeuvre is applied to the subject's airway opening.	Single compartment model parameters: R _{rs} : total respiratory system resistance E _{rs} : total respiratory system elastance C: dynamic compliance
Quick Prime-3	3 second, 1-20.5 Hz broadband low frequency forced oscillations is applied to the subject's airway opening.	Constant phase model parameters: R _N : Newtonian resistance (airway resistance) G: Tissue damping H: Tissue elastance
Partial PV Curve	Ventilator gradually inflates the subject's lungs in a stepwise manner from a positive end expiratory pressure (PEEP) of 3cmH ₂ O to 30cmH ₂ O and deflates them in a similar fashion.	Pressure-volume curve Cst: Static compliance Area: area between inspiratory and expiratory limb of the P-V curve. Salazar-Knowles parameters: κ: shape constant describing the curvature of the upper portion of expiratory limb of the P-V curve. A: estimate of inspiratory capacity.

2.3.2 Calculation of respiratory mechanical parameters

2.3.2.1 P-V curve

The static pressure-driven partial pressure-volume (P-V) loop was used to measure the static compliance of the lung. It was constructed by a stepwise inflation of the lung from positive end expiratory pressure (PEEP, 3cmH₂O) to 30 cmH₂O and a slow deflation in a similar manner.¹²⁸

This procedure was repeated three times and data were averaged to generate a single P-V curve. During the inflation and deflation, lung pressure and volume were recorded. The static compliance was obtained from the slope of a line segment connecting two points within the linear range of the expiratory limb. Therefore, compliance was expressed as a change in volume for a given change in pressure: $C_{st} = (V_2 - V_1) / (P_2 - P_1)$; where C_{st} is static compliance, V is volume and P is pressure.

128

2.3.2.2 Respiratory system resistance and elastance

Total respiratory system resistance (R_{rs}) is a combination of airway, tissue, and chest wall resistance. Likewise, total respiratory system elastance (E_{rs}) consists of lung and chest wall elastance. The piston of the mechanical ventilator can apply small amplitude pressure-driven oscillations to the airway opening (i.e. single frequency oscillation technique, SFOT) which is used to measure dynamic properties of the lung.¹²⁶ The flexiVent software calculates R_{rs} and E_{rs} by fitting the equation of motion of a single compartment linear model to the data generated by the SFOT.¹²⁹

2.3.3 Micro-computed tomography (CT)

2.3.3.1 Image acquisition

Upon completion of the flexiVent measurements, the mouse was disconnected from the Y-tubing, the metal cannula was removed, and an 18-gauge plastic cannula was inserted into the trachea and

secured in place. The cannula was connected to a manometer and lungs were inflated to a pressure of 25cmH₂O to standardize lung inflation and ensure comparability of the morphology of lung sections. The trachea was quickly bound with a string and the cannula was removed.

The mouse was immediately transferred to the nanoScan SPECT/CT for small animals (Mediso Medical Imaging Systems, Budapest, Hungary) and imaged at the Small Animal Imaging Labs (SAIL), RI-MUHC. The following scan parameters were used: 1) number of projections: 480; 2) scan method: semicircular; 3) rotations: 1; 4) x-ray voltage: 35 kilovoltage peak (kVp); 5) amps: 980 microamps (μ A); 6) exposure time: 450 milliseconds (ms), and 7) resolution: 42 micrometers (Mediso Imaging System scan parameters).

2.3.3.2 Image analysis

Analysis was performed by a PET/SPECT specialist at the SAIL, RI-MUHC as described by Lv et al (2013) ¹³⁰. The original CT scan was cropped to obtain only the lung image and automatic segmentation of the whole lung was performed using a MATLAB[®] software developed by SAIL. Airways were then excluded from the segmented lung image. The image was converted from grey levels to CT numbers termed Hounsfield units (HU). This conversion is a linear transformation, setting -1000HU as the density of air and 0 as the density of water. The mean HU and standard deviation were calculated for the whole lung. The software also provided a value representing the sagittal plane which allows the separation into left and right lungs. The mean HU for the left and right lung was then calculated. Similarly, two other values represent two transverse planes which allows the separation of the lung into lower, central and upper parts. The mean HU for these parts of the lung was also calculated.

The poorly aerated tissue refers to a low gas to tissue ratio and was used to assess the extent of injury caused by BLM. The poorly and normal aerated compartments of the lung are defined by a

range of HU. The images of aerated lung are defined as HU between -900 and -500, while affected lung as HU between -500 and -100].¹¹⁷

2.3.4 Bronchoalveolar lavage (BAL) fluid analysis

BAL processing and analysis was adapted from Farahnak et al. (2019).¹²⁷ Following lung mechanics measurements, BAL was performed in animals that did not undergo micro-CT imaging by instilling 1mL of cold PBS via the tracheal cannula and subsequently recovering approximately 0.8mL of fluid by gentle suction. BAL fluid was centrifuged at 3000rpm for 5 minutes. The cell pellet was resuspended in PBS and cells were counted on a haemocytometer. The BAL cell suspension was deposited on a glass slide by cytocentrifugation at 1000rpm for 5 minutes using the EpreDia™ Cytospin™ 4 Cytocentrifuge. Cells were fixed and stained with Diff-Quick (Fisher Scientific, Kalamazoo, MI). Differential cell counts were determined by calculating the percent of macrophages, lymphocytes, neutrophils, and epithelial cells from a count of three hundred cells.

2.3.5 Lung and skin histology

2.3.5.1 Tissue collection

For the HOCl model, on day 42, skin biopsies from the dorsum of the animals within the area of injections were performed. For the BLM model, on day 28, skin biopsies were taken distal to the location of the minipump. For both models, following harvesting, lungs were inflated through the tracheal cannula with 10% buffered formalin with a distending pressure of 25cmH₂O for 10 minutes.¹³¹ The trachea was then tied off with a thread and the inflated lungs were removed. The skin and lungs were both submerged in formalin for 24-48h prior to processing and embedding in paraffin for histology sections.¹³¹

2.3.5.2 Hematoxylin and eosin (H&E) staining

The H&E protocol was adapted from Slaoui and Fiette (2011).¹³² After fixation in formalin, the ASP 300S tissue processor (Leica Microsystems, Germany) was used to process the skin and lung tissues. The Routine Overnight Program was selected, and samples were dehydrated with graded concentrations of ethanol, cleared with xylene and embedded in paraffin wax using the Leica EG1150 H Paraffin Embedding Station. The Leica RM2235 Rotary Microtome was used to cut sections of 4µm thickness and dried at 60°C. Subsequently, sections were dewaxed with xylene for 10 minutes twice and rehydrated with graded concentrations of ethanol (100%, 90%, 70%, 10 minutes in each bath). Sections were stained with Hematoxylin Gill II for 2.5 minutes, washed with tap water, submerged in lithium carbonate solution for 20 seconds, and stained with eosin. Sections were then dehydrated with ethanol (70%, 90% 100%, 10 seconds in each bath), cleared in xylene and coverslips were mounted with Cytoseal. Sections were scanned using the Aperio AT Turbo Scanner. An expert dermatopathologist (Dr Waters) and lung pathologist (Dr Fraser) assessed the skin and lung findings respectively and validated the analysis.

2.3.5.3 Masson's Trichome (MT) staining

Skin and lung sections were deparaffinized, hydrated and stained with Masson's Trichome (Sigma-Aldrich, St. Louis, Missouri) according to the manufacturer's instructions. Briefly, sections were placed in Bouin's solution, a preferred fixative for MT staining as it increases the contrast between tissue components and intensifies the colours. Sections were then rinsed, stained with Working Weigert's Iron Hematoxylin Stain (stains nuclei dark purple/black) and Biebrich Scarlet-Acid Fuchsin Solution (stains cytoplasm, muscle and collagen red).¹³³ Subsequently sections were rinsed and immersed in phosphotungstic-phosphomolybdic acid solution which is used as a decolourizer causing Biebrich Scarlet-Acid Fuchsin to diffuse out of collagen fibers.¹³³ Next,

sections were stained with Aniline blue which stains collagen.¹³³ To better differentiate the colors of the stained tissue structures, slides were incubated in 1% acetic acid.

2.3.5.4 Picrosirius Red (PSR) staining and analysis

Skin and lung sections were deparaffinized, hydrated and stained with picrosirius red (Abcam) for 1 hour at room temperature. Sections were rinsed in acetic acid solution (0.5%) and were subsequently dehydrated and cleared with xylene. PSR-stained slides were scanned and automated image analysis was performed on 3 non-contiguous sections from the left lung using the Aperio Pixel Count Algorithm. The algorithm detects pixels that match the input parameters which are based on the hue, saturation and intensity color model. To detect collagen with PSR, the default hue value was used (0.10), a hue width of 0.40 and color saturation of 0.08 were specified.^{134,135} Collagen content (expressed in pixels) was corrected to the area of each lung determined by manual digitization of the outer perimeter of the lung.

2.3.6 Quantification of dermal thickness

Masson's Trichrome or PSR stained slides of mouse skin sections were scanned using the Aperio® AT Turbo Scanner (Leica Biosystems) and analyzed using the Aperio ImageScope (Leica Microsystems, USA) at 20X magnification. Dermal thickness was measured from the dermal-epidermal junction to the dermal-adipose junction. Either two or three skin biopsies per mouse were used for analysis. Three random measurements were taken per section.

2.3.7 Advanced oxidation protein products (AOPPs)

The protocol used for obtaining serum was adapted from "Blood Collection and Sample Preparation for Rodents" (IDEX BioAnalytics).¹³⁶ Blood from PBS and HOCl injected mice was obtained after the completion of FlexiVent measurement by cardiac puncture and collected in tubes (BD Microtainer®). To prevent hemolysis, the needle was removed from the syringe prior to

depositing the blood in the collection tubes. Tubes were centrifuged at 3800rpm for 10 minutes using a mini centrifuge (Eppendorf® centrifuge 5424). The serum was aliquoted in 1.5mL Eppendorf tubes and stored at -20°C until the levels of advanced oxidation protein products (AOPPs) and anti-Scl70 antibodies were determined.

Serum from PBS and HOCl injected mice was diluted 1/20 in PBS and 200µL was pipetted in a 96-well plate. A solution of Chloramine T (100µM) was used to prepare the standard curve. All samples and standards were run in duplicate. An aliquot of 10µL of 1.16 M potassium iodide was added to each well, mixed and incubated for 5 minutes at room temperature. Next, 20µL of acetic acid solution was added to each well to stop the reaction. Optical density was read at 340nm on a microplate spectrophotometer (LKB Pharmacia 4050 UltroSpec II UV-Vis). The sample AOPP content was calculated using the Chloramine T standard curve.⁸⁹

2.3.8 Anti-topoisomerase I autoantibodies (ELISA)

A mouse Anti-Scl-70 ELISA kit (Signosis, EA-5205) was used to measure anti-Scl-70 antibodies in the serum of HOCl and PBS injected mice. ELISA was conducted following the specifications of the manufacturer. The kit contained a positive and negative control. Optical density was read at 540 nm on a microplate spectrophotometer.

2.3.9 Lung hydroxyproline assay

Lung hydroxyproline content was analyzed with a hydroxyproline colorimetric assay kit (Abcam, Ab222941) following manufacturer's instruction. The lungs from PBS and HOCl mice were hydrolyzed in 10N NaOH for 1 h at 120°C to obtain individual amino acids. Cold samples were neutralized with 10N HCl. Hydroxyproline was converted to pyrrole-2-carboxylate by oxidation via addition of chloramine-T. 3-dimethylamino benzoic acid was added to the intermediate product and incubated at 65°C for 45 minutes forming a colored complex. The absorbance was measured

at 560 nm using a microplate reader (LKB Pharmacia 4050 UltroSpec II UV-Vis) and the micrograms of hydroxyproline per milligram of lung were calculated based on the standard curve.¹³⁷

2.3.10 mRNA expression of pro-fibrotic markers

2.3.10.1 RNA Isolation

The mouse right lung and an amount of skin of approximately 30mg were dissected, transferred to 2mL screw-top tubes (Heathrow Scientific HEA10060), snap frozen and stored at -80°C until RNA isolation. Homogenization beads and lysis buffer with tris(2-carboxyethyl) phosphine (TCEP) was added to the frozen tissues and homogenized (607, Mini-BeadBeater-16). Lung and skin RNA were extracted using the Nucleospin[®] RNA kit (Macherey-NageI[™] 740955.50) and RNeasy Mini Kit (Qiagen, Inc), respectively, according to the manufacturer's instructions. The purity of RNA was verified by a microplate reader (Take3[™] Micro-Volume Plate) using the Gen 5[™] software.

2.3.10.2 Reverse Transcription and Real-Time quantitative PCR

Following RNA isolation, cDNA was synthesized with the LunaScript[®] RT SuperMix Kit (NEB #E3010) according to the manufacturer's instructions using a thermocycler (Applied Biosystems[™] Veriti[™]). A total of 500ng total RNA was reverse transcribed into cDNA. Real time quantitative PCR was performed using SYBR[®] Green PCR Master Mix (Applied Biosystems, Foster City, CA). The primers used are listed in Table 4. cDNA was amplified using Step-One-Plus machine (Applied Biosystems). The following cycling method was used: a holding stage (95°C for 10 min), a cycling stage (45 cycles at 95°C for 15 seconds, 60°C for 30 seconds, 72°C for 25 seconds) and a melting curve stage (95°C for 15 s, 60°C for 45 s, 95°C for 30 s). Relative mRNA expression was calculated using the $\Delta\Delta C_t$ method. Data were normalized to the housekeeping gene, Peptidylprolyl Isomerase A (*PPIA*). The transcriptional stability of commonly

used reference genes (S9, GAPDH, SDHA, PPIA, HPRT-1) was investigated in BLM- and HOCl-treated mouse lungs. PPIA demonstrated the highest transcriptional stability.

Table 4. Primer sequences used for RT-qPCR.

Gene	Forward primer (5'– 3')	Reverse primer (3' – 5')
alpha-smooth muscle actin (α-SMA) (ACTA2)	GAGGCACCACTGAACCCTAA	ATCTCCAGAGTCCAGCACA
Transforming growth factor beta 1 (TGF- β1)	ACGTCACTGGAGTTGTACGG	TGGGGCTGATCCCCGTTGA
Fibronectin (FN)	CGAGGTGACAGAGACCACAA	CTGGAGTCAAGCCAGACACA
Collagen type IV alpha 1 (Col4A1)	AGGGTTACCTGGAGAAAAAGGG	TGGTCTCCTTTCTGTCCCTTC
Collagen Type I alpha 1 (Col1A1)	ACCTTCCTGCGCCTAATGTC	AGTTCGGGTGTGACTCGTG
Collagen Type III alpha 1 (Col3A1)	TCCCCTGGAATCTGTGAATC	TGAGTCGAATTGGGGAGAAT
Peptidylpropyl isomerase A (PPIA)	CTGTAGCTCAGGAGAGCGTC	CCAGCTAGACTTGAAGGGGAA

2.3.11 Lung immune cell repertoires

The flow cytometry protocol was adapted from Kahn et al. 2020.¹³⁸ Both mouse lungs were removed and were placed on ice in a 15mL tube containing 2mL of RPMI-1640 medium. Collagenase (Sigma-Aldrich, C5138) solution was prepared at a concentration of 300U/mL and kept at 37°C until use. Lungs were transferred into a 6-well plate containing collagenase at a final concentration of 150U/mL. Lungs were minced and incubated for 45 minutes at 37°C and 5% CO₂. Using an 18G needle and a 10mL syringe, the minced lung was passed through a 70 μ m nylon strainer into 50mL tube. Using a circular motion, the tissue was pressed against the bottom of the strainer with the plunger of a 5mL syringe. This was repeated for a total volume of 12mL. The cell suspension was centrifuged at 1700rpm for 10 minutes and the supernatant was discarded. Red blood cells (RBC) were then lysed using the RBC lysis buffer (BioLegend, 420301). After 2 minutes of incubation with the RBC lysis buffer, the reaction was stopped by completing to a volume of 25mL with RPMI. The cell suspension was centrifuged at 1700rpm for 7 minutes and the supernatant was discarded. Cells were counted on a hemocytometer.

For immunophenotyping leukocyte subsets in murine lung tissue, 1.5×10^6 cells from each lung sample were plated in 96-well v-bottom plates. Cells were washed two times in 200 μ L of PBS, stained with eFluor506 viability dye (1:1000 dilution, eBioscience™) and incubated at 4°C for 10 minutes. Next, cells were washed once with PBS and incubated at 4°C for 10 minutes with anti-CD32/16 to block Fc receptors (BioLegend, B266361). Cells were then washed twice in FACS buffer (1% BSA in PBS) and incubated at 4°C for 30 minutes with the antibodies outlined in Table 5. Cells were washed twice with FACS buffer and fixed using the fixation reagent and diluent (Invitrogen™) for 20 minutes. All samples were acquired using the LSRFortessa x-20 flow cytometer. Analysis was performed using FlowJo V10 software. Fluorescence minus one (FMO) controls were used to set the upper boundary for background signal on the omitted label, and to identify and gate positive populations.

Table 5. Flow cytometry antibodies.

Antibody/ Fluorophore	Dilution	Company	Catalogue Number
SiglecF – BV786	1/100	BD Biosciences	740956
CD11b – BUV395	1/50	BD Biosciences	563553
CD11c – PeCy7	1/100	BD Biosciences	561022
F4/80 – APC	1/50	BioLegend®	123116
Ly6C – FITC	1/100	BioLegend®	108405
Ly6G – PerCP-eFluor 710	1/100	eBioscience™	46-9668-82

2.3.12 Statistical analysis

GraphPad Prism 9 software (GraphPad Software Inc., San Diego, CA, USA) was used for statistical analysis. A minimum of 3 mice was included in all experiments. Data are expressed as mean \pm standard error of the mean (SEM). non-parametric Mann-Whitney U test was used to

compare two groups. Two-way ANOVA was used for analysis of P-V loops and mouse body weight (repeated measures). A *p*-value less than 0.05 was considered statistically significant.

Chapter 3: Results

3.1 HOCl-SSc model using BALB/c mice

3.1.1 Effect of intradermal HOCl injections on body weight

Weight loss is a known adverse side effect of inducible models of lung fibrosis.¹³⁹ No change in body weight was observed between HOCl and PBS-injected mice over the course of 6 weeks (Figure 7).

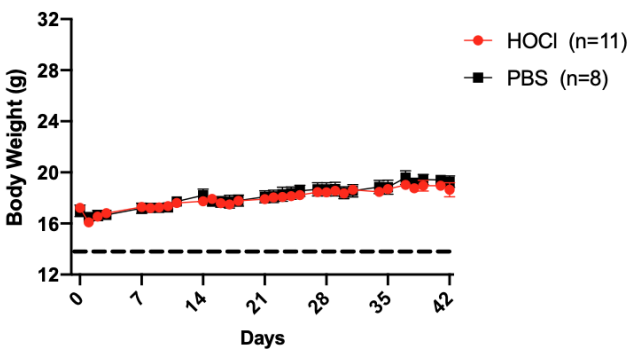


Figure 7. Intradermal HOCl injections did not affect BALB/c mice body weight. Horizontal dashed line represents the weight for euthanasia (weight loss of 20%). $n=8-11$ mice per group, graphs depict mean \pm SEM. Two-way ANOVA, $p>0.05$.

3.1.2 Skin changes following HOCl injections

To assess skin fibrosis in HOCl injected mice, we measured skinfold thickness with calipers, performed histological assessment of H&E and MT stained sections, and evaluated mRNA expression of profibrotic genes. Compared to PBS injected mice, HOCl mice had increased skin thickness at all timepoints except baseline (D0) (Figure 8, a). H&E stained skin sections of HOCl injected mice showed areas of epidermal hyperplasia, hyperkeratosis, and loss of adipose tissue and appendages. Those affected areas alternated with less/non-affected areas (Figure 8, b). Inflammation extending into the superficial layer of the muscle bundles was also observed (Figure 8, b). MT sections showed both areas of irregular and homogeneous collagen bundles in the dermis. In HOCl injected mice, evidence of fibrosis was also observed in the deep reticular dermis (Figure 8, b). Histological assessment showed HOCl mice to have increased dermal thickness compared

to PBS mice (Figure 8, d). Lastly, mRNA expression of *Coll1a1*, *ACTA2* and *Col3a1* was elevated in HOCl treated mice (Figure 8, d).

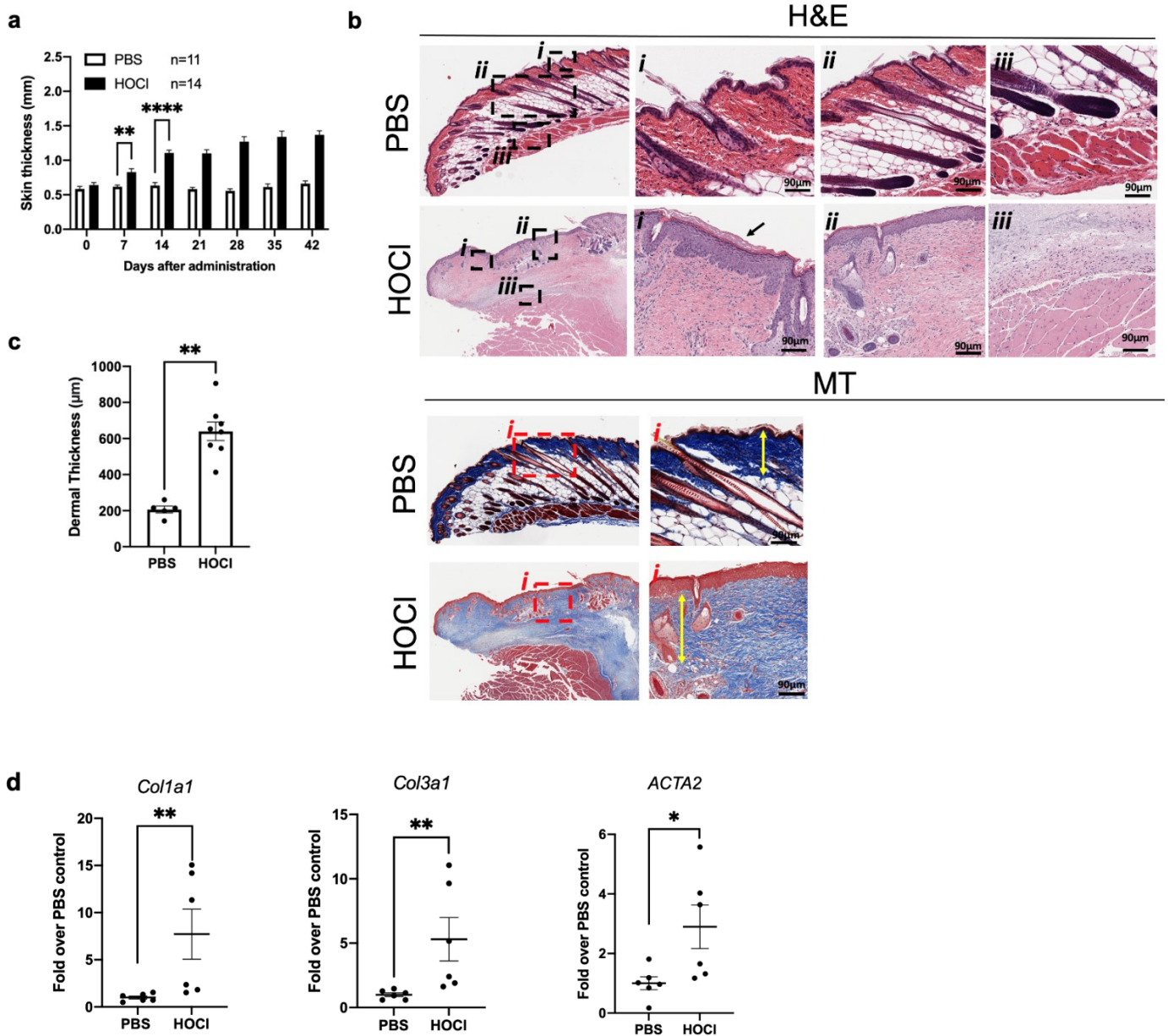


Figure 8. HOCl injections induce local skin fibrosis with spatial heterogeneity. **a.** Mice skin thickness increases over the course of 6-weeks of HOCl injections. $n = 11-14$ mice per group, graphs depict mean \pm SEM. Two-way ANOVA, ** $p=7.50 \times 10^{-3}$, **** $p< 1.00 \times 10^{-4}$. **b.**

Representative skin images of H&E and MT staining of PBS and HOCl-treated mice. Overview and $\times 20$ magnification. Scale bar: 90 μm . H&E sections of HOCl mice show epidermal hyperplasia and hyperkeratosis (black arrow, *i*); loss of adipose tissue/appendages (*ii*); and inflammation extending into the superficial muscle layer (*iii*). Yellow arrows in the MT-stained sections show dermal measurements (MT stained sections, HOCl row, panel *i*). **c.** Average measurements of dermal thickness. $n=5-8$ mice per group, graphs depict mean \pm SEM. Mann-Whitney U test, $**p=1.60 \times 10^{-3}$. **d.** *Colla1*, *ACTA2*, and *Col3a1* mRNA expression in PBS and HOCl mice. $n=6$ mice per group, graphs depict \pm SEM. Mann-Whitney U test, $*p=0.026$, $**p<5.0 \times 10^{-3}$. Abbreviations: ns: not significant.

3.1.3 Effect of HOCl injections on lung function and histology

We determined the effect of HOCl on lung compliance performing *in vivo* lung function measurements (flexiVent). At Day 42, there was no difference between the partial PV loops of PBS and HOCl injected mice (Figure 9, a). Static compliance confirmed the lack of difference between the two groups (PBS vs HOCl, ml/cmH₂O/g: $3.50 \times 10^{-3} \pm 9.30 \times 10^{-5}$ vs $3.36 \times 10^{-3} \pm 4.61 \times 10^{-5}$) (Figure 9, b). H&E, MT and PSR-stained lung tissue sections showed no histological abnormalities (Figure 9, c). Quantitative image analysis performed on PSR-stained slides showed no differences in the number of positive pixels between PBS and HOCl treated mice (PBS vs HOCl, positive PSR pixels/mm²: 2224378 ± 152187 vs 2064449 ± 159647) (Figure 9, d). Furthermore, no difference was observed in the mRNA expression of pro-fibrotic markers *ACTA2*, *TGF- β 1*, *Colla1*, *Col4a1* and *FN* (Figure 9, e-i). A strategy attempted to elicit lung fibrosis involved prolonging the duration of HOCl injections. Administration of HOCl for a period of 8 weeks (instead of 6) had no effect on lung compliance (PBS vs HOCl, ml/cmH₂O/g: $3.19 \times 10^{-3} \pm 4.25 \times 10^{-4}$ vs $2.82 \times 10^{-3} \pm 2.15 \times 10^{-4}$) (Figure 10, a & b). H&E-stained sections from HOCl

injected mice were comparable to those of PBS (Figure 10, c). MT-stained sections did not show any evidence of collagen deposition in the lung parenchyma (Figure 10, c). Together, these data indicate that chronic exposure to intradermal HOCl injections does not result in lung fibrosis.

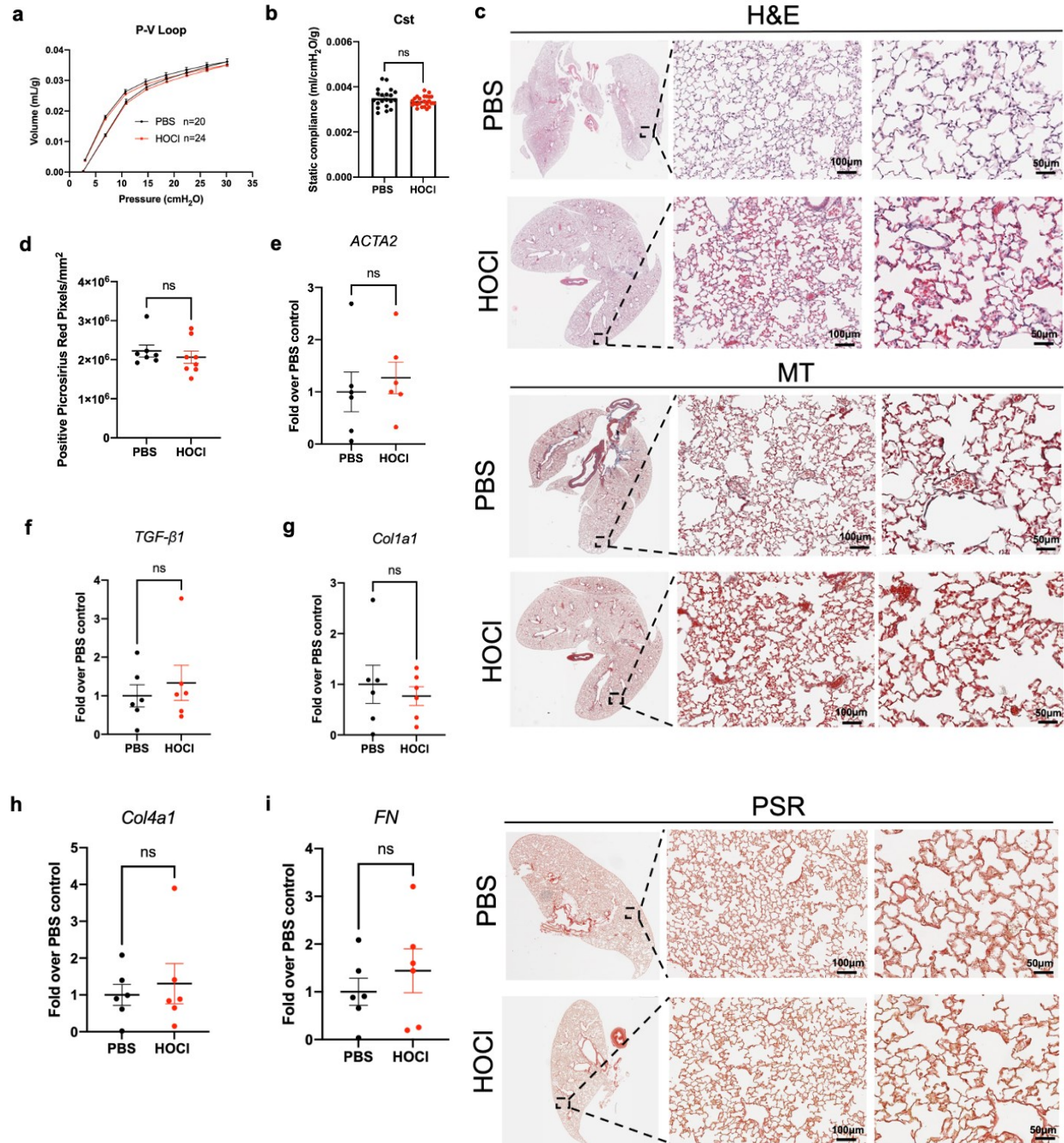


Figure 9. Intradermal HOCl injections (6 weeks) did not impair lung function or induce lung fibrosis. **a.** Mean pressure-volume (P-V) loops for PBS and HOCl-injected mice. **b.** Static lung compliance (C_{st}), $n=20-24$ mice per group, graphs show mean \pm SEM. Mann-Whitney Test, $p=0.18$ **c.** Micrographs of H&E, MT and PSR- stained lung sections (overview and $\times 20$ and $\times 40$ magnification). Scale bar: $100\ \mu\text{m}$ ($\times 20$ magnification) and $50\ \mu\text{m}$ ($\times 40$ magnification). $n=11-15$ **d.** Image analysis of PSR-stained slides. $n=7-8$ mice per group, graphs show mean \pm SEM. Mann-Whitney Test, $p=0.23$. Relative gene expression of **(e)**, α -smooth muscle actin (*ACTA2*), **(f)** transforming growth factor $\beta 1$ (*TGF- $\beta 1$*), **(g)** collagen type I alpha 1 (*Colla1*), **(h)** collagen type IV alpha 1 (*Col4a1*), and **(i)** fibronectin (*FN*) in lung tissue on day 42. Abbreviations: ns: not significant.

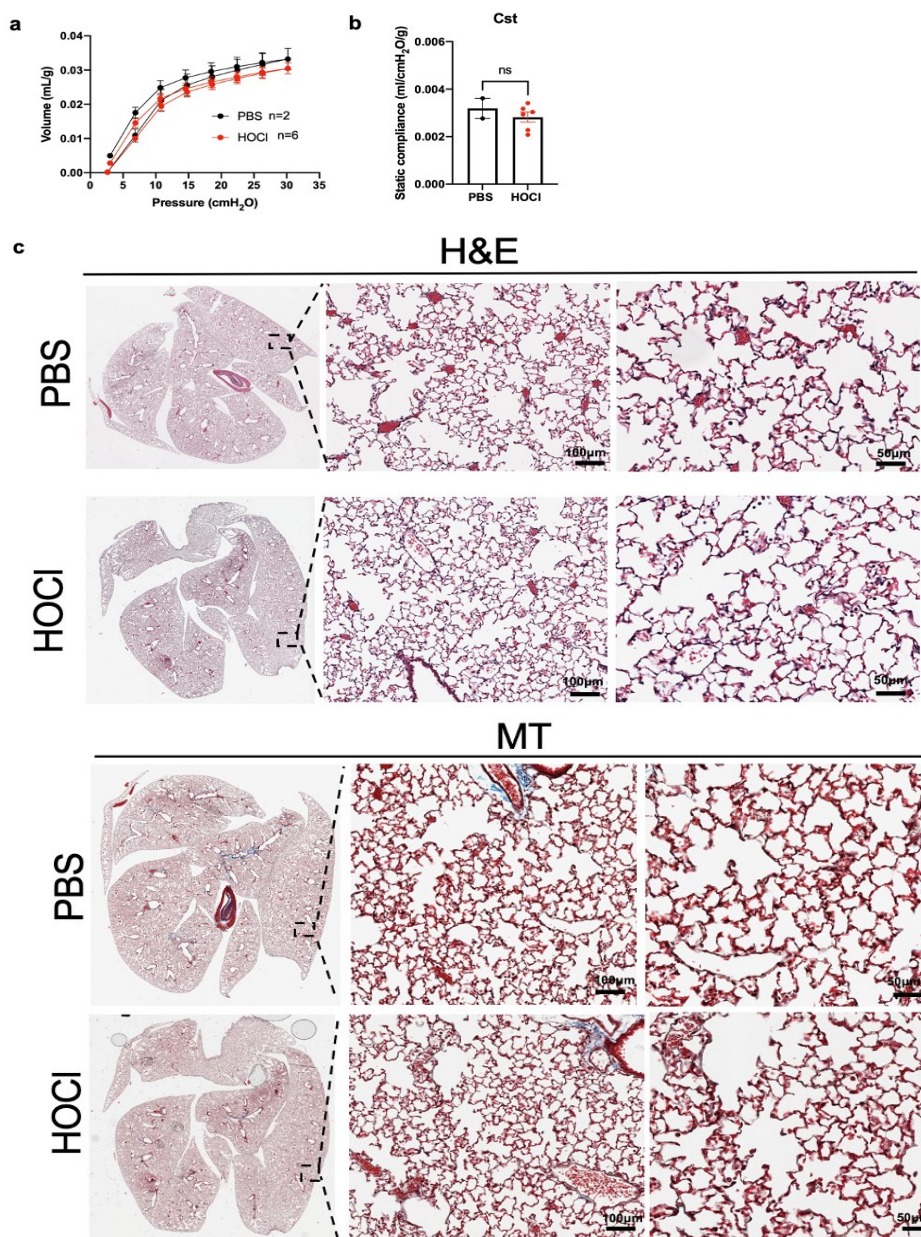


Figure 10. Intradermal HOCl injections (8 weeks) do not impair lung function or induce lung fibrosis. **a.** Mean pressure-volume (P-V) loops for PBS and HOCl-injected mice. **b.** Static lung compliance (C_{st}). $n=5-6$ mice per group, graphs show mean \pm SEM. Mann-Whitney test, $p=0.64$. **c.** Micrographs of H&E and MT-stained lung sections. Images show an overview of the lung and

×20 and ×40 magnification (from left to right). Scale bar: 100 μm (×20 magnification) and 50 μm (×40 magnification). *n*=2-6 mice per group. Abbreviations: ns: not significant.

3.1.4 The effect of HOCl injections on BAL leukocytes and macrophage phenotype

Inflammatory cells are reported to precede and mediate the development of fibrosis by releasing a variety of proinflammatory factors that inflict tissue injury.¹⁴⁰⁻¹⁴³ Therefore, we tested whether intradermal HOCl injections induced lung inflammation. Evaluation of inflammatory cell infiltrates in the BALF showed no difference in total white blood cell counts or differential cell counts between PBS and HOCl-injected animals (Figure 12, a). Lung tissue was analyzed by flow cytometry in a subgroup of mice for a more detailed phenotypic analysis of immune cells. Representative contour plots of the flow cytometry gating strategy are shown in Figure 11. Compared to PBS mice, HOCl injected mice showed no difference in the number of eosinophils (PBS vs HOCl, absolute numbers: 60213 ± 19221 vs 27265 ± 7991), alveolar macrophages (PBS vs HOCl, absolute numbers: 45065 ± 7205 vs 63792 ± 10779), neutrophils (PBS vs HOCl, absolute numbers: 579732 ± 87053 vs 576460 ± 80495), macrophages (PBS vs HOCl, absolute numbers: 324930 ± 40016 vs 459118 ± 43661), inflammatory monocytes (PBS vs HOCl, absolute numbers: 113795 ± 18204 vs 139415 ± 12532), inflammatory monocyte derived macrophages (PBS vs HOCl, absolute numbers: 284930 ± 37756 vs 409492 ± 52010) and interstitial macrophages (PBS vs HOCl, absolute numbers: 35623 ± 7524 vs 35310 ± 4262) (Figure 12, b-h). These findings indicate a lack of an inflammatory response following HOCl treatment.

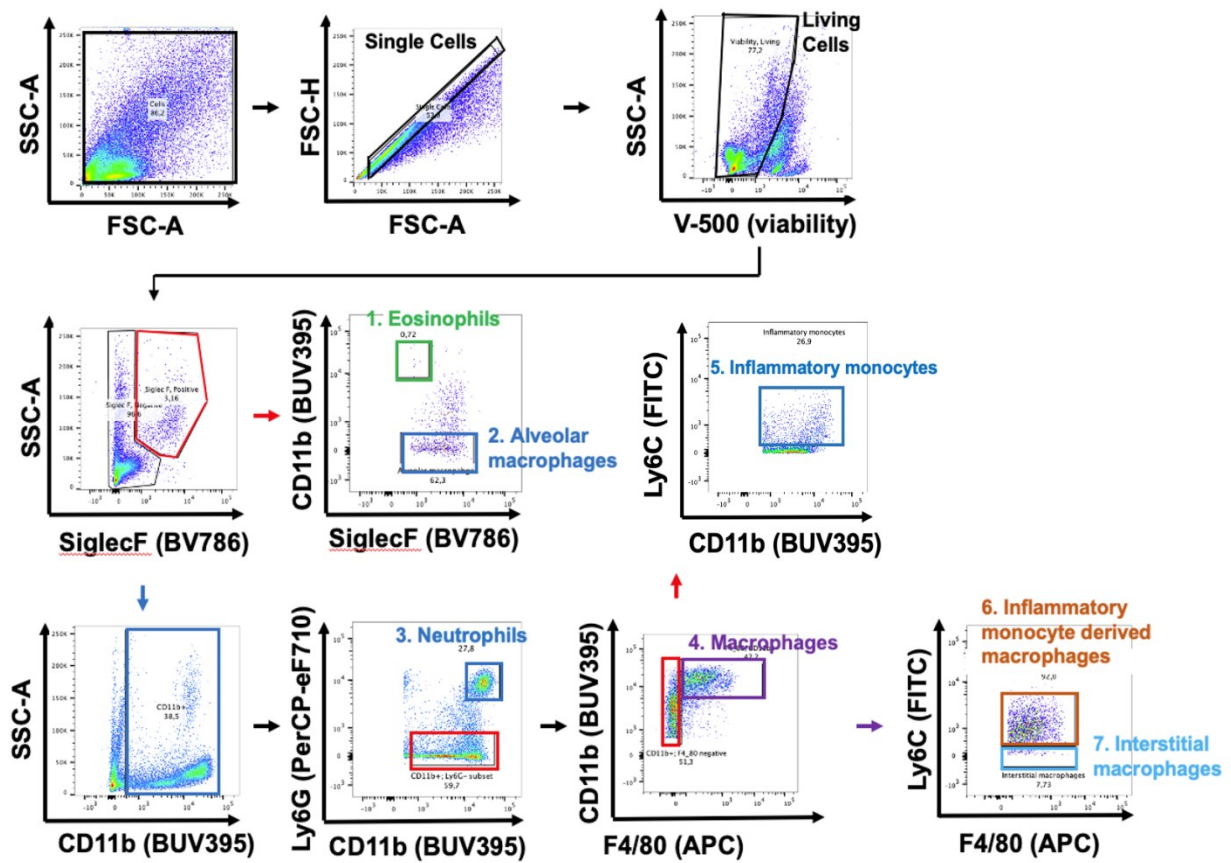


Figure 11. Representative flow cytometry gating strategy adapted from Pernet et al. 2019.¹³⁸ (1) Eosinophils (SiglecF⁺, CD11b⁺); (2) alveolar macrophages SiglecF⁺, CD11b⁻; (3) neutrophils (SiglecF⁻, CD11b⁺, Ly6G⁺); (4) macrophages (SiglecF⁻, CD11b⁺, Ly6G⁻, F4/80⁺, Ly6C^{+/-}); (5) inflammatory monocytes (SiglecF⁻, CD11b⁺, Ly6G⁻, F4/80⁻, Ly6C⁺); (6) inflammatory monocyte derived macrophages (SiglecF⁻, CD11b⁺, F4/80⁺, Ly6C⁺); (7) interstitial macrophages (SiglecF⁻, CD11b⁺, F4/80⁺, Ly6C^{low/neg}).

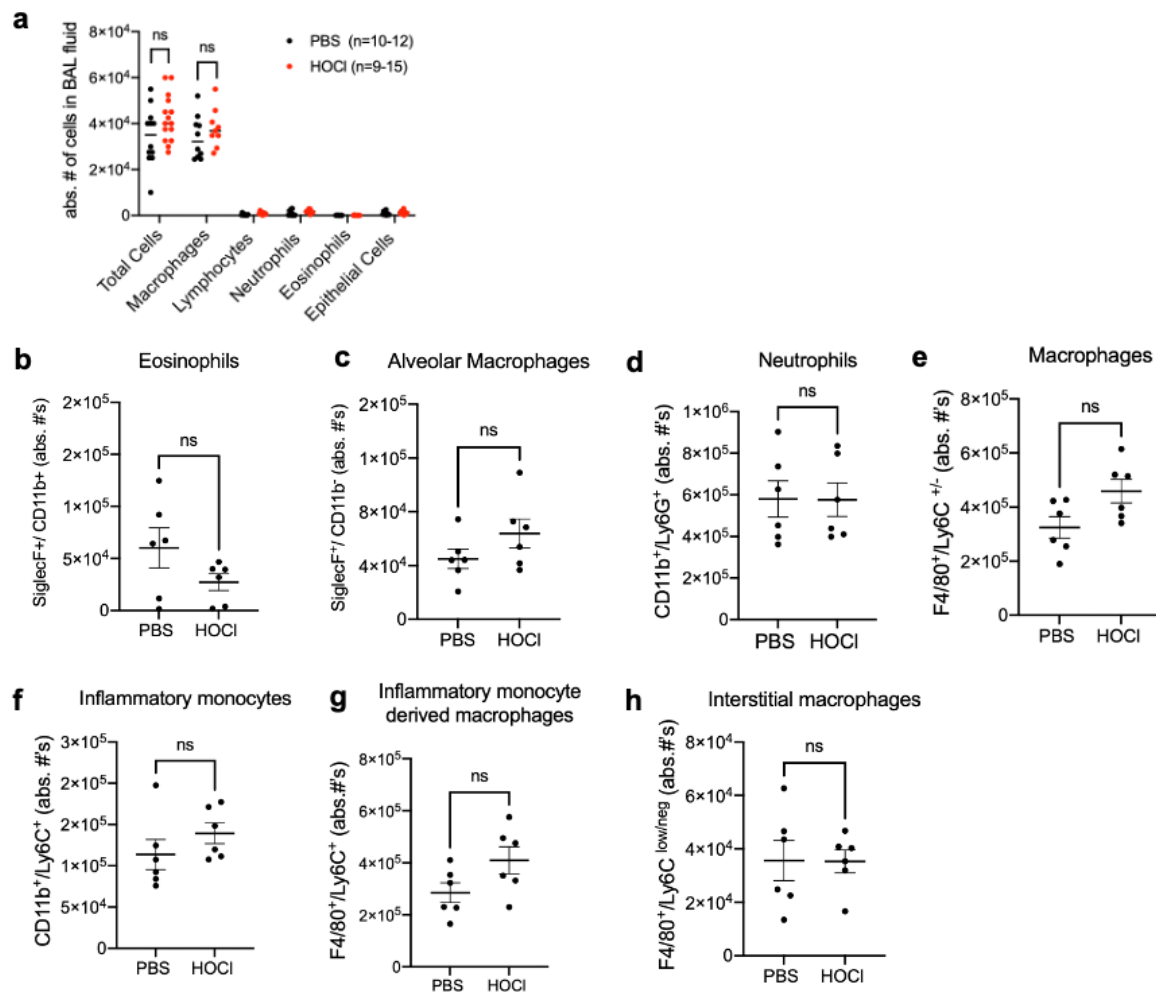


Figure 12. HOCl injections did not induce lung inflammation. **a**. Total and differential cell count from BALF of HOCl and PBS-injected mice. $n=9-15$ mice per group, graphs show mean \pm SEM. Two-way ANOVA, $p>0.05$. Quantification of total numbers of eosinophils (SiglecF⁺, CD11b⁺) (**b**), alveolar macrophages (SiglecF⁺, CD11b⁻) (**c**), neutrophils (SiglecF⁻, CD11b⁺, Ly6G⁺) (**d**), macrophages (SiglecF⁻, CD11b⁺, Ly6G⁻, F4/80⁺, Ly6C^{+/-}) (**e**), inflammatory monocytes (SiglecF⁻, CD11b⁺, Ly6G⁻, F4/80⁻, Ly6C⁺) (**f**), inflammatory monocyte derived macrophages (SiglecF⁻, CD11b⁺, F4/80⁺, Ly6C⁺) (**g**), and interstitial macrophages (SiglecF⁻, CD11b⁺, F4/80⁺, Ly6C^{low/neg}) (**h**). $n=6$ mice per group, graphs show mean \pm SEM. Intergroup differences were tested with Mann-Whitney Test, $p>0.05$. Abbreviations: ns: not significant.

3.1.5 The effect of HOCl injections on the production of AOPPs and anti-Scl70 antibodies

An initial study describing the HOCl-SSc model suggested that HOCl leads to the development of lung fibrosis by promoting oxidative stress.⁸⁹ Specifically, through the generation of AOPPs in the skin with subsequent propagation to the lungs. We did not observe increased concentrations of AOPPs in the sera of HOCl mice (PBS vs HOCl, $\mu\text{mol/L}$: 47.21 ± 11.62 vs 40.12 ± 10.87) (Figure 13, a). The development of fibrosis was also reported to be associated with the production of anti-Scl70 antibodies.⁸⁹ All HOCl mice we report were seronegative for anti-Scl70 (PBS vs HOCl, arbitrary units: 0.19 ± 0.02 vs 0.21 ± 0.01) (Figure 13, b). These data suggest a lack of systemic involvement following HOCl injections.

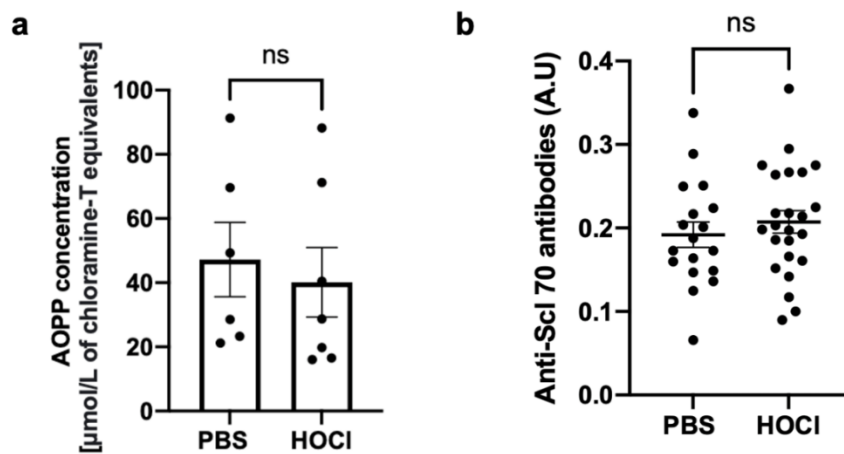


Figure 13. Intradermal HOCl injections neither induced the production of AOPPs nor anti-Scl 70 antibodies. **a.** AOPPs concentration in sera from PBS and HOCl-injected animals. $n=6$ mice per group. **b.** anti-Scl 70 serum levels. $n=18-25$ mice per group. Group comparisons were done with Mann Whitney test. Abbreviations: ns: not significant.

3.2 HOCl-SSc model using $Nrf2^{-/-}$ mice

3.2.1 The effect of intradermal HOCl injections on $Nrf2^{-/-}$ mice body weight

To test the hypothesis that oxidative stress enhances the generation of lung fibrosis in the HOCl model, HOCl was injected in mice more susceptible to oxidative stress ($Nrf2$ knockout mice: $Nrf2^{-/-}$). Under oxidative stress conditions, the $Nrf2$ transcription factor binds to the antioxidant response element (ARE) in the promoter of genes coding for antioxidant enzymes and proteins driving their expression. $Nrf2$ deficient mice have increased susceptibility to oxidative stress as they lack a key antioxidant defense mechanism.¹⁴⁴ We examined the weights of PBS and HOCl-treated C57BL/6 mice since the $Nrf2^{-/-}$ were generated on this background; HOCl treatment did not result in weight loss (Figure 14, a). Likewise, no difference in body weight was observed between $Nrf2^{-/-}$ mice injected with PBS ($Nrf2^{-/-}$ PBS) and $Nrf2^{-/-}$ HOCl animals (Figure 14, b). These results indicate that HOCl treatment does not induce weight loss in the $Nrf2^{-/-}$ model.

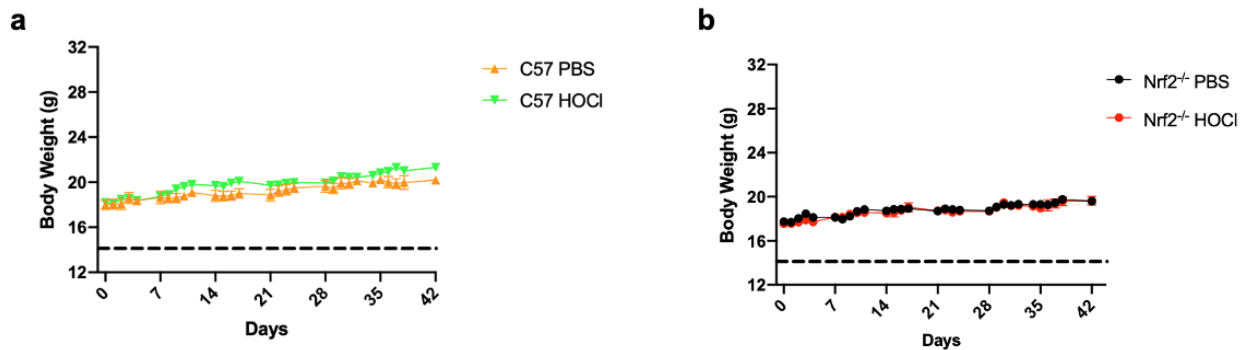


Figure 14. 6 weeks of intradermal injections do not affect the body weight of C57BL/6 nor $Nrf2^{-/-}$ mice. **a.** Body weight of C57BL/6 mice injected with PBS and HOCl. **b.** Body weight of $Nrf2^{-/-}$ animals injected with either PBS or HOCl. Horizontal dashed line represents the 20% weight loss criterion for euthanasia. No animal violated the 20% loss in body weight threshold. $n=4-6$ mice per group, graphs depict mean \pm SEM.

3.2.2 Skin changes in *Nrf2*^{-/-} mice following HOCl injections

Next, we evaluated whether *Nrf2* deficient mice have increased skin fibrosis when exposed to HOCl compared to C57BL/6 controls. Over a period of 6 weeks, no significant difference in skinfold thickness was observed (*Nrf2*^{-/-} HOCl vs C57BL/6 HOCl on day 42, mm: 1.74 ± 0.06 vs 1.51 ± 0.06 , $p = 0.90$) (Figure 15, a). Histology of *Nrf2*^{-/-} HOCl and C57BL/6 HOCl were comparable (Figure 15, b). Consistent with these findings, on day 42 there was no difference between the dermal thickness of *Nrf2*^{-/-} HOCl and C57BL/6 HOCl mice (*Nrf2*^{-/-} HOCl vs C57BL/6 HOCl, mm: 295.80 ± 28.09 vs 320.50 ± 23.64) (Figure 15, c).

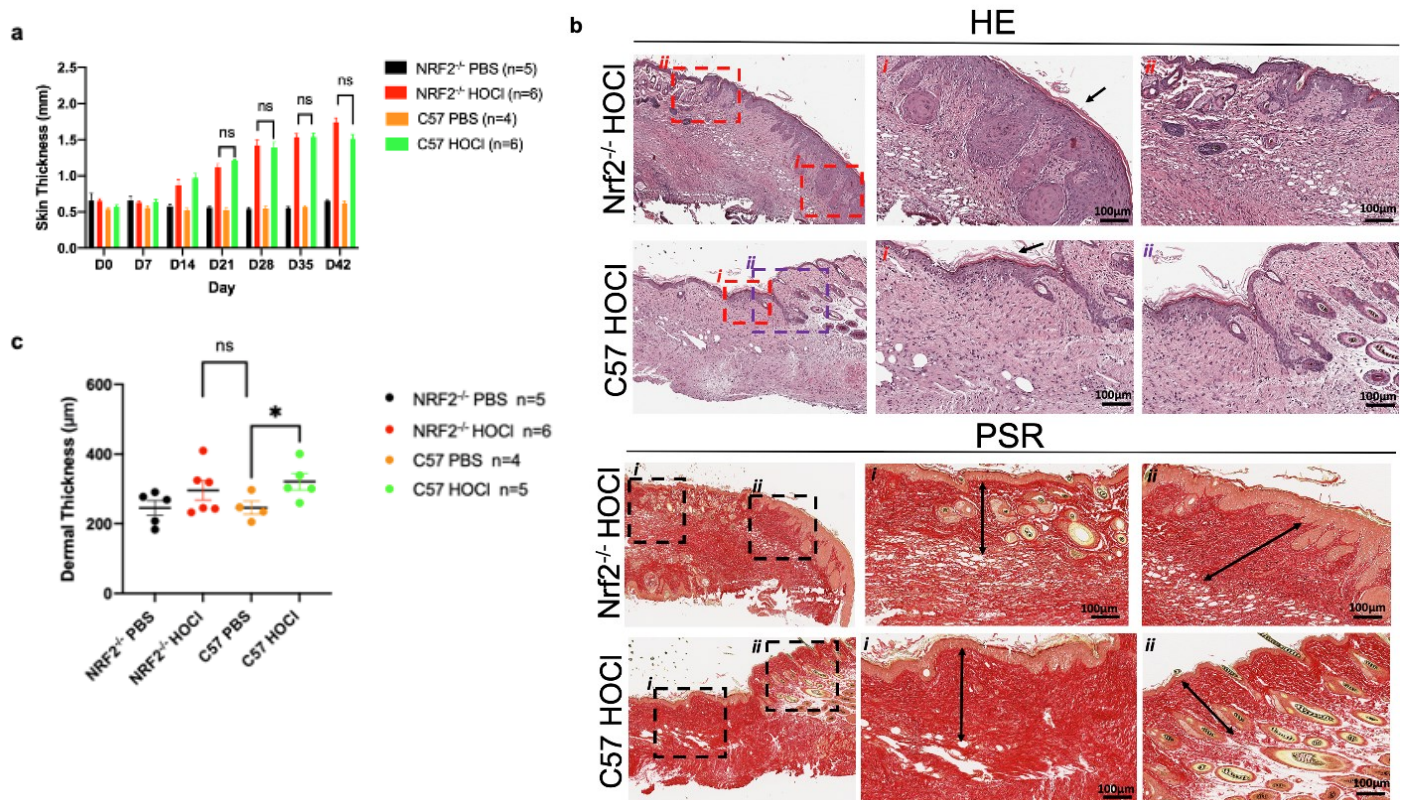


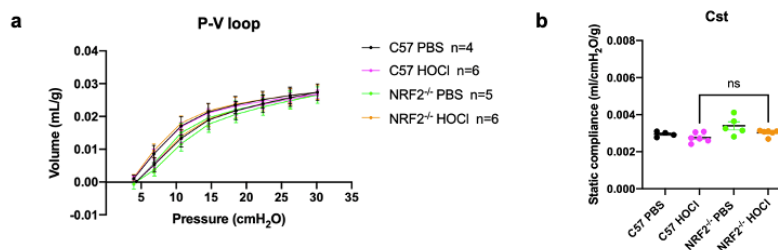
Figure 15. HOCl injections induce comparable skin fibrosis in *Nrf2*^{-/-} and WT control animals.

a. Skin thickness in mice increases over the course of 6-weeks of HOCl injections. $n = 4-6$ mice per group, graphs depict mean \pm SEM. Two-way ANOVA, $p > 0.05$. **b.** Representative images of

H&E and PSR staining of NRF2^{-/-} and C57BL/6 HOCl-treated mice. H&E sections of both NRF2^{-/-} and C57BL/6 mice show epidermal hyperplasia and hyperkeratosis indicated by the black arrow (H&E staining, panels *i*) and loss of adipose tissue/appendages in certain areas with preservation of them in adjacent areas (H&E staining, panels *ii*). Black arrows in the PSR-stained sections show dermal representative measurements. **c.** Mean \pm SEM of dermal thickness. n=4-6 mice per group. Mann-Whitney U test, *p<0.05. Abbreviations: ns: not significant.

3.2.3 Effect of HOCl injections on lung function and histology in Nrf2^{-/-} mice

Lung function measurements showed no difference in compliance between Nrf2^{-/-} and wild type C57BL/6 HOCl-injected mice (Nrf2^{-/-} vs C57BL/6, ml/cmH₂O/g: $3.03 \times 10^{-3} \pm 6.84 \times 10^{-5}$ vs $2.76 \times 10^{-3} \pm 1.07 \times 10^{-4}$) (Figure 16, a & b). Lung histology also confirmed the absence of thickened alveolar septa. Specifically, no visible collagen fibers were detected in PSR-stained slides (Figure 16,d). These results suggest that Nrf2^{-/-} mice were not more susceptible to HOCl-induced lung fibrosis.



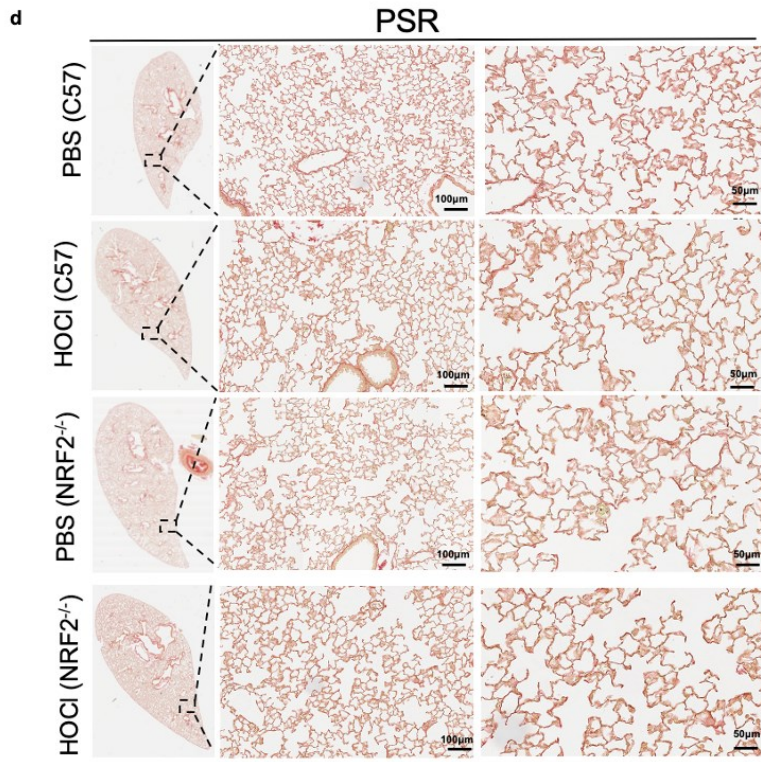
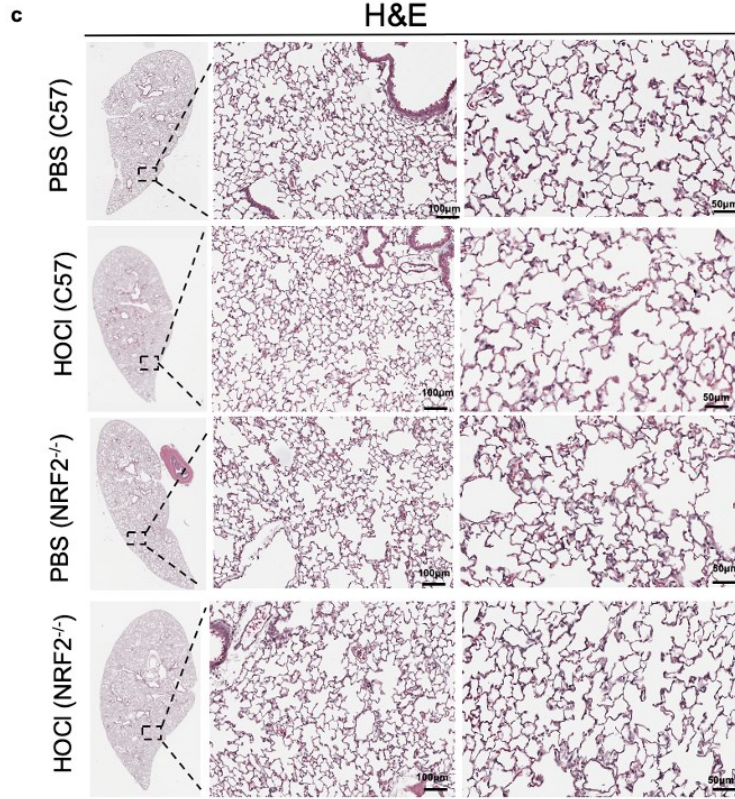


Figure 16. HOCl injections neither impaired lung function nor induced lung fibrosis in Nrf2^{-/-} mice.

a. Mean pressure-volume (P-V) loops for C57BL/6 and Nrf2^{-/-} mice injected with either PBS or HOCl. **b.** Static lung compliance (C_{st}) $n=4-6$ mice per group, graphs show mean \pm SEM. Mann-Whitney test, $p=0.09$. Micrographs of H&E (**c**) and PSR (**d**)-stained lung sections. $n=4-6$ animals per group. Images were obtained to show an overview of the lung and at $\times 20$ and $\times 40$ magnification (from left to right). Scale bar: 100 μm ($\times 20$ magnification) and 50 μm ($\times 40$ magnification). Abbreviations: ns: not significant.

3.2.4 The effect of HOCl on BAL leukocytes in Nrf2^{-/-} mice

It was previously shown that the Nrf2 pathway is involved in attenuating lung inflammation in BLM induced injury.^{145,146} Therefore, in the absence of Nrf2, inflammatory responses are expected to increase. We assessed whether NRF2^{-/-} mice had increased airway inflammation by analyzing total and differential cell counts in BALF. Compared to wild type C57BL/6 HOCl mice, total cells were not increased in Nrf2^{-/-} HOCl mice (C57BL/6 HOCl vs Nrf2^{-/-}, absolute number of cells: 34167 ± 2626 vs 30400 ± 2064) (Figure 17). Moreover, there were no differences in the number of macrophages, eosinophils, neutrophils, and lymphocytes between these two groups. These data show that HOCl-generated oxidative stress does not play a role in the development of pulmonary inflammation following intradermal HOCl administration.

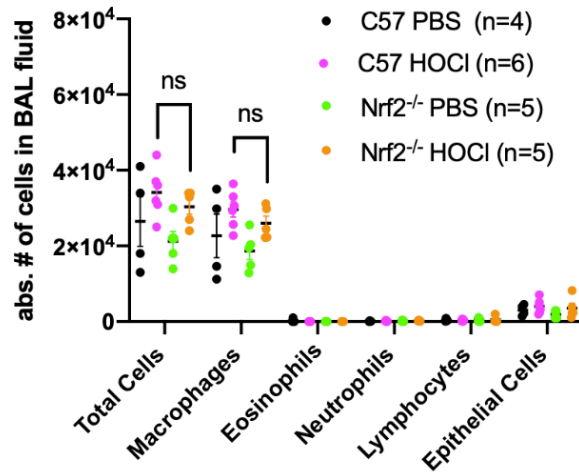


Figure 17. HOCl treatment did not induce lung inflammation in Nrf2^{-/-} mice. Total and differential cell counts in BALF of C57BL/6 and Nrf2^{-/-} mice injected with HOCl and PBS. *n*=4-6 mice per group, graphs show mean ± SEM. Two-way ANOVA, *p*>0.05.

3.3 BLM-MP mouse model

3.3.1 Effect of different BLM doses on body weight and lung function

Since neither the described HOCl-SSc model nor the sensitized (NRF2^{-/-}) model recapitulate pulmonary fibrosis, we switched to the BLM-MP, a SSc mouse model that is suggested to recapitulate two key features of human SSc: lung and skin fibrosis. We first established the optimal dose of BLM to be used testing doses reported in previous papers (i.e. 60mg/kg, 67mg/kg and 100mg/kg).^{116,117} BLM induced a dose-dependent reduction in body weight in the first 14 days post pump implantation. Weight recovery started on day 15/16 for doses of 60mg/kg and 67mg/kg, respectively. A precipitous decline in body weight was observed in mice receiving 100mg/kg with 50% mortality. No mortality was observed in mice receiving 60mg/kg and 67mg/kg (Figure 18). Regarding lung function, BLM induced a dose dependent reduction in compliance and an increase

in resistance and elastance (Figure 19, a-d). We selected the dose of 60mg/kg for subsequent experiments.

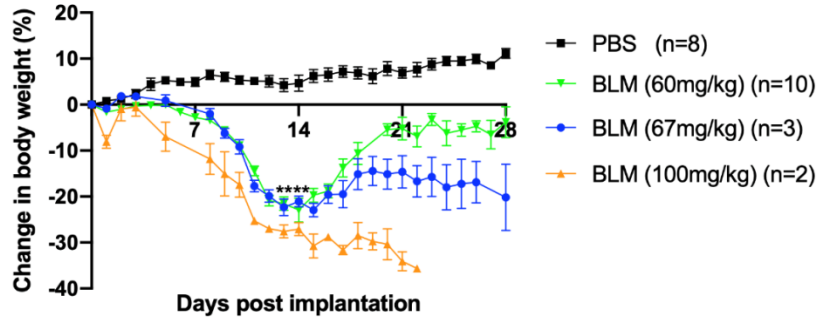


Figure 18. Time course of percent body weight change following exposure to different bleomycin doses or saline treatment. $n=2-10$ mice per group, graphs show mean \pm SEM. Two-way ANOVA, **** $p < 0.0001$.

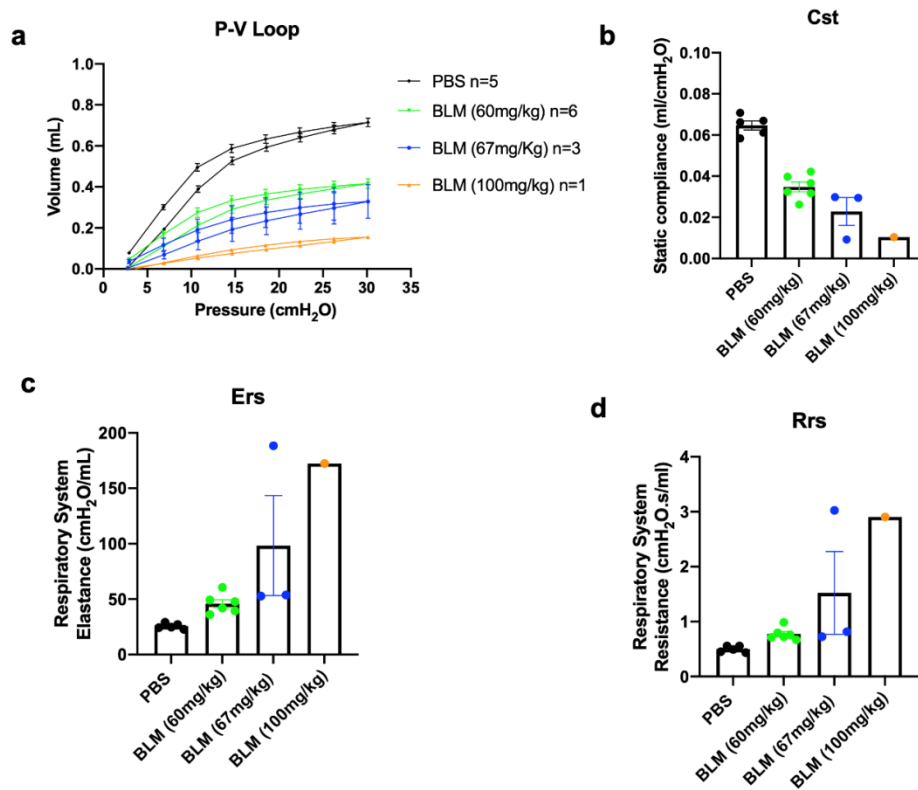


Figure 19. Dose dependent decline in lung function associated with increasing BLM doses. **a.** Mean pressure-volume (P-V) loops for PBS and BLM-treated mice. **b.** Static lung compliance (C_{st}) **c.** Respiratory system elastance (E_{rs}) and resistance (R_{rs}) (**d**) $n=1-6$ mice per group, graphs show mean \pm SEM.

3.3.2 Skin changes following systemic administration of BLM

BLM-MP treated animals develop skin fibrosis.^{117,118} This was confirmed in our model. BLM treated animals had ulcers lined with granulation tissue (Figure 20, panel A; H&E, BLM-MP, panel *i*), epidermal hyperplasia and hyperkeratosis (Figure 20, panel A; H&E, BLM-MP, panel *ii*). There was evidence of skin fibrosis in areas proximal and distal to the minipump (Figure 20, panel A; PSR, BLM-MP, panel *i&ii*). Preliminary results ($n=3$ per group) on the quantification of PSR-stained slides showed increased dermal thickness in BLM-MP animals (Figure 20, panel B).

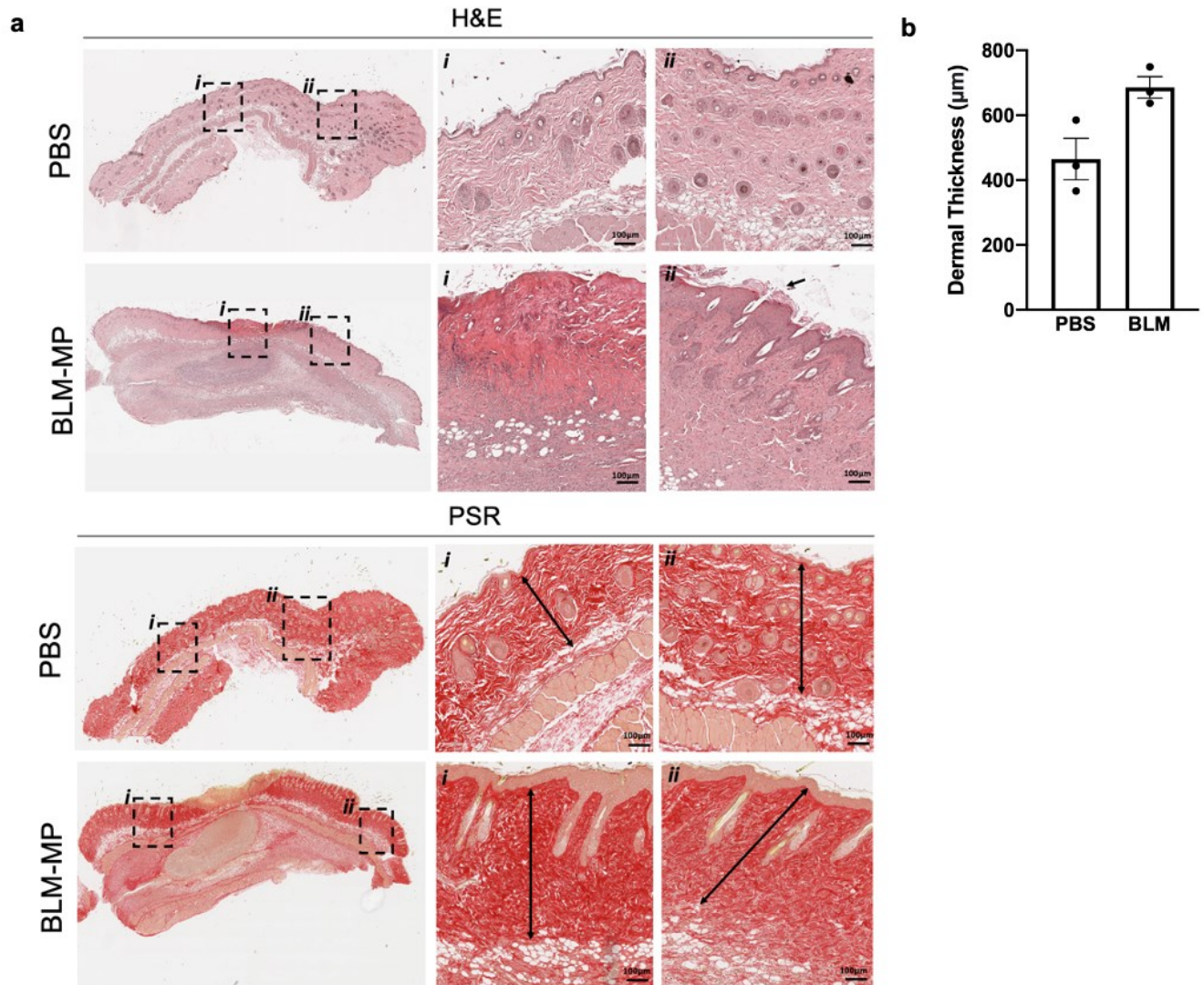


Figure 20. Systemic administration of bleomycin via minipump leads to skin fibrosis. **a.** Representative skin images of H&E and PSR-stained sections of PBS and BLM-treated mice. Images show a skin overview (first micrograph in each row) and $\times 20$ magnification. Scale bar: 100 μm . **b.** H&E sections of BLM-MP mice show an area of ulceration (panel *i*), epidermal hyperplasia and hyperkeratosis indicated by the black arrow (H&E stained sections, BLM-MP row, panel *ii*). Black arrows in the PSR- stained sections show dermal thickness measurements. **b.** Dermal thickness quantification, graph shows mean \pm SEM. $n=3$ mice per group.

3.3.3 Lung function, histology, and micro-CT following BLM administration

The degree of lung injury induced by bleomycin was evaluated by histology, pulmonary function tests and micro-CT imaging. Four weeks post pump implantation, BLM-MP mice had decreased lung compliance, increased resistance, and dynamic elastance compared to control animals (Figure 21, panels a-d). H&E-stained lung sections showed a predominantly inflammatory process with minimal evidence of fibrosis. The distribution of parenchymal injury was largely peripheral which resembles the pattern in ILD (Figure 21, e). In the histology quantification, BLM-MP animals tend to have higher number of positive picosirius red pixels and affected lung area (Figure 21, f & g). The presence of increased areas of attenuation on micro CT corroborated the BLM-induced lung injury (Figure 22, a-d). Notably, on day 14 BLM-MP mice had restrictive lung function whereas histology showed minimal architectural abnormalities (Figure 23). Compared to 28 days post pump implantation, on day 38 an improvement in lung function was observed; however, histological changes were comparable between the two days (Figure 24).

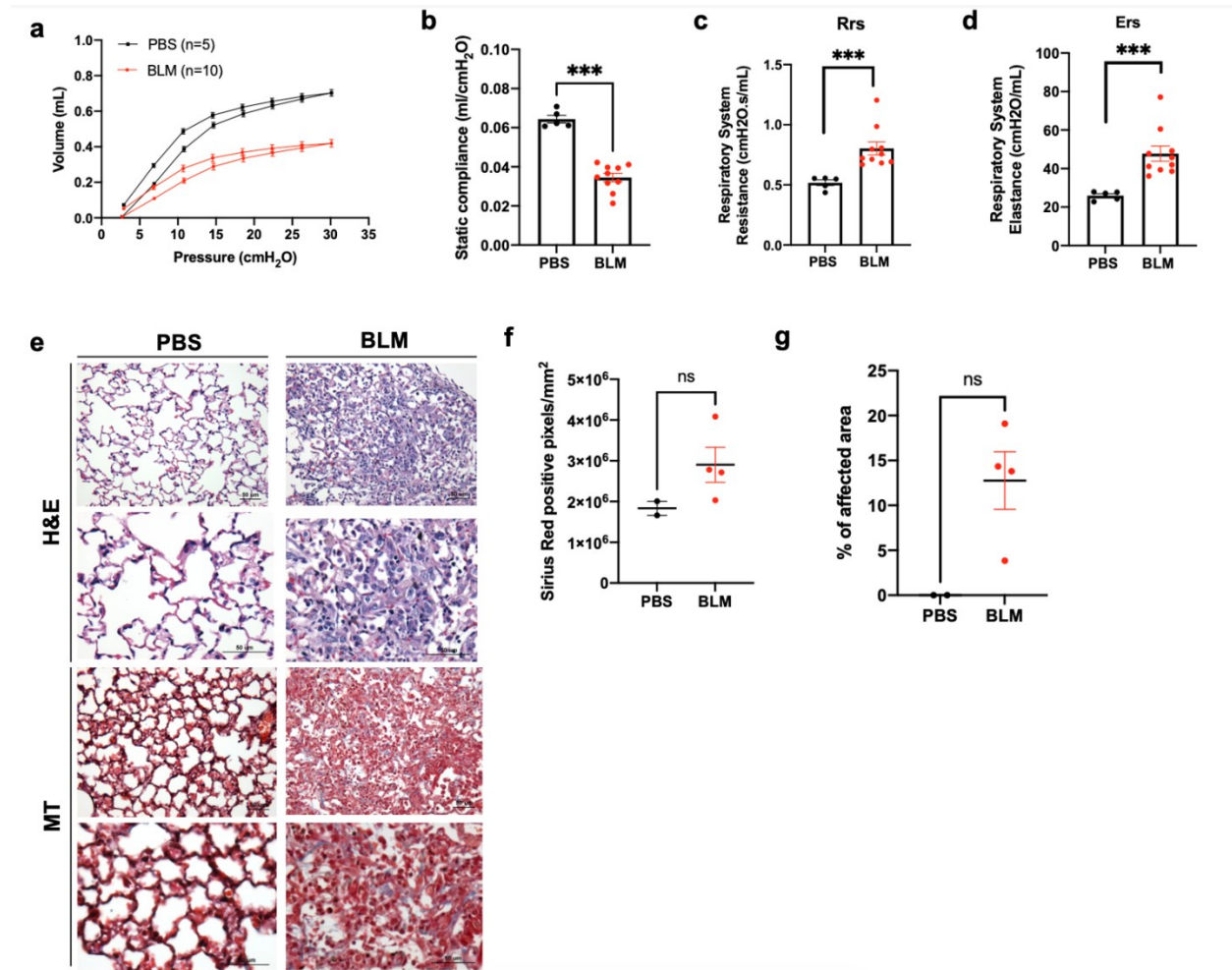


Figure 21. 28 days post pump implantation BLM impairs lung mechanics as it generates interstitial inflammation with few fibroblastic foci. **a**. Mean pressure-volume (P-V) loops for PBS and BLM-treated mice. **b**. Static lung compliance (C_{st}). **c**. Lung resistance (R_{rs}) and elastance (E_{rs}) (**d**.) calculated by the flexiVent software by fitting the data from the single frequency forced oscillation manoeuvre to the single-compartment model. $n=5-10$ mice per group, graphs show mean \pm SEM. Two tailed t test, * $p < 0.005$ **e**. Hematoxylin and eosin (HE) and Masson's Trichrome (MT)- stained lung sections. First row of HE and MT $\times 20$ images and bottom row $\times 40$ magnification. Scale bar: 50 μm . **f**. Image analysis on PSR-stained slides and **g**. Abnormal lung areas quantified by the Positive Pixel Count V9 Aperio Algorithm (airways and large vessels were excluded). Three

transverse sections per left lung were analyzed (lower, middle, upper lobe). Mann-Whitney U Test was used for comparisons. Abbreviations: ns: not significant.

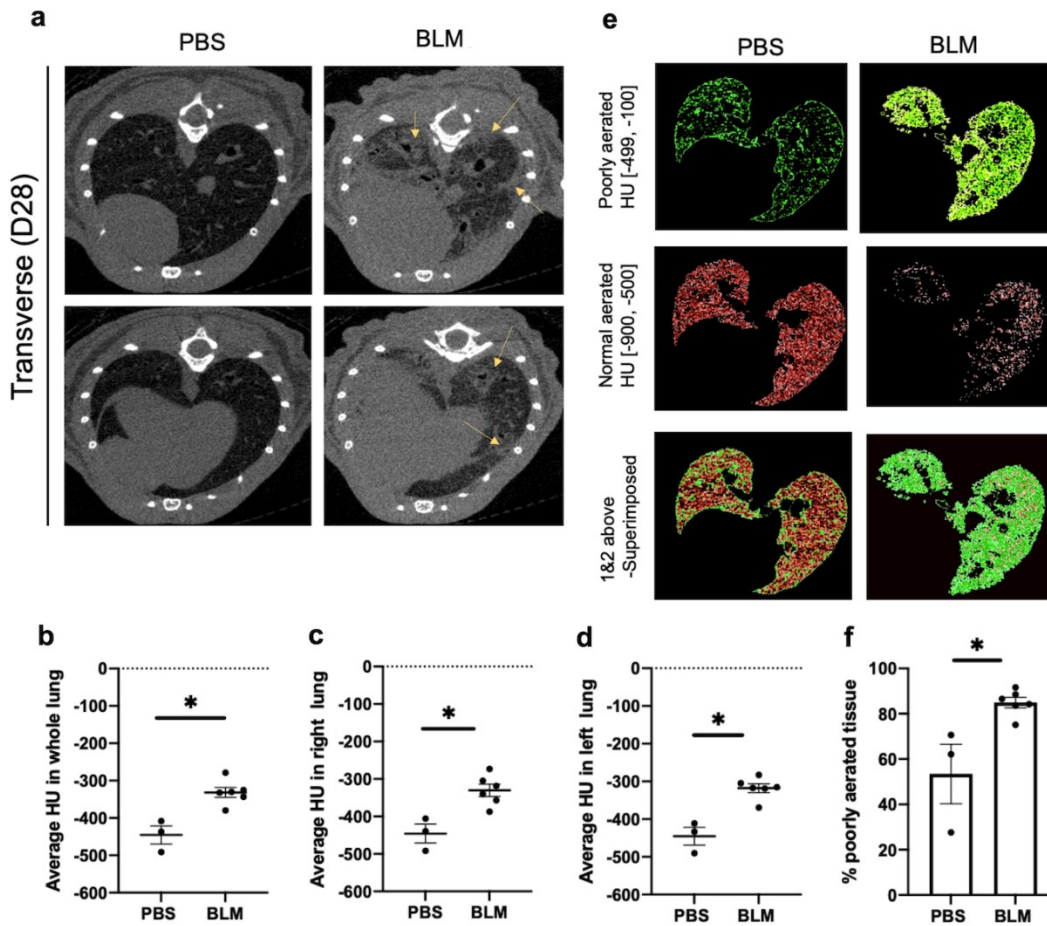


Figure 22. Osmotic minipump delivery of BLM increases lung density and the percent of poorly aerated tissue. **a**. Representative micro-CT scans of PBS and BLM animals. Yellow arrows indicate areas of increased lung attenuation. Density of lung parenchyma in whole lung (**b**), right lung (**c**) and left lung (**d**). **e**. Micro-CT scans of BLM mice evaluated with the image analysis software AMIDE have increase in poorly- aerated tissue. **f**. Quantification of poorly aerated tissue according to Hounsfield units (HU) range assessed with the MATLAB software. $n=3-6$ mice per group, graphs show \pm SEM. Two tailed t test, * $p < 0.05$

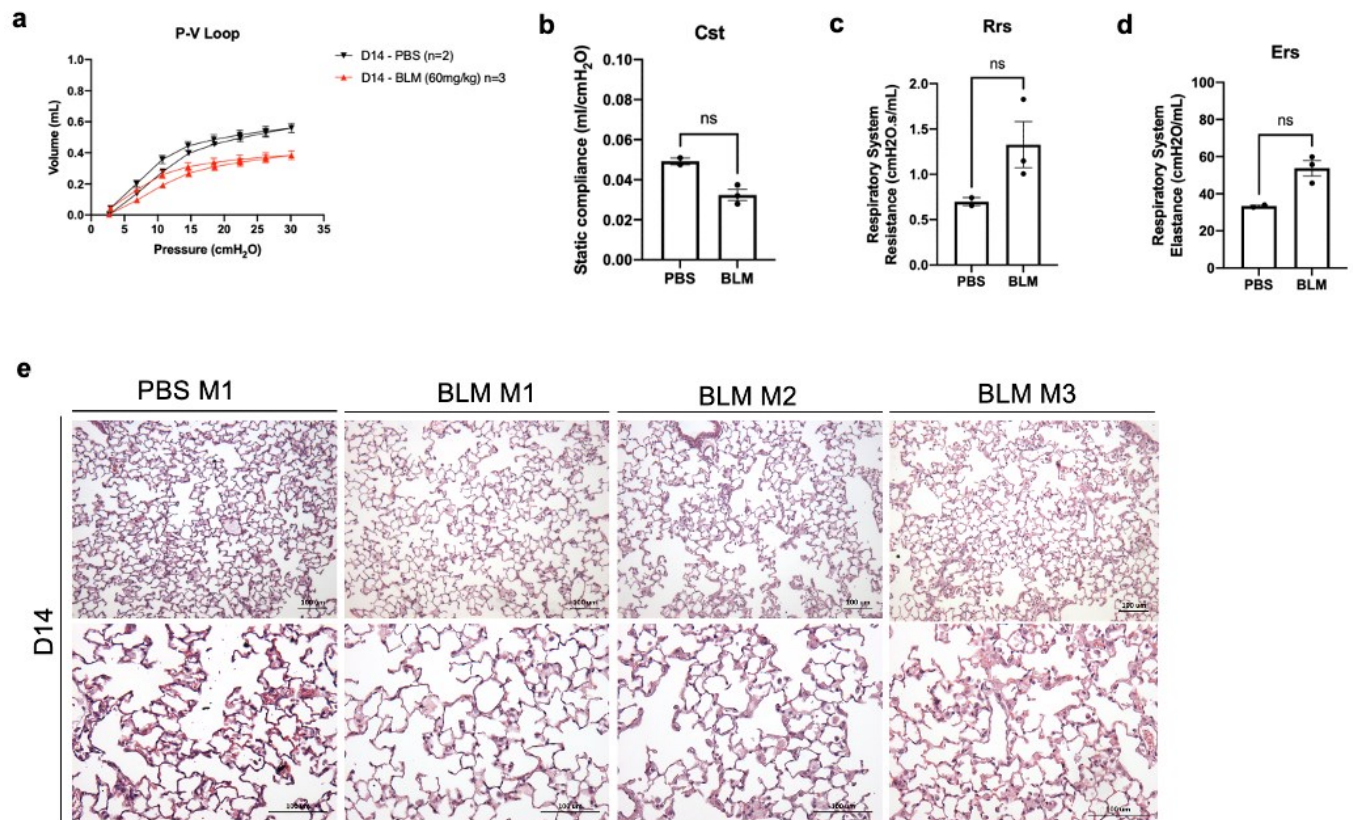


Figure 23. 14 days post pump implantation BLM impairs lung mechanics in the absence of evident fibrosis. **a.** Mean pressure-volume (P-V) loops for PBS and BLM-treated mice. **b.** Static lung compliance (C_{st}). **c.** Lung resistance (Rrs) and elastance (Ers) (**d.**). $n=2-3$ mice per group, graphs show \pm SEM. **e.** Hematoxylin and eosin (HE)- stained lung sections. First row of HE $\times 20$ images and bottom row $\times 40$ magnification. Scale bar: 100 μ m.

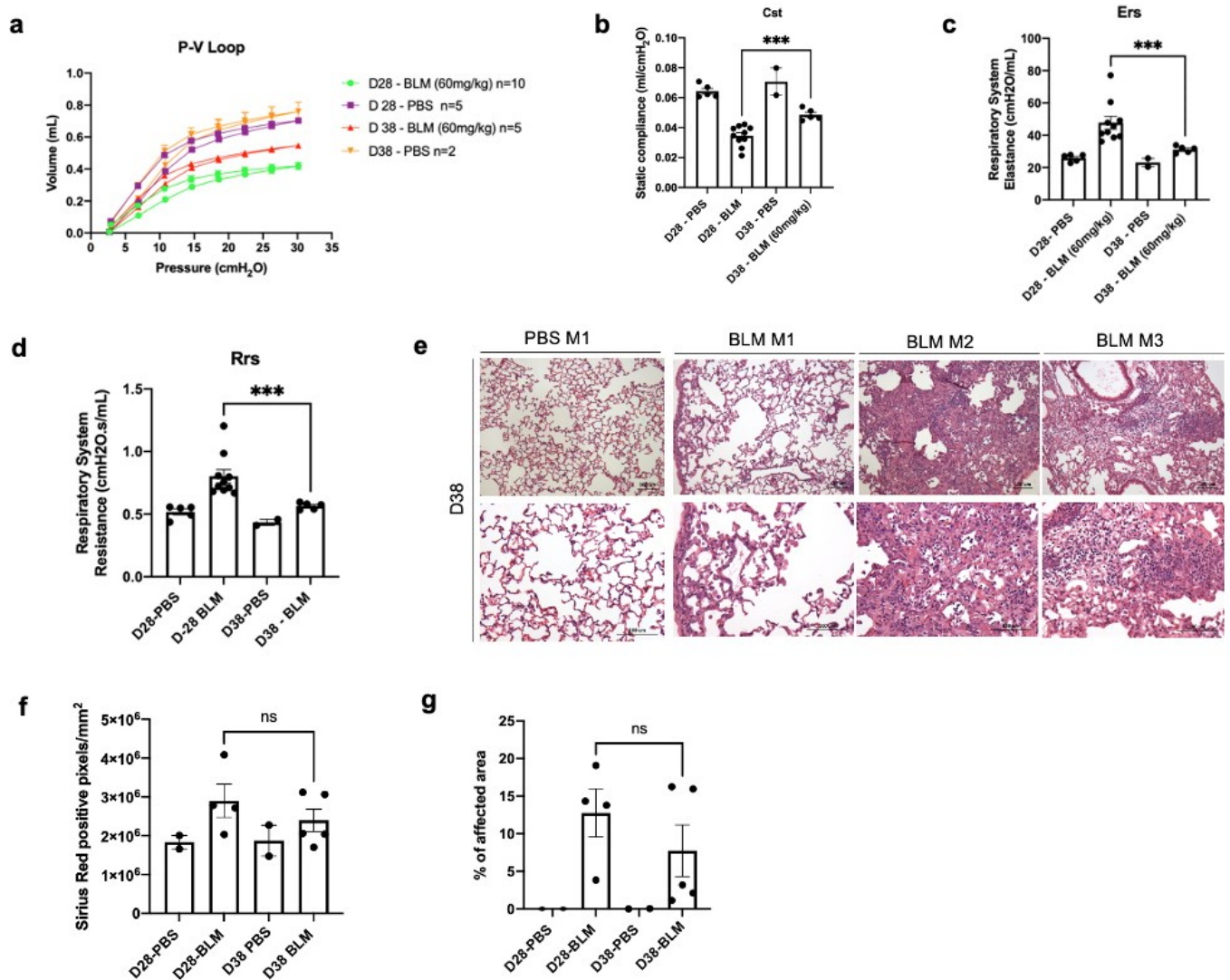


Figure 24. 38 days post pump implantation lung function in BLM-MP mice improved while histological changes were similar to day 28. **a.** Mean pressure-volume (P-V) loops for PBS and BLM-treated mice at day 28 and 38. **b.** Static lung compliance (C_{st}). **c.** and **d.** Lung elastance (E_{rs}) and resistance (R_{rs}) calculated by the flexiVent software. *** $n=5-10$ mice per group, graphs show \pm SEM, Two tailed t test, *** $p=7 \times 10^{-4}$ **e.** Hematoxylin and eosin (HE)- stained lung sections. First row of HE images were obtained at $\times 20$ and bottom row at $\times 40$ magnification. Scale bar: 100 μ m. **f.** Image analysis on PSR-stained slides and **g.** abnormal lung areas according to the Positive Pixel Count V9 Aperio Algorithm (airways and large vessels were excluded). Three transverse

sections per left lung were analyzed (lower, middle, upper lobe). n= 2-5 mice per group, graphs depict mean \pm SEM. Abbreviations: ns: not significant.

Chapter 4: Discussion

Animal models are valuable for studying mechanisms of human diseases and for testing potential therapeutic interventions. However robust animal models of SSc are scarce. We performed an in-depth characterization of two models favoured in the literature - the HOCl-SSc^{87,89} and BLM-MP mouse model.¹¹⁶ Over the course of 6 weeks, the body weight of HOCl-injected mice remained unchanged compared to PBS controls. Skin fold and dermal thickness of HOCl mice increased approximately 2- and 3-fold, respectively. Skin histology was characterized by patchy areas of fibrosis adjacent to unaffected skin. Consistent with these data, skin of HOCl-treated mice showed upregulated expression of fibrosis-related genes including *Coll1a1*, *Col3a1*, and *Acta2*. However, pertaining to the lungs, there were no differences in static compliance, histology, expression of pro-fibrotic genes, and immune cell compositions between PBS and HOCl animals. Additionally, neither AOPPs nor anti-Scl70 were elevated in the sera of HOCl mice. Furthermore, to test the hypothesis that a model that enhances the oxidative damage caused by HOCl results in lung fibrosis, experiments were conducted using the *Nrf2*^{-/-} mouse. *Nrf2*^{-/-} mice that received HOCl injections had comparable body weight, skin fibrosis, lung function, lung histology and BALF cellularity to *Nrf2*^{-/-} controls. In contrast, BLM-MP mice lost approximately 20% of their body weight within 15 days of pump implantation which was followed by a gradual recovery until day 28. Analogous to the HOCl model, BLM induced heterogeneous skin fibrosis with increased dermal thickening. Twenty-eight days after pump implantation lung histology showed a pattern of injury that was predominately inflammatory with some evidence of patchy fibrosis. As a result, these mice had significant lung function impairment and micro-CT abnormalities. Interestingly, lung function impairment was also observed 14 days post-pump implantation in the absence of evident histological abnormalities.

The lack of weight loss during the course of 6 weeks of HOCl injections was not previously reported in the literature. However, Dr Alexandre Maria shared with us that he did not observe any weight loss (personal communication). In contrast, BLM caused an initial drop in body weight followed by a recovery phase which was previously described in this model.¹¹⁶ Several papers also reported HOCl to induce a gradual increase in skinfold and dermal thickness within a range similar to our results.^{88,147} H&E- and MT-stained skin sections from HOCl animals showed a pattern of fibrotic injury characterized by spatial heterogeneity, epidermal hyperplasia and hyperkeratosis, consistent with prior reports^{88,125,147} and also seen in SSc patients.¹⁴⁸ In some sections fibrosis was predominantly localized to the deep reticular dermis as opposed to the papillary dermis.¹⁴⁷ It is important to emphasize that the HOCl-induced skin manifestations were only observed in the lower back of the animal where injections were administered suggesting a lack of a generalized fibrotic cutaneous response. The skin lesions induced by BLM also resulted in a phenotype resembling SSc; however, the observed effect was distal to the site of the minipump. Several papers have reported that BLM-MP mice developed skin fibrosis^{117,118}, however, this was not a uniform finding among the different groups using the model.¹¹⁹ Differences in the site of skin biopsies collection may account for those discrepancies.

Following 6 weeks of HOCl injections, the lung function of BALB/c mice remained unchanged which corresponded with the lack of morphological alterations in the lung. Although lung function measurements were not previously reported, several papers claim evidence of pulmonary fibrosis.^{88,125,149} However, an expert pulmonary pathologist (Dr Richard Fraser) reviewed the published images of lung histology and could not definitively confirm the presence of fibrosis.

Poor lung inflation with areas of atelectasis¹⁵⁰ and thick histological sections were noted and suggested architectural abnormalities that could account for erroneous interpretations of putative lung fibrosis. We also performed automated and manual image analysis, which was not previously conducted, on PSR-stained lung sections and no differences were detected between PBS- and HOCl-injected mice. Assessment of inflammatory cells in the BAL fluid did not show any evidence of an inflammatory response in HOCl-injected mice. We proceeded to characterize macrophage subsets in PBS and HOCl treated mice as macrophages are known to influence mechanisms of fibrosis.^{151,152} Although there is a dearth of data on human macrophages, the characterization of monocyte/macrophages in murine models reveals three distinct subsets: tissue resident alveolar macrophages (TR-AM), monocyte derived alveolar macrophages (Mo-AM), and interstitial macrophages (IM).¹⁵¹ TR-AM are a long lived, self-renewing population that is derived from cells that originate in the fetal liver and yolk sac.¹⁵³ They are in close contact with type I and type II alveolar epithelial cells and express high levels of CD11c and low levels CD11b.¹⁵² Under normal conditions TR-AM are the most abundant immune cell in the lung. Conversely, in the setting of lung inflammation, circulating monocytes are recruited to the lung via the activation of chemokine receptor 2 (CCR2) and differentiate into Mo-AMs.¹⁵¹ Initially Mo-AMs drive the inflammatory and fibrotic response; however, during repair it is proposed that Mo-AMs can either differentiate into cells that phenotypically resemble TR-AM or undergo apoptosis.¹⁵¹ Similar to TR-AM, interstitial macrophages are also derived from embryonic progenitors but reside in the lung parenchyma between the alveolar epithelium and capillaries and express high levels of CD11b and low levels of CD11c.^{151,153} Several groups reported that depletion of circulating monocytes by intratracheal administration of liposomal clodronate¹⁵⁴ or using monocyte-chemoattractant protein-1 chemokine receptor knockout animals (CCR2^{-/-})¹⁵⁵ attenuated BLM-induced lung injury.

These findings show that monocytes contribute to facilitating the progression of lung fibrosis. It has been suggested that monocytes differentiate into Mo-AMs and in combination with TR-AM acquire a profibrotic phenotype.¹⁵¹ Indeed, inducing cell death of Mo-AM ameliorates the severity of lung fibrosis.¹⁵² Following 42 days of HOCl injections, an increase in the number of Mo-AM was expected provided the literature showing that Mo-AMs are causally related to fibrosis severity.¹⁵² During the fibrotic phase of BLM-induced lung injury, a decrease in the number of interstitial macrophages and an increase in the number of Mo-AM was reported.¹⁵¹ This is likely attributed to the large inflammatory response induced by BLM which causes the loss of most macrophages present under homeostatic conditions (TR-AM and IM) and their replacement by Mo-AM. The absence of an inflammatory response in our HOCl model contrasts with a previous report which showed increased CD4⁺ and CD8⁺ T cells, and CD19⁺ B cells in the lung by immunohistochemical analysis.¹⁵⁶ Moreover, we did not observe an upregulation of profibrotic genes in HOCl-injected mice whereas the mRNA expression of *α SMA*, *TGF- β 1*, and *collagen type I* and *III* were upregulated in previous studies.^{88,91}

HOCl has been proposed to generate lung fibrosis through excess formation of reactive oxygen species (ROS) and the induction of oxidative stress. Specifically, oxidized serum proteins (i.e. AOPPs) were suggested to be involved in the propagation of oxidative stress from the skin to the lungs.⁸⁹ However, our experiments showed that administering HOCl by the intradermal route does not induce the development of AOPPs. It is known that prolonged exposure to ROS results in oxidative stress. In this case, there is an imbalance between the production of ROS and cellular antioxidant defense mechanisms. Since we did not observe elevated AOPPs following HOCl injections, we hypothesized that the ROS generated by HOCl is countered by physiological antioxidant defense mechanisms that maintain redox homeostasis. The antioxidant response

element (ARE) is a regulatory enhancer sequence present in the promoters of many antioxidant genes and Phase II detoxifying enzymes (i.e. glutathione S-transferases).¹⁵⁷ Many transcription factors interact with the ARE to induce the expression of cytoprotective genes in response to oxidative stress, one of which is Nrf2.¹⁵⁷ Under homeostatic conditions, Nrf2 is sequestered in the cytoplasm by Kelch-like ECH-associated protein 1 (Keap1) resulting in E3 ligase mediated polyubiquitination of the complex and subsequent proteosomal degradation.¹⁵⁷ When the cellular redox potential is altered by oxidative stress conditions, Keap 1 undergoes a conformational change and is no longer able to bind Nrf2.¹⁵⁷ This allows Nrf2 to translocate into the nucleus where it dimerizes with the transcriptional co-activator musculoaponeurotic fibrosarcoma oncogene homolog (MAF) and this complex binds to the ARE within the promoter region of cytoprotective genes to activate their transcription.¹⁵⁷ Cytoprotective genes regulated by Nrf2 include genes involved in redox homeostasis (i.e. glutathione peroxidase 2 and thioredoxin), glutathione biosynthesis (i.e. glutamate-cysteine ligase catalytic subunit), detoxification of xenobiotics (glutathione s-transferase).¹⁵⁸ Given that Nrf2 regulates the transcription of a vast array of antioxidant genes, to test the hypothesis that deficient antioxidant responses increase the skin and lung toxicity of intradermal HOCl, we subjected Nrf2^{-/-} animals to daily HOCl injections, which should increase intracellular ROS levels. Nrf2^{-/-} animals injected with HOCl were comparable to C57BL/6 HOCl injected animals in their skin fold thickness, skin histology, dermal thickness, BAL cellularity, lung mechanics, and lung histology. Conversely, one paper reported an increase in skin thickness, collagen content in the skin and lungs, and exacerbated skin and lung pathology in Nrf2^{-/-} HOCl-treated animals.⁹¹ The lack of a positive control for the induction of oxidative stress is a limitation of our experiments.

In contrast to the HOCl-SSc mouse model, the lung function of BLM-MP animals was adversely affected. Treated animals had reduced lung compliance and an increase in elastic recoil and resistance, all of which are observations consistent with a previous report.¹⁵⁹ These observations were likely a consequence of the severe morphological alterations occurring 28- and 38-days post pump implantation, which manifested as a heterogeneous distribution of inflammatory cells in the alveolar spaces and interstitial fibrosis as previously described.¹¹⁶ However, this is an unlikely explanation for the day 14 observations where there was a profound restrictive abnormality but minimal evidence of histological involvement. This effect may be attributed to increased surface tension either due to BLM-induced alveolar type II epithelial cell injury, affecting synthesis and secretion of surfactant proteins, or injury to endothelial cells, causing leakage of plasma proteins in lung parenchyma affecting the function of surfactant molecules¹⁶⁰. The alveolar epithelium consists of two cell types: alveolar type I and type II cells.¹⁶¹ Type I cells are less abundant than type II cells but provide the major surface area of the alveoli to facilitate gas exchange.¹⁶¹ Type II cells produce surfactant and are important in alveolar epithelial repair. Surfactant is a complex mixture composed primarily of lipids (i.e phosphatidylcholine) and associated proteins (surfactant proteins A, B, C, D) that are necessary for its function of reducing surface tension.¹⁶² Between the alveolar epithelial cells and the air within the alveoli there is an aqueous layer which forms an air-liquid interface within the lung.¹⁶¹ This is the site where surface tension occurs.¹⁶¹ Water molecules within the bulk of the liquid solution are surrounded by other water molecules in each direction, resulting in a net attractive force of zero on a given water molecule. However, water molecules located immediately at the air-liquid interface have a net attraction into the bulk of the liquid (downwards) due to the lack of water molecules above them. This downward force causes high surface tension and promotes the aggregation of water molecules in order to reduce the overall

surface area exposed to air. As a consequence of this high surface tension, the alveoli have a tendency to collapse therefore inhibiting gas exchange^{162,163}. To reduce this surface tension within the lungs, a lipoprotein complex termed pulmonary surfactant is produced. Specifically, surfactant can reduce surface tension through adsorption, the process in which surfactant lipids and proteins can form a surface-active film at the air liquid interface of alveoli. Since surfactants are amphiphilic molecules, they are able to orient themselves at the air liquid interface with their hydrophobic acyl tails directed towards the airspace and their hydrophilic polar head groups towards the hypophase (thin layer of fluid that is in contact with the air). In this orientation, the hydrophilic heads can displace the water molecules and reduce surface tension. Type I cells are fairly susceptible to injury and when they are damaged the reparative process involves hyperplasia and proliferation of type II cells and their subsequent differentiation to alveolar type I cells.¹⁶¹ However, in lung fibrosis, type II cells are damaged which can impair their ability to produce surfactant resulting in decreased compliance.^{164,165} Specifically, surfactant protein C, a marker of type II alveolar epithelial cells, was found to be important not only for the biophysical function of surfactant but for lung function as well.¹⁶⁶ Mice receiving two doses of BLM via minipump showed a reduction in the number of SP-C positive cells whereas an increase was observed in BLM-treated mice that received keratinocyte growth factor (KGF), a potent mitogen for type II alveolar cells.¹⁶⁷ These findings suggest that BLM reduces the number of type II alveolar cells which is restored by the administration of KGF.¹⁶⁷ Furthermore, intratracheal transplantation of alveolar type II cells has been shown to stop and reverse BLM-induced lung fibrosis suggesting these cells are damaged or lost during fibrotic lung injury.¹⁶⁸

In conclusion, despite administering HOCl intradermally following published protocols we were unable to reproduce the putative lung fibrosis. Despite sensitizing the model to the potential development of fibrosis by studying Nrf2^{-/-} mice with defective antioxidant responses, there was no lung pathology identified by careful histological examination, quantification of lung collagen and lung function. In contrast, systemic bleomycin administration led to functional and histological skin and lung fibrotic changes. Early in the development of bleomycin induced lung damage there was evidence of a restrictive impairment, which was not accompanied by histological abnormalities, leading us to conclude that disruption of surfactant function or synthesis was the likely explanation for the findings. Further study of microvascular permeability will help to clarify the basis for the early impairment in lung function. To assess vascular permeability, Evans blue dye may be injected in mice intravenously which binds to circulating albumin.¹⁶⁹ The accumulation of the dye in the lung can be visualized macroscopically (lungs with increased permeability will appear dark blue) or quantified by spectrophotometry.¹⁶⁹ Fibrinogen levels in BAL fluid can also be measured by ELISA to determine whether BLM induces microvascular leakage. Similarly, an assessment of alveolar type II cell apoptosis may prove to be informative. Apoptosis will be assessed by terminal deoxynucleotidyl transferase dUTP nick end labeling (TUNEL) staining. Although several papers have reported spontaneous resolution in the BLM model, some have shown that fibrosis persists for extended periods.^{170,171} Since the lung injury observed following BLM is largely inflammatory, we may quantify fibrosis in MT-stained lung sections and measure hydroxyproline content at a later time point (e.g. day 49) to determine whether more established fibrotic lesions will develop. Compared to a single BLM intratracheal instillation, a multiple dose regimen resulted in greater lung fibrosis and reduced inflammation.¹⁷² Therefore, administering a second dose of BLM following minipump implantation may prove to

be effective in obtaining a predominantly fibrotic lesion. Alternatively, the effect of prolonged infusion of BLM (e.g. infusion over 4 weeks as opposed to 7 days) can be tested.

We found that HOCl-injected mice developed a SSc-like skin phenotype without pulmonary involvement. In the skin of HOCl mice, the subcutaneous fat tissue was partly replaced by connective tissue resulting in increased dermal thickness. Lungs from HOCl-injected mice did not display any histological abnormalities and there was no evidence of functional impairment. The basis for the discrepancy between our pulmonary findings and those described in the literature is not clear. However, it should be noted that the lung phenotype in this model has not been sufficiently characterized. Prior publications do not report lung function measurements nor histological quantification of lung fibrosis, both of which can provide a more accurate assessment. Studies have frequently relied upon the measurement of hydroxyproline, an indirect surrogate for collagen synthesis. Our findings can inform the research community to discourage experiments employing this model as a means to study the pathogenesis and treatment of pulmonary fibrosis. The HOCl mouse can be used to model SSc-like skin fibrosis; however, given the heterogeneity in fibrotic lesions, investigators should be cautious and selective in their readouts when testing the effect of potential interventions. Following these unexpected results, we proceeded to characterize the BLM-MP model. BLM-MP mice developed skin fibrosis as well as lung features reminiscent of human NSIP. These structural changes manifested in severe functional impairment characterized by restrictive lung function and increased lung density on micro-CT. This model has greater promise for the study of the contribution of inflammation to the fibrotic phenotype and can enable the testing of antifibrotic agents.

References

- 1 Cottin, V. *et al.* Presentation, diagnosis and clinical course of the spectrum of progressive-fibrosing interstitial lung diseases. *European Respiratory Review* **27**, 180076, doi:10.1183/16000617.0076-2018 (2018).
- 2 C, M.-M., H, R. & C, H. - Interstitial Lung Diseases. *Multislice CT* **24**, 261-288 (2017).
- 3 Cottin, V. *et al.* Fibrosing interstitial lung diseases: knowns and unknowns. *European Respiratory Review* **28**, 180100, doi:10.1183/16000617.0100-2018 (2019).
- 4 Olson, A. *et al.* Estimation of the Prevalence of Progressive Fibrosing Interstitial Lung Diseases: Systematic Literature Review and Data from a Physician Survey. *Adv Ther* **38**, 854-867, doi:10.1007/s12325-020-01578-6 (2021).
- 5 Faverio, P. *et al.* Management of acute respiratory failure in interstitial lung diseases: overview and clinical insights. *BMC Pulm Med* **18**, 70, doi:10.1186/s12890-018-0643-3 (2018).
- 6 Antoniou, K. M. *et al.* Interstitial lung disease. *European Respiratory Review* **23**, 40, doi:10.1183/09059180.00009113 (2014).
- 7 Travis, W. D. *et al.* An official American Thoracic Society/European Respiratory Society statement: Update of the international multidisciplinary classification of the idiopathic interstitial pneumonias. *Am J Respir Crit Care Med* **188**, 733-748, doi:10.1164/rccm.201308-1483ST (2013).
- 8 Bairkdar, M. *et al.* Incidence and prevalence of systemic sclerosis globally: a comprehensive systematic review and meta-analysis. *Rheumatology* **60**, 3121-3133, doi:10.1093/rheumatology/keab190 (2021).
- 9 Allanore, Y. *et al.* Systemic sclerosis. *Nat Rev Dis Primers* **1**, 15002, doi:10.1038/nrdp.2015.2 (2015).
- 10 Varga, J. & Abraham, D. Systemic sclerosis: a prototypic multisystem fibrotic disorder. *The Journal of Clinical Investigation* **117**, 557-567, doi:10.1172/JCI31139 (2007).
- 11 Abbot, S., Bossingham, D., Proudman, S., de Costa, C. & Ho-Huynh, A. Risk factors for the development of systemic sclerosis: a systematic review of the literature. *Rheumatology Advances in Practice* **2**, rky041, doi:10.1093/rap/rky041 (2018).
- 12 Johnson, S. R., Glaman, D. D., Schentag, C. T. & Lee, P. Quality of life and functional status in systemic sclerosis compared to other rheumatic diseases. *J Rheumatol* **33**, 1117-1122 (2006).
- 13 Hoffmann-Vold, A.-M., Molberg, Ø., Midtvedt, Ø., Garen, T. & Gran, J. T. Survival and Causes of Death in an Unselected and Complete Cohort of Norwegian Patients with Systemic Sclerosis. *The Journal of Rheumatology* **40**, 1127, doi:10.3899/jrheum.121390 (2013).
- 14 Distler, O. *et al.* Predictors of progression in systemic sclerosis patients with interstitial lung disease. *European Respiratory Journal* **55**, 1902026, doi:10.1183/13993003.02026-2019 (2020).
- 15 Hao, Y. *et al.* Early Mortality in a Multinational Systemic Sclerosis Inception Cohort. *Arthritis Rheumatol* **69**, 1067-1077, doi:10.1002/art.40027 (2017).
- 16 Khanna, D. *et al.* Diagnosis and monitoring of systemic sclerosis-associated interstitial lung disease using high-resolution computed tomography. *Journal of Scleroderma and Related Disorders*, 23971983211064463, doi:10.1177/23971983211064463 (2022).

- 17 Steele, R., Hudson, M., Lo, E. & Baron, M. Clinical decision rule to predict the presence of interstitial lung disease in systemic sclerosis. *Arthritis Care Res (Hoboken)* **64**, 519-524, doi:10.1002/acr.21583 (2012).
- 18 Ruaro, B. *et al.* High-Resolution Computed Tomography: Lights and Shadows in Improving Care for SSc-ILD Patients. *Diagnostics* **11** (2021).
- 19 Steen, V. D., Conte, C., Owens, G. R. & Medsger, T. A., Jr. Severe restrictive lung disease in systemic sclerosis. *Arthritis Rheum* **37**, 1283-1289, doi:10.1002/art.1780370903 (1994).
- 20 Steen, V. D., Owens, G. R., Fino, G. J., Rodnan, G. P. & Medsger, T. A., Jr. Pulmonary involvement in systemic sclerosis (scleroderma). *Arthritis Rheum* **28**, 759-767, doi:10.1002/art.1780280706 (1985).
- 21 Vonk, M. C. *et al.* Natural variability in the disease course of SSc-ILD: implications for treatment. *European Respiratory Review* **30**, 200340, doi:10.1183/16000617.0340-2020 (2021).
- 22 Fischer, A. *et al.* Clinically Significant Interstitial Lung Disease in Limited Scleroderma: Histopathology, Clinical Features, and Survival. *Chest* **134**, 601-605, doi:<https://doi.org/10.1378/chest.08-0053> (2008).
- 23 Hansell, D. M. *et al.* Fleischner Society: glossary of terms for thoracic imaging. *Radiology* **246**, 697-722, doi:10.1148/radiol.2462070712 (2008).
- 24 Bouros, D. *et al.* Histopathologic subsets of fibrosing alveolitis in patients with systemic sclerosis and their relationship to outcome. *Am J Respir Crit Care Med* **165**, 1581-1586, doi:10.1164/rccm.2106012 (2002).
- 25 Visscher, D. W. & Myers, J. L. Histologic Spectrum of Idiopathic Interstitial Pneumonias. *Proceedings of the American Thoracic Society* **3**, 322-329, doi:10.1513/pats.200602-019TK (2006).
- 26 Fischer, A., Patel, N. M. & Volkmann, E. R. Interstitial Lung Disease in Systemic Sclerosis: Focus on Early Detection and Intervention. *Open Access Rheumatol* **11**, 283-307, doi:10.2147/oarr.S226695 (2019).
- 27 Di Saia, P. J. C. W. T. M. R. S. M. S. M. D. G. Clinical gynecologic oncology. (2018).
- 28 Tashkin, D. P. *et al.* Cyclophosphamide versus Placebo in Scleroderma Lung Disease. *New England Journal of Medicine* **354**, 2655-2666, doi:10.1056/NEJMoa055120 (2006).
- 29 Tashkin, D. P. *et al.* Mycophenolate mofetil versus oral cyclophosphamide in scleroderma-related interstitial lung disease (SLS II): a randomised controlled, double-blind, parallel group trial. *Lancet Respir Med* **4**, 708-719, doi:10.1016/s2213-2600(16)30152-7 (2016).
- 30 Poormoghim, H. *et al.* Systemic sclerosis: comparison of efficacy of oral cyclophosphamide and azathioprine on skin score and pulmonary involvement-a retrospective study. *Rheumatol Int* **34**, 1691-1699, doi:10.1007/s00296-014-3026-y (2014).
- 31 Hoyles, R. K. *et al.* A multicenter, prospective, randomized, double-blind, placebo-controlled trial of corticosteroids and intravenous cyclophosphamide followed by oral azathioprine for the treatment of pulmonary fibrosis in scleroderma. *Arthritis Rheum* **54**, 3962-3970, doi:10.1002/art.22204 (2006).
- 32 Wallace, B., Vummidi, D. & Khanna, D. Management of connective tissue diseases associated interstitial lung disease: a review of the published literature. *Curr Opin Rheumatol* **28**, 236-245, doi:10.1097/bor.0000000000000270 (2016).

- 33 Smith, V. *et al.* Rituximab in diffuse cutaneous systemic sclerosis: an open-label clinical and histopathological study. *Annals of the Rheumatic Diseases* **69**, 193, doi:10.1136/ard.2008.095463 (2010).
- 34 Lafyatis, R. *et al.* B cell depletion with rituximab in patients with diffuse cutaneous systemic sclerosis. *Arthritis Rheum* **60**, 578-583, doi:10.1002/art.24249 (2009).
- 35 Bosello, S. *et al.* B cell depletion in diffuse progressive systemic sclerosis: safety, skin score modification and IL-6 modulation in an up to thirty-six months follow-up open-label trial. *Arthritis Res Ther* **12**, R54, doi:10.1186/ar2965 (2010).
- 36 Elhai, M. *et al.* Outcomes of patients with systemic sclerosis treated with rituximab in contemporary practice: a prospective cohort study. *Annals of the Rheumatic Diseases* **78**, 979, doi:10.1136/annrheumdis-2018-214816 (2019).
- 37 Sircar, G., Goswami, R. P., Sircar, D., Ghosh, A. & Ghosh, P. Intravenous cyclophosphamide vs rituximab for the treatment of early diffuse scleroderma lung disease: open label, randomized, controlled trial. *Rheumatology (Oxford)* **57**, 2106-2113, doi:10.1093/rheumatology/key213 (2018).
- 38 Ebata, S. *et al.* Rituximab therapy is more effective than cyclophosphamide therapy for Japanese patients with anti-topoisomerase I-positive systemic sclerosis-associated interstitial lung disease. *J Dermatol* **46**, 1006-1013, doi:10.1111/1346-8138.15079 (2019).
- 39 Khanna, D. *et al.* Safety and efficacy of subcutaneous tocilizumab in adults with systemic sclerosis (faSScinate): a phase 2, randomised, controlled trial. *Lancet* **387**, 2630-2640, doi:10.1016/s0140-6736(16)00232-4 (2016).
- 40 Fernandes das Neves, M., Oliveira, S., Amaral, M. C. & Delgado Alves, J. Treatment of systemic sclerosis with tocilizumab. *Rheumatology* **54**, 371-372, doi:10.1093/rheumatology/keu435 (2015).
- 41 Khanna, D. *et al.* Tocilizumab in systemic sclerosis: a randomised, double-blind, placebo-controlled, phase 3 trial. *Lancet Respir Med* **8**, 963-974, doi:10.1016/s2213-2600(20)30318-0 (2020).
- 42 King, T. E. *et al.* A Phase 3 Trial of Pirfenidone in Patients with Idiopathic Pulmonary Fibrosis. *New England Journal of Medicine* **370**, 2083-2092, doi:10.1056/NEJMoa1402582 (2014).
- 43 Richeldi, L. *et al.* Efficacy and safety of nintedanib in idiopathic pulmonary fibrosis. *N Engl J Med* **370**, 2071-2082, doi:10.1056/NEJMoa1402584 (2014).
- 44 Noble, P. W. *et al.* Pirfenidone in patients with idiopathic pulmonary fibrosis (CAPACITY): two randomised trials. *Lancet* **377**, 1760-1769, doi:10.1016/s0140-6736(11)60405-4 (2011).
- 45 Flaherty, K. R. *et al.* Nintedanib in Progressive Fibrosing Interstitial Lung Diseases. *New England Journal of Medicine* **381**, 1718-1727, doi:10.1056/NEJMoa1908681 (2019).
- 46 Richeldi, L. *et al.* Efficacy of a Tyrosine Kinase Inhibitor in Idiopathic Pulmonary Fibrosis. *New England Journal of Medicine* **365**, 1079-1087, doi:10.1056/NEJMoa1103690 (2011).
- 47 Huang, J. *et al.* Nintedanib inhibits fibroblast activation and ameliorates fibrosis in preclinical models of systemic sclerosis. *Annals of the Rheumatic Diseases* **75**, 883, doi:10.1136/annrheumdis-2014-207109 (2016).
- 48 Wollin, L., Maillet, I., Quesniaux, V., Holweg, A. & Ryffel, B. Antifibrotic and Anti-inflammatory Activity of the Tyrosine Kinase Inhibitor Nintedanib in Experimental

- Models of Lung Fibrosis. *Journal of Pharmacology and Experimental Therapeutics* **349**, 209, doi:10.1124/jpet.113.208223 (2014).
- 49 Distler, O. *et al.* Nintedanib for Systemic Sclerosis–Associated Interstitial Lung Disease. *New England Journal of Medicine* **380**, 2518-2528, doi:10.1056/NEJMoa1903076 (2019).
- 50 Conte, E. *et al.* Effect of pirfenidone on proliferation, TGF- β -induced myofibroblast differentiation and fibrogenic activity of primary human lung fibroblasts. *European Journal of Pharmaceutical Sciences* **58**, 13-19, doi:<https://doi.org/10.1016/j.ejps.2014.02.014> (2014).
- 51 Miura, Y. *et al.* Clinical experience with pirfenidone in five patients with scleroderma-related interstitial lung disease. *Sarcoidosis Vasc Diffuse Lung Dis* **31**, 235-238 (2014).
- 52 Khanna, D. *et al.* An Open-label, Phase II Study of the Safety and Tolerability of Pirfenidone in Patients with Scleroderma-associated Interstitial Lung Disease: the LOTUSS Trial. *J Rheumatol* **43**, 1672-1679, doi:10.3899/jrheum.151322 (2016).
- 53 Chambers, R. C. Preferential PDE4B Inhibition — A Step toward a New Treatment for Idiopathic Pulmonary Fibrosis. *New England Journal of Medicine* **386**, 2235-2236, doi:10.1056/NEJMe2205411 (2022).
- 54 Richeldi, L. *et al.* Trial of a Preferential Phosphodiesterase 4B Inhibitor for Idiopathic Pulmonary Fibrosis. *New England Journal of Medicine* **386**, 2178-2187, doi:10.1056/NEJMoa2201737 (2022).
- 55 Sullivan, K. M. *et al.* Systemic Sclerosis as an Indication for Autologous Hematopoietic Cell Transplantation: Position Statement from the American Society for Blood and Marrow Transplantation. *Biol Blood Marrow Transplant* **24**, 1961-1964, doi:10.1016/j.bbmt.2018.06.025 (2018).
- 56 Levy, O. *et al.* Shattering barriers toward clinically meaningful MSC therapies. *Science Advances* **6**, eaba6884, doi:10.1126/sciadv.aba6884.
- 57 Artlett, C. M. Animal models of systemic sclerosis: their utility and limitations. *Open Access Rheumatol* **6**, 65-81, doi:10.2147/oarr.S50009 (2014).
- 58 Kielty, C. M. *et al.* The Tight skin mouse: demonstration of mutant fibrillin-1 production and assembly into abnormal microfibrils. *J Cell Biol* **140**, 1159-1166, doi:10.1083/jcb.140.5.1159 (1998).
- 59 Cale, J. M., Greer, K., Fletcher, S. & Wilton, S. D. Proof-of-Concept: Antisense Oligonucleotide Mediated Skipping of Fibrillin-1 Exon 52. *Int J Mol Sci* **22** (2021).
- 60 Ramirez, F., Sakai, L. Y., Dietz, H. C. & Rifkin, D. B. Fibrillin microfibrils: multipurpose extracellular networks in organismal physiology. *Physiological Genomics* **19**, 151-154, doi:10.1152/physiolgenomics.00092.2004 (2004).
- 61 Zhou, X. *et al.* Autoantibodies to Fibrillin-1 Activate Normal Human Fibroblasts in Culture through the TGF- β Pathway to Recapitulate the “Scleroderma Phenotype”. *The Journal of Immunology* **175**, 4555, doi:10.4049/jimmunol.175.7.4555 (2005).
- 62 Long, K. B. *et al.* The Tsk2/+ mouse fibrotic phenotype is due to a gain-of-function mutation in the PIIINP segment of the Col3a1 gene. *J Invest Dermatol* **135**, 718-727, doi:10.1038/jid.2014.455 (2015).
- 63 Long, K. B., Artlett, C. M. & Blankenhorn, E. P. Tight skin 2 mice exhibit a novel time line of events leading to increased extracellular matrix deposition and dermal fibrosis. *Matrix Biology* **38**, 91-100, doi:<https://doi.org/10.1016/j.matbio.2014.05.002> (2014).

- 64 Nguyen, V. A., Sgonc, R., Dietrich, H. & Wick, G. Endothelial injury in internal organs of University of California at Davis line 200 (UCD 200) chickens, an animal model for systemic sclerosis (Scleroderma). *J Autoimmun* **14**, 143-149, doi:10.1006/jaut.1999.0355 (2000).
- 65 Aggarwal, N. R., King, L. S. & D'Alessio, F. R. Diverse macrophage populations mediate acute lung inflammation and resolution. *American Journal of Physiology-Lung Cellular and Molecular Physiology* **306**, L709-L725, doi:10.1152/ajplung.00341.2013 (2014).
- 66 Sgonc, R. & Wick, G. Pro- and anti-fibrotic effects of TGF-beta in scleroderma. *Rheumatology (Oxford)* **47 Suppl 5**, v5-7, doi:10.1093/rheumatology/ken275 (2008).
- 67 Leach, H. G., Chrobak, I., Han, R. & Trojanowska, M. Endothelial cells recruit macrophages and contribute to a fibrotic milieu in bleomycin lung injury. *Am J Respir Cell Mol Biol* **49**, 1093-1101, doi:10.1165/rcmb.2013-0152OC (2013).
- 68 Chung, L. & Utz, P. J. Antibodies in scleroderma: direct pathogenicity and phenotypic associations. *Curr Rheumatol Rep* **6**, 156-163, doi:10.1007/s11926-004-0061-9 (2004).
- 69 Eferl, R. & Wagner, E. F. AP-1: a double-edged sword in tumorigenesis. *Nature Reviews Cancer* **3**, 859-868, doi:10.1038/nrc1209 (2003).
- 70 Maurer, B. *et al.* Fra-2 transgenic mice as a novel model of pulmonary hypertension associated with systemic sclerosis. *Annals of the Rheumatic Diseases* **71**, 1382, doi:10.1136/annrheumdis-2011-200940 (2012).
- 71 Maurer, B. *et al.* Transcription factor fos-related antigen-2 induces progressive peripheral vasculopathy in mice closely resembling human systemic sclerosis. *Circulation* **120**, 2367-2376, doi:10.1161/circulationaha.109.855114 (2009).
- 72 Birnhuber, A. *et al.* IL-1 receptor blockade skews inflammation towards Th2 in a mouse model of systemic sclerosis. *European Respiratory Journal* **54**, 1900154, doi:10.1183/13993003.00154-2019 (2019).
- 73 Noda, S. *et al.* Simultaneous downregulation of KLF5 and Fli1 is a key feature underlying systemic sclerosis. *Nat Commun* **5**, 5797, doi:10.1038/ncomms6797 (2014).
- 74 Asano, Y., Bujor, A. M. & Trojanowska, M. The impact of Fli1 deficiency on the pathogenesis of systemic sclerosis. *J Dermatol Sci* **59**, 153-162, doi:10.1016/j.jdermsci.2010.06.008 (2010).
- 75 Pardali, E., Goumans, M. J. & ten Dijke, P. Signaling by members of the TGF-beta family in vascular morphogenesis and disease. *Trends Cell Biol* **20**, 556-567, doi:10.1016/j.tcb.2010.06.006 (2010).
- 76 Sonnylal, S. *et al.* Postnatal induction of transforming growth factor beta signaling in fibroblasts of mice recapitulates clinical, histologic, and biochemical features of scleroderma. *Arthritis Rheum* **56**, 334-344, doi:10.1002/art.22328 (2007).
- 77 Wang, W. *et al.* Fibroblast A20 governs fibrosis susceptibility and its repression by DREAM promotes fibrosis in multiple organs. *Nature Communications* **13**, 6358, doi:10.1038/s41467-022-33767-y (2022).
- 78 Park, M. J. *et al.* Establishment of a humanized animal model of systemic sclerosis in which T helper-17 cells from patients with systemic sclerosis infiltrate and cause fibrosis in the lungs and skin. *Exp Mol Med* **54**, 1577-1585, doi:10.1038/s12276-022-00860-7 (2022).
- 79 Shu, Y. *et al.* Both T and B cells are indispensable for the development of a PBMC transfer-induced humanized mouse model for SSc. *Arthritis Res Ther* **24**, 209, doi:10.1186/s13075-022-02896-6 (2022).

- 80 Di Guglielmo, G. M., Le Roy, C., Goodfellow, A. F. & Wrana, J. L. Distinct endocytic pathways regulate TGF-beta receptor signalling and turnover. *Nat Cell Biol* **5**, 410-421, doi:10.1038/ncb975 (2003).
- 81 Del Galdo, F. *et al.* Decreased expression of caveolin 1 in patients with systemic sclerosis: crucial role in the pathogenesis of tissue fibrosis. *Arthritis Rheum* **58**, 2854-2865, doi:10.1002/art.23791 (2008).
- 82 Drab, M. *et al.* Loss of Caveolae, Vascular Dysfunction, and Pulmonary Defects in Caveolin-1 Gene-Disrupted Mice. *Science* **293**, 2449-2452, doi:10.1126/science.1062688 (2001).
- 83 Zhao, Y. Y. *et al.* Defects in caveolin-1 cause dilated cardiomyopathy and pulmonary hypertension in knockout mice. *Proc Natl Acad Sci U S A* **99**, 11375-11380, doi:10.1073/pnas.172360799 (2002).
- 84 Breuss, J. M. & Uhrin, P. VEGF-initiated angiogenesis and the uPA/uPAR system. *Cell Adh Migr* **6**, 535-615, doi:10.4161/cam.22243 (2012).
- 85 Manetti, M. *et al.* Inactivation of urokinase-type plasminogen activator receptor (uPAR) gene induces dermal and pulmonary fibrosis and peripheral microvasculopathy in mice: a new model of experimental scleroderma? *Annals of the Rheumatic Diseases* **73**, 1700, doi:10.1136/annrheumdis-2013-203706 (2014).
- 86 D'Alessio, S. *et al.* Matrix metalloproteinase 12-dependent cleavage of urokinase receptor in systemic sclerosis microvascular endothelial cells results in impaired angiogenesis. *Arthritis Rheum* **50**, 3275-3285, doi:10.1002/art.20562 (2004).
- 87 Maria, A. T. J. *et al.* Fibrosis Development in HOCl-Induced Systemic Sclerosis: A Multistage Process Hampered by Mesenchymal Stem Cells. *Frontiers in Immunology* **9**, doi:10.3389/fimmu.2018.02571 (2018).
- 88 Maria, A. T. *et al.* Antifibrotic, Antioxidant, and Immunomodulatory Effects of Mesenchymal Stem Cells in HOCl-Induced Systemic Sclerosis. *Arthritis Rheumatol* **68**, 1013-1025, doi:10.1002/art.39477 (2016).
- 89 Servettaz, A. *et al.* Selective oxidation of DNA topoisomerase 1 induces systemic sclerosis in the mouse. *J Immunol* **182**, 5855-5864, doi:10.4049/jimmunol.0803705 (2009).
- 90 Bei, Y. *et al.* RhoA/Rho-kinase activation promotes lung fibrosis in an animal model of systemic sclerosis. *Exp Lung Res* **42**, 44-55, doi:10.3109/01902148.2016.1141263 (2016).
- 91 Kavian, N. *et al.* The Nrf2-Antioxidant Response Element Signaling Pathway Controls Fibrosis and Autoimmunity in Scleroderma. *Frontiers in Immunology* **9**, doi:10.3389/fimmu.2018.01896 (2018).
- 92 Furukawa, M. & Xiong, Y. BTB protein Keap1 targets antioxidant transcription factor Nrf2 for ubiquitination by the Cullin 3-Roc1 ligase. *Mol Cell Biol* **25**, 162-171, doi:10.1128/mcb.25.1.162-171.2005 (2005).
- 93 Yamamoto, T. *et al.* Physiological significance of reactive cysteine residues of Keap1 in determining Nrf2 activity. *Mol Cell Biol* **28**, 2758-2770, doi:10.1128/mcb.01704-07 (2008).
- 94 Chen, J. K., Yang, D., Shen, B., Neilan, B. A. & Murray, V. Zorbamycin has a different DNA sequence selectivity compared with bleomycin and analogues. *Bioorg Med Chem* **24**, 6094-6101, doi:10.1016/j.bmc.2016.09.072 (2016).

- 95 Kawai, K. & Akaza, H. Bleomycin-induced pulmonary toxicity in chemotherapy for testicular cancer. *Expert Opin Drug Saf* **2**, 587-596, doi:10.1517/14740338.2.6.587 (2003).
- 96 Umezawa, H., Maeda, K., Takeuchi, T. & Okami, Y. New antibiotics, bleomycin A and B. *J Antibiot (Tokyo)* **19**, 200-209 (1966).
- 97 in *Fresenius Kabi Canada Ltd* (2016).
- 98 Sausville, E. A., Stein, R. W., Peisach, J. & Horwitz, S. B. Properties and products of the degradation of DNA by bleomycin and iron(II). *Biochemistry* **17**, 2746-2754, doi:10.1021/bi00607a008 (1978).
- 99 Ekimoto, H., Takahashi, K., Matsuda, A., Takita, T. & Umezawa, H. Lipid peroxidation by bleomycin-iron complexes in vitro. *J Antibiot (Tokyo)* **38**, 1077-1082, doi:10.7164/antibiotics.38.1077 (1985).
- 100 Ali, M. K. *et al.* Critical role for iron accumulation in the pathogenesis of fibrotic lung disease. *J Pathol* **251**, 49-62, doi:10.1002/path.5401 (2020).
- 101 Oury, T. D. *et al.* Attenuation of bleomycin-induced pulmonary fibrosis by a catalytic antioxidant metalloporphyrin. *Am J Respir Cell Mol Biol* **25**, 164-169, doi:10.1165/ajrcmb.25.2.4235 (2001).
- 102 Yan, B. *et al.* Sulforaphane prevents bleomycin-induced pulmonary fibrosis in mice by inhibiting oxidative stress via nuclear factor erythroid 2-related factor-2 activation. *Mol Med Rep* **15**, 4005-4014, doi:10.3892/mmr.2017.6546 (2017).
- 103 Filderman, A. E. & Lazo, J. S. Murine strain differences in pulmonary bleomycin metabolism. *Biochemical Pharmacology* **42**, 195-198, doi:[https://doi.org/10.1016/0006-2952\(91\)90702-7](https://doi.org/10.1016/0006-2952(91)90702-7) (1991).
- 104 Reinert, T., Baldotto, C. S. d. R., Nunes, F. A. P. & Scheliga, A. A. d. S. Bleomycin-Induced Lung Injury. *Journal of Cancer Research* **2013**, 480608, doi:10.1155/2013/480608 (2013).
- 105 Chung, M. P. *et al.* Role of repeated lung injury and genetic background in bleomycin-induced fibrosis. *Am J Respir Cell Mol Biol* **29**, 375-380, doi:10.1165/rcmb.2003-0029OC (2003).
- 106 Faffe, D. S. & Zin, W. A. Lung parenchymal mechanics in health and disease. *Physiol Rev* **89**, 759-775, doi:10.1152/physrev.00019.2007 (2009).
- 107 Upagupta, C., Shimbori, C., Alsilmi, R. & Kolb, M. Matrix abnormalities in pulmonary fibrosis. *European Respiratory Review* **27**, 180033, doi:10.1183/16000617.0033-2018 (2018).
- 108 Knudsen, L. *et al.* Alveolar Micromechanics in Bleomycin-induced Lung Injury. *Am J Respir Cell Mol Biol* **59**, 757-769, doi:10.1165/rcmb.2018-0044OC (2018).
- 109 Slutsky, A. S. & Ranieri, V. M. Ventilator-induced lung injury. *N Engl J Med* **370**, 980, doi:10.1056/NEJMc1400293 (2014).
- 110 Moore, B. B. & Hogaboam, C. M. Murine models of pulmonary fibrosis. *Am J Physiol Lung Cell Mol Physiol* **294**, L152-160, doi:10.1152/ajplung.00313.2007 (2008).
- 111 Chua, F., Gauldie, J. & Laurent, G. J. Pulmonary Fibrosis. *American Journal of Respiratory Cell and Molecular Biology* **33**, 9-13, doi:10.1165/rcmb.2005-0062TR (2005).
- 112 Goldstein, R. H., Lucey, E. C., Franzblau, C. & Snider, G. L. Failure of mechanical properties to parallel changes in lung connective tissue composition in bleomycin-

- induced pulmonary fibrosis in hamsters. *Am Rev Respir Dis* **120**, 67-73, doi:10.1164/arrd.1979.120.1.67 (1979).
- 113 Starcher, B. C., Kuhn, C. & Overton, J. E. Increased elastin and collagen content in the lungs of hamsters receiving an intratracheal injection of bleomycin. *Am Rev Respir Dis* **117**, 299-305, doi:10.1164/arrd.1978.117.2.299 (1978).
- 114 Chung, M. P. *et al.* Role of Repeated Lung Injury and Genetic Background in Bleomycin-Induced Fibrosis. *American Journal of Respiratory Cell and Molecular Biology* **29**, 375-380, doi:10.1165/rcmb.2003-0029OC (2003).
- 115 Lawson, W. E. *et al.* Increased and prolonged pulmonary fibrosis in surfactant protein C-deficient mice following intratracheal bleomycin. *Am J Pathol* **167**, 1267-1277, doi:10.1016/S0002-9440(10)61214-X (2005).
- 116 Lee, R. *et al.* Bleomycin delivery by osmotic minipump: similarity to human scleroderma interstitial lung disease. *Am J Physiol Lung Cell Mol Physiol* **306**, L736-L748, doi:10.1152/ajplung.00210.2013 (2014).
- 117 Ravanetti, F. *et al.* Modeling pulmonary fibrosis through bleomycin delivered by osmotic minipump: a new histomorphometric method of evaluation. *Am J Physiol Lung Cell Mol Physiol* **318**, L376-L385, doi:10.1152/ajplung.00311.2019 (2020).
- 118 Liang, M. *et al.* A modified murine model of systemic sclerosis: bleomycin given by pump infusion induced skin and pulmonary inflammation and fibrosis. *Lab Invest* **95**, 342-350, doi:10.1038/labinvest.2014.145 (2015).
- 119 Watanabe, T. *et al.* Optimization of a murine and human tissue model to recapitulate dermal and pulmonary features of systemic sclerosis. *PLoS One* **12**, e0179917, doi:10.1371/journal.pone.0179917 (2017).
- 120 Harrison, J. H., Jr. & Lazo, J. S. High dose continuous infusion of bleomycin in mice: a new model for drug-induced pulmonary fibrosis. *J Pharmacol Exp Ther* **243**, 1185-1194 (1987).
- 121 Percie du Sert, N. *et al.* Reporting animal research: Explanation and elaboration for the ARRIVE guidelines 2.0. *PLoS Biol* **18**, e3000411, doi:10.1371/journal.pbio.3000411 (2020).
- 122 Hughes, M. *et al.* Gender-related differences in systemic sclerosis. *Autoimmunity Reviews* **19**, 102494, doi:<https://doi.org/10.1016/j.autrev.2020.102494> (2020).
- 123 Redente, E. F. *et al.* Age and sex dimorphisms contribute to the severity of bleomycin-induced lung injury and fibrosis. *Am J Physiol Lung Cell Mol Physiol* **301**, L510-518, doi:10.1152/ajplung.00122.2011 (2011).
- 124 Maria, A. T. J. *et al.* iNOS Activity Is Required for the Therapeutic Effect of Mesenchymal Stem Cells in Experimental Systemic Sclerosis. *Front Immunol* **9**, 3056, doi:10.3389/fimmu.2018.03056 (2018).
- 125 Maria, A. T. *et al.* Human adipose mesenchymal stem cells as potent anti-fibrosis therapy for systemic sclerosis. *J Autoimmun* **70**, 31-39, doi:10.1016/j.jaut.2016.03.013 (2016).
- 126 McGovern, T. K., Robichaud, A., Fereydoonzad, L., Schuessler, T. F. & Martin, J. G. Evaluation of respiratory system mechanics in mice using the forced oscillation technique. *J Vis Exp*, e50172, doi:10.3791/50172 (2013).
- 127 Farahnak, S. *et al.* HB-EGF Synthesized by CD4 T Cells Modulates Allergic Airway Eosinophilia by Regulating IL-5 Synthesis. *The Journal of Immunology* **203**, 39-47, doi:10.4049/jimmunol.1801686 (2019).

- 128 Robichaud, A. *et al.* Automated full-range pressure-volume curves in mice and rats. *J Appl Physiol (1985)* **123**, 746-756, doi:10.1152/jappphysiol.00856.2016 (2017).
- 129 Shalaby, K. H., Gold, L. G., Schuessler, T. F., Martin, J. G. & Robichaud, A. Combined forced oscillation and forced expiration measurements in mice for the assessment of airway hyperresponsiveness. *Respir Res* **11**, 82, doi:10.1186/1465-9921-11-82 (2010).
- 130 Lv, X.-x. *et al.* Rupatadine Protects against Pulmonary Fibrosis by Attenuating PAF-Mediated Senescence in Rodents. *PLOS ONE* **8**, e68631, doi:10.1371/journal.pone.0068631 (2013).
- 131 McGovern, T. K. *et al.* Neutrophilic oxidative stress mediates organic dust-induced pulmonary inflammation and airway hyperresponsiveness. *American Journal of Physiology-Lung Cellular and Molecular Physiology* **310**, L155-L165, doi:10.1152/ajplung.00172.2015 (2016).
- 132 Slaoui, M. & Fiette, L. in *Drug Safety Evaluation: Methods and Protocols* (ed Jean-Charles Gautier) 69-82 (Humana Press, 2011).
- 133 Van De Vlekkert, D., Machado, E. & d'Azzo, A. Analysis of Generalized Fibrosis in Mouse Tissue Sections with Masson's Trichrome Staining. *Bio Protoc* **10**, e3629, doi:10.21769/BioProtoc.3629 (2020).
- 134 Farris, A. B. *et al.* Morphometric and Visual Evaluation of Fibrosis in Renal Biopsies. *Journal of the American Society of Nephrology* **22**, 176, doi:10.1681/ASN.2009091005 (2011).
- 135 Watson, C. J. *et al.* Epigenetic Therapy for the Treatment of Hypertension-Induced Cardiac Hypertrophy and Fibrosis. *Journal of Cardiovascular Pharmacology and Therapeutics* **21**, 127-137, doi:10.1177/1074248415591698 (2016).
- 136 in *Idexx Bioanalytics*.
- 137 Lee, J. K. *et al.* Effect of Muscle Cell Preservation on Viability and Differentiation of Hamstring Tendon Graft In Vitro. *Cells* **10**, doi:10.3390/cells10040740 (2021).
- 138 Khan, N. *et al.* M. tuberculosis Reprograms Hematopoietic Stem Cells to Limit Myelopoiesis and Impair Trained Immunity. *Cell* **183**, 752-770.e722, doi:10.1016/j.cell.2020.09.062 (2020).
- 139 Cowley, P. M., Roberts, C. R. & Baker, A. J. Monitoring the Health Status of Mice with Bleomycin-induced Lung Injury by Using Body Condition Scoring. *Comp Med* **69**, 95-102, doi:10.30802/AALAS-CM-18-000060 (2019).
- 140 Lee, C. G. *et al.* Interleukin-13 induces tissue fibrosis by selectively stimulating and activating transforming growth factor beta(1). *J Exp Med* **194**, 809-821, doi:10.1084/jem.194.6.809 (2001).
- 141 Belperio, J. A. *et al.* The Role of the Th2 CC Chemokine Ligand CCL17 in Pulmonary Fibrosis. *The Journal of Immunology* **173**, 4692, doi:10.4049/jimmunol.173.7.4692 (2004).
- 142 Kolb, M., Margetts, P. J., Anthony, D. C., Pitossi, F. & Gauldie, J. Transient expression of IL-1beta induces acute lung injury and chronic repair leading to pulmonary fibrosis. *J Clin Invest* **107**, 1529-1536, doi:10.1172/jci12568 (2001).
- 143 Sime, P. J. *et al.* Transfer of tumor necrosis factor-alpha to rat lung induces severe pulmonary inflammation and patchy interstitial fibrogenesis with induction of transforming growth factor-beta1 and myofibroblasts. *Am J Pathol* **153**, 825-832, doi:10.1016/s0002-9440(10)65624-6 (1998).

- 144 Lee, J. M., Chan, K., Kan, Y. W. & Johnson, J. A. Targeted disruption of Nrf2 causes regenerative immune-mediated hemolytic anemia. *Proc Natl Acad Sci U S A* **101**, 9751-9756, doi:10.1073/pnas.0403620101 (2004).
- 145 Cho, H.-Y., Reddy, S. P. M., Yamamoto, M. & Kleeberger, S. R. The transcription factor NRF2 protects against pulmonary fibrosis. *The FASEB Journal* **18**, 1258-1260, doi:<https://doi.org/10.1096/fj.03-1127fje> (2004).
- 146 Kikuchi, N. *et al.* Nrf2 protects against pulmonary fibrosis by regulating the lung oxidant level and Th1/Th2 balance. *Respir Res* **11**, 31, doi:10.1186/1465-9921-11-31 (2010).
- 147 Morin, F. *et al.* Niclosamide Prevents Systemic Sclerosis in a Reactive Oxygen Species–Induced Mouse Model. *The Journal of Immunology* **197**, 3018, doi:10.4049/jimmunol.1502482 (2016).
- 148 Nikitorowicz-Buniak, J., Shiwen, X., Denton, C. P., Abraham, D. & Stratton, R. Abnormally Differentiating Keratinocytes in the Epidermis of Systemic Sclerosis Patients Show Enhanced Secretion of CCN2 and S100A9. *Journal of Investigative Dermatology* **134**, 2693-2702, doi:<https://doi.org/10.1038/jid.2014.253> (2014).
- 149 Kaviani, N. *et al.* Reactive oxygen species-mediated killing of activated fibroblasts by arsenic trioxide ameliorates fibrosis in a murine model of systemic sclerosis. *Arthritis Rheum* **64**, 3430-3440, doi:10.1002/art.34534 (2012).
- 150 Pérez-Bravo, D. *et al.* A comparison of airway pressures for inflation fixation of developing mouse lungs for stereological analyses. *Histochem Cell Biol* **155**, 203-214, doi:10.1007/s00418-020-01951-0 (2021).
- 151 Misharin, A. V. *et al.* Monocyte-derived alveolar macrophages drive lung fibrosis and persist in the lung over the life span. *Journal of Experimental Medicine* **214**, 2387-2404, doi:10.1084/jem.20162152 (2017).
- 152 McCubbrey, A. L. *et al.* Deletion of c-FLIP from CD11b(hi) Macrophages Prevents Development of Bleomycin-induced Lung Fibrosis. *Am J Respir Cell Mol Biol* **58**, 66-78, doi:10.1165/rcmb.2017-0154OC (2018).
- 153 Watanabe, S., Alexander, M., Misharin, A. V. & Budinger, G. R. S. The role of macrophages in the resolution of inflammation. *The Journal of Clinical Investigation* **129**, 2619-2628, doi:10.1172/JCI124615 (2019).
- 154 Gibbons, M. A. *et al.* Ly6Chi monocytes direct alternatively activated profibrotic macrophage regulation of lung fibrosis. *Am J Respir Crit Care Med* **184**, 569-581, doi:10.1164/rccm.201010-1719OC (2011).
- 155 Moore, B. B. *et al.* Protection from Pulmonary Fibrosis in the Absence of CCR2 Signaling. *The Journal of Immunology* **167**, 4368, doi:10.4049/jimmunol.167.8.4368 (2001).
- 156 Meng, M. *et al.* The Fibrosis and Immunological Features of Hypochlorous Acid Induced Mouse Model of Systemic Sclerosis. *Frontiers in Immunology* **10**, doi:10.3389/fimmu.2019.01861 (2019).
- 157 Raghunath, A. *et al.* Antioxidant response elements: Discovery, classes, regulation and potential applications. *Redox Biol* **17**, 297-314, doi:10.1016/j.redox.2018.05.002 (2018).
- 158 Tonelli, C., Chio, I. I. C. & Tuveson, D. A. Transcriptional Regulation by Nrf2. *Antioxidants & Redox Signaling* **29**, 1727-1745, doi:10.1089/ars.2017.7342 (2017).
- 159 Park, J. K. *et al.* Bleomycin Induces Drug Efflux in Lungs. A Pitfall for Pharmacological Studies of Pulmonary Fibrosis. *Am J Respir Cell Mol Biol* **62**, 178-190, doi:10.1165/rcmb.2018-0147OC (2020).

- 160 Balis, J. U., Shelley, S. A., McCue, M. J. & Rappaport, E. S. Mechanisms of damage to the lung surfactant system. Ultrastructure and quantitation of normal and in vitro inactivated lung surfactant. *Experimental and molecular pathology* **14**, 243-262, doi:10.1016/0014-4800(71)90069-4 (1971).
- 161 Weinberger, S. E., Cockrill, B.A, & Mandel, J. . *Principles of pulmonary medicine* (Elsevier, 2019).
- 162 Veldhuizen, E. J. A. & Haagsman, H. P. Role of pulmonary surfactant components in surface film formation and dynamics. *Biochimica et Biophysica Acta (BBA) - Biomembranes* **1467**, 255-270, doi:[https://doi.org/10.1016/S0005-2736\(00\)00256-X](https://doi.org/10.1016/S0005-2736(00)00256-X) (2000).
- 163 Abman, S. H. *et al.* in *Avery's Diseases of the Newborn (Tenth Edition)* (eds Christine A. Gleason & Sandra E. Juul) vii-xx (Elsevier, 2018).
- 164 Katzenstein, A. L. & Myers, J. L. Idiopathic pulmonary fibrosis: clinical relevance of pathologic classification. *Am J Respir Crit Care Med* **157**, 1301-1315, doi:10.1164/ajrcm.157.4.9707039 (1998).
- 165 Sisson, T. H. *et al.* Targeted injury of type II alveolar epithelial cells induces pulmonary fibrosis. *Am J Respir Crit Care Med* **181**, 254-263, doi:10.1164/rccm.200810-1615OC (2010).
- 166 Mulugeta, S. & Beers, M. F. Surfactant protein C: Its unique properties and emerging immunomodulatory role in the lung. *Microbes and Infection* **8**, 2317-2323, doi:<https://doi.org/10.1016/j.micinf.2006.04.009> (2006).
- 167 Sakamoto, S. *et al.* Keratinocyte growth factor gene transduction ameliorates pulmonary fibrosis induced by bleomycin in mice. *Am J Respir Cell Mol Biol* **45**, 489-497, doi:10.1165/rcmb.2010-0092OC (2011).
- 168 Serrano-Mollar, A. *et al.* Intratracheal transplantation of alveolar type II cells reverses bleomycin-induced lung fibrosis. *Am J Respir Crit Care Med* **176**, 1261-1268, doi:10.1164/rccm.200610-1491OC (2007).
- 169 Radu, M. & Chernoff, J. An in vivo assay to test blood vessel permeability. *J Vis Exp*, e50062, doi:10.3791/50062 (2013).
- 170 García-Prieto, E. *et al.* Resistance to bleomycin-induced lung fibrosis in MMP-8 deficient mice is mediated by interleukin-10. *PLoS One* **5**, e13242, doi:10.1371/journal.pone.0013242 (2010).
- 171 Scotton, C. J. *et al.* *Ex vivo* μ CT analysis of bleomycin-induced lung fibrosis for pre-clinical drug evaluation. *European Respiratory Journal*, erj01824-02012, doi:10.1183/09031936.00182412 (2013).
- 172 Degryse, A. L. *et al.* Repetitive intratracheal bleomycin models several features of idiopathic pulmonary fibrosis. *Am J Physiol Lung Cell Mol Physiol* **299**, L442-452, doi:10.1152/ajplung.00026.2010 (2010).